

A Crack-Closure Model for the Fatigue Behavior of Notched Components and Welded Joints

by
Chien-Yuan Hou
and
F. V. Lawrence
Civil Engineering

A report of
MATERIALS ENGINEERING — MECHANICAL BEHAVIOR
College of Engineering, University of Illinois at Urbana-Champaign
May 1994

ABSTRACT

Newman's Dugdale strip-yield model for crack closure was modified to estimate the crack-closure behavior of cracks emanating from notches. The results obtained using this crack-tip plastic deformation model showed that the estimated effective stress-intensity ratio $U(a)$ ($= \Delta K_{\text{eff}}(a)/\Delta K(a)$) does not exhibit the commonly observed "dip" caused by the notch plasticity. A finite element procedure was used to calculate the magnitude of the notch plastic stretches. It was found that the magnitude of notch plastic stretches is much larger than that of the crack-tip plastic stretches, and that the notch plastic stretches are the main source of the plastic wake when the crack length is much smaller than the notch plastic zone.

A model termed the Strip-Yield Model for Notched Components (SYMNC) that incorporates the notch plastic stretches into the original strip-yield model was proposed for simulating the crack-closure behavior of cracks propagating in the vicinity of a notch. The validity and the efficiency of this model was verified by comparing the predicted results with the published experimental data of various notched components and stress-relieved weldments.

The effect of residual stress on the crack propagation behavior was studied using the crack-closure concept with the SYMNC model. The SYMNC model combined the weld toe plastic deformation and the residual stress effects, and in this form was used to study the crack-closure behavior of as-welded joints. The fatigue lives of weldments were simulated using the SYMNC model.

ACKNOWLEDGEMENTS

Acknowledgement is due to all the faculty and staff members at the University of Illinois for their invaluable input during the course of the author's graduate study.

The author would like to express his sincere gratitude to Professor F. V. Lawrence, Jr. for his guidance, encouragement and many generous contributions to his personal and professional development.

The invaluable advice and guidance of Dr. J. C. Newman, Jr. and Professor H. Sehitoglu are also sincerely acknowledged.

The author wish to express his appreciation to Dr. G. Banas, Mr. H. Y. Hsieh, Mr. G. Fry and Mr. S. Dimitrakis for their help in preparing this report.

The author would like to express his deepest thanks to his brother K. Y. Hour for his invaluable patience and support.

The initial funding of this research was provided by the Fracture Control Program at the University of Illinois at Urbana-Champaign. Additional funding was provided by the Cooperative Research Program of Edison Welding Institute, Columbus, Ohio.

TABLE OF CONTENTS

CHAPTER I:	INTRODUCTION.....	1
1.1	BACKGROUND.....	1
1.2	OBJECTIVE AND SCOPE.....	1
1.3	THESIS ORGANIZATION.....	1
CHAPTER II:	LITERATURE REVIEW.....	3
2.1	FATIGUE CRACK CLOSURE.....	3
2.1.1	Mechanisms of Crack Closure.....	3
2.1.2	Theoretical and Numerical Approach for Plasticity-Induced Crack Closure.....	4
2.2	FATIGUE CRACK PROPAGATION BEHAVIOR IN NOTCHED COMPONENTS.....	5
2.3	THE EFFECTS OF RESIDUAL STRESSES ON FATIGUE CRACK INITIATION AND PROPAGATION OF WELDED JOINTS.....	7
2.4	FATIGUE LIFE PREDICTION MODELS FOR WELDED JOINTS.....	9
2.4.1	Linear Elastic Fracture Mechanics.....	9
2.4.2	Crack Initiation-Propagation Approach.....	9
2.4.3	Crack Closure at a Notch Model.....	10
2.5	SUMMARY.....	12
CHAPTER III:	NEWMAN'S MODIFIED DUGDALE STRIP-YIELD MODEL FOR PLASTICITY-INDUCED CRACK CLOSURE.....	13
3.1	DUGDALE-TYPE CRACK.....	13
3.2	STRIP-YIELD MODEL FOR CRACK CLOSURE.....	13
3.3	DIFFICULTIES WITH THE NEWMAN'S STRIP-YIELD MODEL WHEN APPLIED TO NOTCHED COMPONENTS.....	14
CHAPTER IV:	THE DEVELOPMENT OF A STRIP-YIELD MODEL FOR A NOTCHED COMPONENT (SYMNC).....	16
4.1	MODIFICATION OF NEWMAN'S STRIP-YIELD MODEL TO INCLUDE THE EFFECTS OF THE NOTCH PLASTIC ZONE.....	16
4.1.1	A Method for the Determination of the Notch Plastic Stretches (NPS).....	16
4.1.2	Comparison of the Magnitude of the NPS with the Magnitude of the CTPS	17
4.1.3	Incorporating the NPS into the Strip-Yield Model.....	18
4.2	COMPARISON OF PREDICTED RESULTS WITH EXPERIMENTAL DATA.....	19
4.2.1	Sharp, Single-Edge Notch in a BS4360 50B Steel Plate.....	19
4.2.2	Blunt Center Notch in a 1020 Steel Plate.....	20

4.2.3	Sharp, Double-Edge Notch in a 1070 Steel Plate.....	21
4.2.4	Sharp Center Notch in a JIS SM41B Steel Plate.....	22
4.3	SUMMARY.....	22
CHAPTER V:	THE PREDICTION OF THE PLASTICITY-INDUCED CRACK CLOSURE IN WELDMENTS USING THE STRIP-YIELD MODEL FOR A NOTCHED COMPONENT (SYMNC).....	24
5.1	STRESS-RELIEVED WELDMENTS.....	24
5.1.1	A Special Finite Element Mesh for Determining the Notch Plastic Stretches at Weld Toes.....	24
5.1.2	Comparison of Predicted Results with the Experimental Data of Cruciform Weldments.....	25
5.2	AS-WELDED WELDMENTS.....	27
5.2.1	The Development of Strip-Yield Model Including Residual Stress Effects.....	27
5.2.2	Comparison of Predicted Results with the Test Data: Case I.....	27
5.2.3	Comparison of Predicted Results with the Test Data: Case II.....	29
5.2.4	Comparison of Predicted Results with the Test Data of an As-Welded T-Joint.....	31
5.3	SUMMARY.....	32
CHAPTER VI:	DISCUSSION.....	33
6.1	EFFECTS OF STRESS RATIO R ON CRACK CLOSURE IN THE VICINITY OF A NOTCH.....	33
6.2	GENERAL DISCUSSION OF THE SYMNC MODEL FOR FATIGUE LIFE PREDICTIONS.....	34
6.3	COMPARISON OF VARIOUS MODEL PREDICTIONS FOR WELDMENT FATIGUE LIFE.....	36
6.3.1	Crack Propagation Life.....	36
6.3.2	Total Fatigue Life.....	38
6.4	THE IMPORTANCE OF CRACK INITIATION IN WELDMENTS.....	39
CHAPTER VII:	CONCLUSIONS AND PROPOSED FUTURE WORK.....	41
7.1	CONCLUSIONS.....	41
7.2	PROPOSED FUTURE WORK.....	41
TABLES.....		43
FIGURES.....		48
REFERENCES.....		94
APPENDIX A:	ADAPTATION OF NEWMAN'S STRIP-YIELD MODEL TO ESTIMATE THE CRACK CLOSURE OF NOTCHED COMPONENTS.....	99
A.1	MATHEMATICAL FORMULATION OF THE STRIP-YIELD	

MODEL FOR NOTCHED COMPONENTS.....	99
A.2 CONSTRAINT FACTOR.....	101
APPENDIX B: INTRODUCING THE EFFECTS OF RESIDUAL STRESSES INTO THE STRIP-YIELD MODEL.....	105

LIST OF SYMBOLS

a	Crack length
α, α_g	Constraint factor, global constraint factor of Newman
b	Fatigue strength exponent
c/a	Aspect ratio of surface crack
C, C', m	Paris law and modified Paris law material constants
D	Notch depth
ϵ_p	Plastic strain in the loading direction
K_c	Fracture toughness
K_f	Fatigue notch factor
K_{\max}, K_{\min}	Applied maximum and minimum stress-intensity factor
K_{open}	Crack-opening stress-intensity factor
K_p	Stress-intensity factor caused by strip yield stress
K_{res}	Residual stress induced stress-intensity factor
K_S	Stress intensity caused by uniform remote stress
K_t	Stress concentration factor
κ	Residual stress relaxation exponent
l_t	Transition crack length
N_I	Crack initiation life
N_N	Crack nucleation life
N_{P1}	Short crack propagation life
N_{P2}	Long crack propagation life
N_T	Total fatigue life
R	Stress ratio
r	Notch radius
R'	Effective stress ratio
ρ_c	Crack-tip plastic zone size
ρ_n	Notch plastic zone size
σ'_f	Fatigue strength coefficient
$\sigma(x)$	Unflawed notch stress distribution
σ_0	Flow stress
σ_{0s}	mean stress calculated by the set-up-cycle
σ_{cs}	current value of mean stress at crack initiation site
S_a	Applied stress amplitude

σ_c	Current value of mean stress at crack initiation site
σ_m	Crack initiation site mean stress
S_{\max}, S_{\min}	Applied maximum and minimum stress
S_{open}	Crack-opening stress
t	Plate thickness or base plate thickness of weldments
U	Effective stress-intensity factor ratio
u	Crack-face displacement
W	Plate width
$\Delta K', K'_{\max}, K'_{\min}$	Stress intensities in residual stress field
$\Delta K, \Delta K_{\text{eff}}$	Stress-intensity range and effective stress-intensity range
ΔK_{th}	Threshold stress-intensity range
S_y, S_u	Yield and ultimate strength of material
x_c	Coordinate system located at the moving crack tip
x	Coordinate system located at notch root

LIST OF ABBREVIATIONS

CTPS	Crack-Tip Plastic Stretches
FEA	Finite Element Analysis
LEFM	Linear Elastic Fracture Mechanics
NPS	Notch Plastic Stretches
OICC	Oxide-Induced Crack Closure
PICC	Plasticity-Induced Crack Closure
RICC	Roughness-Induced Crack Closure
SIF	Stress-Intensity Factor
SYMNC	Strip-Yield Model for Notched Components

CHAPTER I: INTRODUCTION

1.1 BACKGROUND

A large fraction of observed structural failures result from the development of fatigue cracks at sites of stress concentration and particularly at the geometric discontinuities provided by the weldments that join their components. Based on the observed fatigue processes of crack nucleation, crack initiation, and crack propagation, various analytical fatigue-life models have been proposed to predict component fatigue life. A linear elastic fracture mechanics (LEFM) approach to estimate the crack propagation life has been widely accepted for years. However, many shortcomings of this approach such as dealing with short crack behavior and the anomalous behavior of cracks emanating from notches limit the application of this model.

Since crack closure explains (mechanically) short crack propagation and residual stress effects, a sophisticated crack-closure model might make better fatigue life predictions of notched components and welded joints. Many numerical techniques for estimating crack closure have been developed, but none of them is adequate and efficient for the design of notched components or welded joints. This problem has to be solved before the crack-closure concept can be widely used in computer simulations of fatigue crack development.

1.2 OBJECTIVE AND SCOPE

The objective of this study is to develop an efficient numerical technique to estimate crack closure, and hence, to apply the crack-closure concept to the fatigue design of notched components and welded joints. Newman's modified Dugdale strip-yield model for plasticity-induced crack closure will be used in this study. Many improvements such as considering the notch or weld toe plasticity, and including the effects of residual stresses will be made to make this model more applicable to the notch and weldment problems. The validity of this approach will be confirmed by comparing the model predictions with test data under various conditions.

1.3 THESIS ORGANIZATION

Chapter II, Literature Review, reviews the related published papers and reports. Important crack-closure mechanisms and the analytical models for these mechanisms are summarized. Research dealing with the effect of residual stresses on the crack initiation and

crack propagation are surveyed. Finally, models predicting the fatigue lives of welded joints are presented.

Chapter III, Newman's Modified Dugdale Strip-Yield Model for Plasticity-Induced Crack Closure, briefly describes Newman's strip-yield model and discusses the difficulty encountered when this model is applied to notched components.

Chapter IV, The Modified Dugdale Strip-Yield Model for Plasticity-Induced Crack Closure of Notched Components, focuses on the crack-closure behavior of notched components. A finite element procedure for the notch plastic stretches is presented. The notch plastic stretches are included in the modified Dugdale strip-yield model to study crack closure in notch plastic zones. Various notch crack closure experimental data are compared with predicted results.

Chapter V, The Prediction of Plasticity-Induced Crack Closure in Weldments by the Strip-Yield Model of Notched Components (SYMNC), focuses on estimating the crack-closure behavior of welded joints. Modifications of the finite element technique for the notch plastic stretches are made to make the approach applicable to the special condition at the weld toe. Residual stress effects on crack closure are considered in the strip-yield model. Crack closure of stress-relieved and as-welded weldments is predicted and is compared with the experimental data.

Chapter VI, Discussion, deals with the effects of stress ratio (R) on notch crack-closure behavior. Various models are applied to estimate the crack propagation life and the total fatigue life of T-joints. Finally, the ratio of predicted crack initiation life to the total fatigue life by different models is compared.

Chapter VII, Conclusion and Future Work, presents the conclusions of this study and the proposed future work directions.

Appendix A, Adaptation of Newman's Strip-Yield Model to Estimate the Crack Closure of Notched Components, develops the mathematical formulations of the strip-yield model for notched components in this study.

Appendix B, Introducing the Effects of the Residual Stresses into the Strip-Yield Model, presents the approach employed to include residual stresses in the strip-yield model.

CHAPTER II: LITERATURE REVIEW

2.1 FATIGUE CRACK CLOSURE

2.1.1 Mechanisms of Crack Closure

Fatigue cracks often close during part of a load cycle. Such events are termed crack closure. Because no fatigue crack growth occurs when the crack is closed, the effective stress-intensity range $\Delta K_{\text{eff}} (= K_{\text{max}} - K_{\text{open}})$ is often used instead of the conventional fatigue crack-tip driving force (ΔK) to represent the stimulus causing fatigue crack growth. The effective stress-intensity ratio U is defined as:

$$U(a) = \frac{\Delta K_{\text{eff}}(a)}{\Delta K(a)} = \frac{K_{\text{max}}(a) - K_{\text{open}}(a)}{K_{\text{max}}(a) - K_{\text{min}}(a)} = \frac{S_{\text{max}} - S_{\text{open}}(a)}{S_{\text{max}} - S_{\text{min}}} \quad (2.1)$$

where

a	=	crack length
ΔK_{eff}	=	effective stress-intensity range ($\text{MPa}\sqrt{\text{m}}$)
$K_{\text{max}}, K_{\text{min}}$	=	maximum and minimum stress-intensity factor ($\text{MPa}\sqrt{\text{m}}$)
$S_{\text{max}}, S_{\text{min}}$	=	maximum and minimum remote stress (MPa)
$S_{\text{open}}, K_{\text{open}}$	=	crack-opening stress and crack-opening stress-intensity factor

Various crack-closure mechanisms have been observed in fatigue crack propagation tests. Elber [1] first reported that the residual crack-tip plastic deformations are left behind the crack tip which close the crack faces even when the external load is tensile. This closure mechanism has been termed plasticity-induced crack closure (PICC). The PICC has been used to explain the mean stress effect (R ratio effect), the crack growth retardation after overloads, the short crack behavior and the existence of non-propagating cracks at notches. Since it is caused by plastic deformation, the PICC is dependent upon the external load, material yielding properties, and crack length.

Walker and Beever [2] found the roughness-induced crack closure (RICC). This crack-closure mechanism is caused by the contact of asperities on crack faces when the Mode II displacements occur. Steward [3] and Ritchie et al. [4] found that the thin layer of fillings produced by the corrosion products and oxides residing on crack faces cause the oxide-induced crack closure (OICC). These two closure mechanisms are strongly affected by the microstructure and the environments and are more significant at near-threshold conditions.

Many models have been proposed to predict crack-closure effects caused by these mechanisms. Suresh [5] calculated the reduction of nominal stress-intensity factor at crack tip based on the simplified geometry of a kinked crack and concluded that a small net Mode II displacement causes a significant reduction of stress-intensity factor. LLorca [6] used a finite difference method to calculate the RICC based on an idealized saw-cut crack face geometry. Suresh et al. [7] measured the thickness of oxide film on crack faces and estimated the increase of threshold stress-intensity factor due to the OICC by calculating the stress-intensity factor induced by the prescribed crack-face displacements which are caused by the oxide film.

Modeling RICC and OICC is challenging. However, the nature of irregular microstructures obstructs the accuracy of model predictions. It seems that the PICC is the only closure mechanism which can be accurately estimated because of the well established plasticity theory.

2.1.2 Theoretical and Numerical Approach for Plasticity-Induced Crack Closure

Budiansky and Hutchinson [8] calculated the stable value of $U(a)$ using the Dugdale-type crack and theoretically proved the existence of PICC under plane-stress conditions. They also pointed out that further analyses were required to solve the uncertainty of the existence of PICC under plane-strain conditions. Despite the fact that the theoretical analyses successfully predict the PICC, difficulties encountered in solving more complex crack-closure problems limit the applicability of this approach.

Newman [9] first developed an elastic-plastic finite element technique to estimate the crack-opening and closing stresses. In this finite element model, crack propagation was simulated by releasing element nodes on crack path and large stiffness spring elements were attached to the crack-face nodes to avoid the penetration of these nodes during unloading. After Newman's original work, numerous studies by other researchers using this technique have been reported. This numerical approach has also been used to identify the sources of residual plastic deformation producing the plastic wake. These researches have explained the existence of PICC under plane-strain conditions [10,11].

The advantage of FEA for the PICC is that the model can be applied for any crack geometry and loading condition. However, when applying this technique to short cracks propagating under plane-strain conditions, practical difficulties will arise because the element size has to be small enough to catch the small crack-tip plastic zone. Thus, FEA methods are laborious and costly. Furthermore, the calculated crack-opening stresses are affected by the mesh element size and the crack-tip node releasing scheme used [12].

Another numerical method which deals with PICC is the modified Dugdale strip-yield model developed by Newman [13,14]. Based on the theory of Dugdale-type crack, this model estimates the crack-face contact stresses by calculating the magnitude of the plastic wake left behind the crack tip, and hence, the crack-opening stresses. Many researchers have reported that this strip-yield model is capable of predicting the crack-closure behavior caused by overloads and random loading spectrums [15,16].

A controversial issue entailed with the use of the strip-yield model is its constraint factor (α). Originally, the theory of the Dugdale-type crack was developed for a 2-D crack under plane-stress conditions. When plate thickness increases and the plane-stress state no longer prevails, the stress required to yield the material ahead of the crack tip is larger than the material yield strength (S_y) or flow stress (σ_0) because of the constraints from the thickness direction. To consider plate thickness effects in the strip-yield model, uniformly distributed strip-yield load with magnitude of ($\alpha\sigma_0$) is assumed in the crack-tip plastic zone. For plane stress, $\alpha = 1$; and for plane strain, α is 2.7 from finite element results [17]. Based on a theoretical analysis, Irwin [18] found that α is 1.73 for the plane-strain condition.

The value of α used in the strip-yield model has a large influence on the calculated crack-tip plastic zone size (ρ_c), and hence, the calculated crack-opening stresses. For various plate thickness, the value of α should be between the value of plane stress and that of plane strain. In the original paper [13] of the strip-yield model for crack closure, Newman used $\alpha = 2.3$ for plane-strain conditions. In a subsequent report, Newman [14] used a linear relationship between α and the logarithm value of the calculated crack growth rate. Wang and Blom [16] used a crack-tip plastic zone size (ρ_c) dependent function for α calculations. Because ρ_c is dependent on α in the strip-yield model, an iteration procedure was required to obtain α for their calculations.

2.2 FATIGUE CRACK PROPAGATION BEHAVIOR IN NOTCHED COMPONENTS

The LEFM approach assumes that the fatigue crack tip experiences a K-field stress state, and Paris [19] found a simple relationship between crack growth rate and stress-intensity factor range:

$$da/dN = C(\Delta K)^m \quad (2.2)$$

where

$$\begin{aligned} da/dN &= \text{crack growth rate} \\ C, m &= \text{material constants} \end{aligned}$$

To apply Eq. 2.2 to the case of cracks emanating from notches, one must estimate ΔK accurately. It is obvious that when a crack is long enough, the notch-stress field has no effect on the crack-tip stress state. In this latter case, the stress-intensity factor can be calculated by taking the notch depth as part of the crack length (see Fig. 1):

$$K(a) = f(a+D)S\sqrt{\pi(a+D)} \quad (2.3)$$

where

$$\begin{aligned} f(a+D) &= \text{correction factor} \\ D &= \text{notch depth} \end{aligned}$$

For crack lengths which are affected by the notch-stress field, FEA with special stress singular elements located at the crack tip is commonly used. Another numerical alternative is the weight function method. Bueckner [20] and Rice [21] proved that the stress intensity of a 2-D crack subjected to a symmetrical load system can be written as:

$$K(a) = \int_0^a \sigma(x)m(a,x)dx \quad (2.4)$$

where

$$\begin{aligned} \sigma(x) &= \text{elastic unflawed notch-stress distribution on the crack path: see Fig. 1} \\ m(a,x) &= \text{weight function} \end{aligned}$$

For various notch geometries, $\sigma(x)$ can be easily obtained by the close-form solutions using theory of elasticity or by performing FEA. Numerous of weight functions for various crack geometries have been published. Therefore, using of weight function method for stress-intensity factor is simple and straightforward.

The transition from a stress-intensity factor which is influenced by notch-stress field (Eq. 2.4) to the stress-intensity factor which is affected only by the remote stresses (Eq. 2.3) is shown by the intersection of the two curves in Fig. 1. The transition crack length l_t is dependent on notch geometry. Dowling's notch-stress intensity equation gives l_t ranging from $r/20$ to $r/4$ [22]. Smith and Miller [23] suggested that l_t should be $0.13\sqrt{Dr}$.

It is well known that a higher crack growth rate than that predicted by the LEFM has been observed at notches. To explain this anomalous crack growth behavior, many researchers [24-27] used elastic-plastic fracture mechanics parameters to correlate the

experimental data since the small-scale yielding assumption in LEFM is invalid in notch plastic zone. Crack closure [28,29] has also been used and successfully explains this anomalous crack growth behavior.

Because the closure effects reduce the nominal crack-tip driving force (ΔK), the stress-intensity range during which the crack is open was introduced to the Paris equation by Elber [1]. Hence, the crack growth rate is estimated by the modified Paris equation:

$$da/dN = C'(\Delta K_{\text{eff}}(a))^m = C'(U(a)\Delta K(a))^m \quad (2.5)$$

where C' is the material constants for the modified Paris equation.

2.3 THE EFFECTS OF RESIDUAL STRESSES ON FATIGUE CRACK INITIATION AND PROPAGATION OF WELDED JOINTS

Residual stresses in weldments are caused by the non-uniform thermal distortions during the welding process. Any residual stress field must be in self-equilibrium, and the magnitude of maximum tensile component in weldments can be as high as the yield strength of base plate. It is known that residual stresses increase the mean stress and reduce the weldment fatigue strength. The effects of residual stresses on weldment fatigue can be separated into the effects on crack initiation stage and crack propagation stage.

Lawrence et al. [30] proposed a set-up-cycle procedure to calculate the mean stress induced by residual stresses at first cycle. Because the residual stresses could be relaxed during cycling, the mean stress at crack initiation site was corrected by [31]:

$$\sigma_{cs}/\sigma_{0s} = (2N_I - 1)^\kappa \quad (2.6)$$

where

σ_{cs}	=	current value of mean stress at crack initiation site
σ_{0s}	=	the mean stress calculated by the set-up-cycle procedure at the first cycle
$2N_I$	=	elapsed crack initiation reversals
κ	=	relaxation exponent which is a function of applied strain amplitude

For crack propagation, Parker [32] proposed using the superposition principle to account for the additional stress intensity induced by residual stresses. The weight function

method is commonly used to estimate the residual stress-intensity factor $K_{\text{res}}(a)$. When the $K_{\text{res}}(a)$ is introduced, the actual crack-tip driving forces during cyclic loading are:

$$\begin{aligned} K'_{\text{max}}(a) &= K_{\text{max}}(a) + K_{\text{res}}(a) \\ K'_{\text{min}}(a) &= K_{\text{min}}(a) + K_{\text{res}}(a) \\ \Delta K'(a) &= K'_{\text{max}}(a) - K'_{\text{min}}(a) = \Delta K(a) \end{aligned} \quad (2.7)$$

However, the effective stress ratio R' varies as a function of crack length:

$$R'(a) = \frac{K'_{\text{min}}(a)}{K'_{\text{max}}(a)} \quad (2.8)$$

Glinka [33] observed the crack growth rate under various types of residual stress field and found that tensile residual stresses increase crack growth rate. As cracks propagate into the region of compressive residual stress, the test data approached and merged with the baseline data (crack growth rate tested at plain plate without residual stresses). He also used Forman's equation which considers the stress ratio R effects to predict his experimental data:

$$\frac{da}{dN} = \frac{C \Delta K^m}{(1 - R') - K_c} \quad (2.9)$$

where K_c is the fracture toughness. The predicted crack growth rate showed a sharp decrease for increasing ΔK which was not demonstrated by the experimental data.

Nelson [34] argued that this discrepancy was due to the superposition method used. Instead of using the superposition method, he tried to avoid this artificial effect by using the crack-closure concept. Ohta et al. [35] tested cracks propagating in weldment tensile residual field and found that crack closure occurred only at high compressive external load. In a subsequent work, Ohta and coworkers [36] applied a two-step loading on a fatigue crack propagating in a tensile residual stress field. A constant stress-intensity range was first applied followed by another constant stress-intensity range loading. Transient crack growth rate is expected to be observed after changing of applied load level due to change of crack-closure level. However, no transient effects on crack growth behavior were observed because of the tensile residual stresses. Again, they concluded that no crack closure existed in weld tensile residual stress field. Itoh et al. [37] and Kang et al. [38] studied the crack growth behavior influenced by residual stresses under various stress ratios. They both concluded that crack closure successfully correlated the test data.

Wang and Blom [16] first applied the Newman's strip-yield model to study the problem of crack closure in residual stress fields. They converted the $K_{res}(a)$ to an equivalent uniformly distributed remote load which induces the same value of $K_{res}(a)$ at crack tip. A total remote load (the sum of the applied remote load and the converted remote load) was then used to predict crack growth rate affected by residual stresses in a CT specimen.

2.4 FATIGUE LIFE PREDICTION MODELS FOR WELDED JOINTS

2.4.1 Linear Elastic Fracture Mechanics

Because the preexisting crack-like defects or serious geometry discontinuities in weldments, cracks are assumed to be presented at the first load cycle. Thus, the fatigue life devoted to propagating these initial cracks to final failure is assumed to be the total fatigue life (N_T) of weldments. The LEFM approach using Eq. 2.10 with a proper initial flaw size a_i is commonly used to estimate N_T of welded joints:

$$N_T = N_{P2} = \int_{a_i}^{a_f} \frac{da}{C \Delta K^m} \quad (2.10)$$

2.4.2 Crack Initiation-Propagation Approach

Based on the facts that the observed fatigue strengths of weldments are always higher than those predicted using Eq. 2.10, which indicates that N_T can not be predicted by only considering the N_{P2} . Lawrence et al. [39-41] proposed that N_T of welded joints should be composed of a crack initiation life (N_I) and a crack propagation life (N_{P2}):

$$N_T = N_I + N_{P2} \quad (2.11)$$

The fatigue life spent to initiate a crack was estimated by the Basquin-Morrow equation assuming that the stress state at the crack initiation sites is $K_f \Delta S$. The simplest form of this equation for N_I is:

$$N_I = \frac{1}{2} \left(\frac{S_a K_f}{\sigma_f - \sigma_m} \right)^{\frac{1}{b}} \quad (2.12)$$

where

K_f = fatigue notch factor

σ_f	=	fatigue strength coefficient (MPa)
b	=	fatigue strength exponent
S_a	=	stress amplitude (MPa)
σ_m	=	mean stress at crack initiation site (MPa)

At about the same time, Dowling [22] also suggested the same concept of crack initiation-propagation for notched components. Because $K_t \Delta S$ was used for the notch-root stress, the estimated crack initiation life was always a small fraction of the estimated total fatigue life ($K_t \geq K_f$) at any stress level. In a different crack initiation-propagation approach developed by Miller and coworkers [42], they estimated N_I and N_{P2} by calculating the notch root and crack-tip shear deformations.

Another important difficulty with the I-P model is defining the crack length at which the crack initiation stage ends. This crack length is used as the initial crack length a_i for the integration of the Paris equation, therefore, controls the estimated N_{P2} . Because the transition from crack initiation to crack propagation is not well defined, Lawrence et al. [40,41] assumes this is an arbitrary chosen "engineering-size" crack (≈ 0.25 mm) for weldments. Taking notch depth D as part of crack length, Dowling assumed crack initiation ends at the existence of a crack emanating from notch root with a crack length of l_t . Therefore, crack length of $D+l_t$ is used as a_i in Eq. 2.10 for notched components. It is evident that different definition of a_i leads to different perspectives of crack initiation: see the different stress states assumed at crack initiation sites between Lawrence et al. and Dowling. Socie et al. [43] used notch depth D as a_i to avoid the complicated short crack propagation and also obtained good predictions for N_T .

2.4.3 Crack Closure at a Notch Model

Newman used the modified Dugdale strip-yield model to calculate $U(a)$ [14] and estimated the N_T of notched aluminum plates by integrating Eq. 2.5. Based on other researcher's results, Ting and Lawrence [44,45] determined the $U(a)$ for cracks emanating from notches and calculated the crack propagation life and threshold stresses of notched components. They termed this approach as crack closure at a notch (CCN) model. Figure 2 shows the concepts of the CCN model. Assuming that crack closure is the dominant factor for crack growth behavior in notched components, they estimated the total crack propagation life (N_F , including both the short crack propagation life, N_{P1} , and long crack propagation life, N_{P2}) using Eq. 2.5. Hence, an important concept regarding the total fatigue life partition of notched components has been brought out by the CCN model:

$$N_T = N_I + N_{P2} = (N_N + N_{P1}) + N_{P2} = N_N + (N_{P1} + N_{P2}) = N_N + N_F \quad (2.13)$$

where N_N is the crack nucleation life which is assumed to be small compared with the total fatigue life and is neglectable.

Obviously, the $U(a)$ is the most important function in the crack-closure approach. Acquainted with the fact that the U value is affected by the notch plastic zone, Ogura et al. [46] normalized the measured U values of various load levels by the cyclic notch plastic zone size and showed that U value reached its stable value after crack length is larger than the cyclic notch plastic zone size. Verreman et al. [47] also idealized the $U(a)$ by a linearly decreasing function in the notch plastic zone after which they assumed $U(a)$ is a constant.

After modifying the original formulation for cracks in smooth specimens, Newman [14] applied his strip-yield model to estimate $U(a)$ for cracks propagating in an aluminum notched panel. However, his formulation was restricted to circular notches and center cracks. The weight functions used by Wang and Blom [16] provided a chance to apply this crack-closure model to various notch geometries, but they focused their study on the overload and block loading effects and the notch cases they studied never went beyond circular notches.

McClung and Sehitoglu [48] studied the crack-opening stresses of circular and elliptical notches ($K_t = 3$ and 7) by finite element method and concluded that the anomalous short crack effects can occur even beyond the notch plastic zone. This observation indicates that the calculated $U(a)$ was not stabilized when the crack tip reached the boundary of notch plastic zone. Based on the calculated results of FEA, Sun and Sehitoglu [11] gave the $S_{open}(a)$ for cracks emanating from various notches as a function of maximum applied load, stress concentration factor, and stress ratio R .

Ting and Lawrence [44,45] modeled $U(a)$ by combining two sets of equations for notched components. The S_{open} functions proposed by Sun and Sehitoglu were used to account for closure effects caused by notch and crack-tip plasticity. The RICC and OICC at near-threshold regime was considered by converting Tanaka's equation [49] for the relationship between threshold stress-intensity range (ΔK_{th}) and the crack length. This approach offered more applicability of crack-closure model for the fatigue behavior of notched components.

Lacking information on $U(a)$ for cracks emanating from a weld toe, Hou and Lawrence [50] used an equivalent notch concept which transformed a weld toe notch to an elliptical notch to estimate $U(a)$ of weldments using Ting's $U(a)$ approach. However, lack of the numerical results for plane-strain conditions in steel plates of Sun and Sehitoglu's S_{open} function and the nature of differences between a weld toe notch and an elliptical notch limit the validity of this equivalent notch concept for welded joints.

2.5 SUMMARY

The plasticity-induced crack closure is the only crack-closure mechanism which can be analytically modeled without involving the uncertainty of microstructural effects. Finite element technique and Newman's modified Dugdale strip-yield model are two approaches to estimate PICC. Difficulties may be encountered when applying the finite element technique to weldments. Newman's strip-yield model is an efficient approach to estimate PICC. However, modifications must be made to apply this model to notch components and welded joints.

The crack-closure model is a possible alternative method for estimating total fatigue life of welded joints. The crucial function $U(a)$ for weldments is unavailable, and some simple method for its calculation must be found before the crack-closure concept can be widely used for the computer simulation of fatigue crack development in weldments.

CHAPTER III: NEWMAN'S MODIFIED DUGDALE STRIP-YIELD MODEL FOR PLASTICITY-INDUCED CRACK CLOSURE

3.1 DUGDALE-TYPE CRACK

As shown in Fig. 3(a), a Dugdale-type crack in a plate subjected to remote load contains two regions: (1) plastically deformed material ahead of crack tip (darkly shaded area), and (2) regions other than this region which remain elastic. The crack-tip plastic zone size (ρ_c) which will be subsequently seen to control the crack-closure phenomenon can be calculated by assuming a fictitious crack of length $a+\rho_c$ loaded by two load systems: (1) the remote load S (see Fig. 3(b)) and (2) the uniformly distributed flow stress (σ_0) extending from a to $a+\rho_c$ (see Fig. 3(c)). These two loading conditions produce stress-intensity factors K_S and K_σ at the fictitious crack tip. Because the stress intensity experienced at the fictitious crack tip must be zero, the value of ρ_c can be obtained from the relation:

$$K_S + K_\sigma = 0 \quad (3.1)$$

where

$$\begin{aligned} K_S &= \text{the stress-intensity factor at the fictitious crack tip caused by the remote load} \\ K_\sigma &= \text{the stress-intensity factor at the fictitious crack tip caused by the strip-yield load} \end{aligned}$$

For elastic-perfectly plastic materials, the material yield strength S_y is used as the strip-yield load (or flow stress) σ_0 for a Dugdale-type crack under plane-stress conditions. To make this model applicable to strain-hardening materials such as steel, the average of yield strength and ultimate strength is often used for σ_0

3.2 STRIP-YIELD MODEL FOR CRACK CLOSURE

The permanent deformations parallel to the loading direction produced by crack-tip stress field are termed the "crack-tip plastic stretches" (or CTPS, see Fig. 3(a)). During the fatigue process, fatigue cracks propagate by breaking a small regions of the CTPS ahead of the crack tip. This broken CTPS becomes a "plastic wake" left behind the crack tip. During unloading part of every loading cycle, contact stresses along the crack faces are induced due to the compatibility requirements of the plastic wake and the plastic deformations in the

crack-tip plastic zone. These contact stresses are related to the crack-opening stress of next load cycle (see Fig. 4). Based on the theory of the Dugdale-type crack, Newman [13] developed a numerical scheme (the modified Dugdale strip-yield model for crack closure) to simulate the PICC by calculating the magnitude of CTPS and the height of plastic wake. Contact stresses along crack faces at minimum load and the crack-opening stress were then calculated. Newman's original formulations as described above were modified in this study to estimate the PICC of cracks emanating from notches.

3.3 DIFFICULTIES WITH THE NEWMAN'S STRIP-YIELD MODEL WHEN APPLIED TO NOTCHED COMPONENTS

It is well known that application of an overload to a fatigue-cracked component induces crack-growth retardation. Crack closure successfully explains this phenomenon. Fleck [51] found "bumps" on crack faces after an overload was applied. He concluded that these bumps were caused by the larger crack-tip plastic deformations induced by the overload and that these "bumps" were responsible for the observed change of crack-closure levels. The "bumps" cause larger crack-face contact stresses during unloading, and hence, induce larger crack-closure effects; therefore, as shown in Fig. 5(a), many test results exhibit a pattern in which $U(a)$ shows a "dip" after an overload is applied.

For cracks propagating from notch roots, experimental values of $U(a)$ frequently show a "dip" similar to that observed in overload experiments (see Fig. 5(b)). Many researchers suggest that this dip is due to the plasticity induced by the notch. This idea is reasonable because the notch plastic zone produces loading-direction permanent deformations which are similar to the "bumps" caused by overloads.

If one neglects the above mentioned phenomenon, the PICC of cracks emanating from notches can be easily calculated using Newman's strip-yield model¹. Figure 6(a) shows the calculated crack-closure levels for a cracks emanating from circular notches of various radii. All the predicted closure levels reach the same stable state after cracks propagate a sufficient distance. This distance increases as the notch size increases. This notch-size effect results from the fact that the (elastic) notch-induced stresses extend larger distances for larger notches. Figure 6(b) shows the calculated results for different load levels. The results of Fig. 6(b) are consistent with the results of other researcher's works which show that different load levels induce different stable closure states and different distances to reach the stable state. Based on the results obtained from these two cases, it is apparent that the closure level at any crack length (a) is strongly dependent on the notch size and load level.

¹See Appendix A for details of the formulation of the strip-yield model in this study.

Unfortunately, the above mentioned "dip" of $U(a)$ is not captured by Newman's strip-yield model: see Fig. 6. The absence of the "dip" is believed due to the fact that the strip-yield model accounts for crack-tip plasticity but does not consider the plastic deformation contributed by the notch itself during first quarter cycle. This notch plasticity would add to the crack-tip plasticity, and hence, it must affect the closure levels for cracks propagating within the notch plastic zone.

Thus, Newman's original formulation should be modified to estimate the PICC of cracks emanating from notches.

CHAPTER IV: THE DEVELOPMENT OF A STRIP-YIELD MODEL FOR A NOTCHED COMPONENT (SYMNC)

4.1 MODIFICATION OF NEWMAN'S STRIP-YIELD MODEL TO INCLUDE THE EFFECTS OF THE NOTCH PLASTIC ZONE

Since the crack-tip plastic deformations parallel to the loading direction (CTPS) are the key concept of Newman's strip-yield model for the calculations of the PICC caused by the crack-tip plasticity, a simple way to gauge the effects of the notch plastic zone on crack closure would be to determine the monotonic notch plastic stretches (NPS) and (in some way) add these to those caused by crack-tip plasticity, that is, to superpose the NPS on the CTPS.

4.1.1 A Method for the Determination of the Notch Plastic Stretches (NPS)

First consider a notched plate (Fig. 7) loaded by a remote load S which induces a notch plastic zone: see Fig. 7(a). Next, a crack of length a_A is introduced: see Fig. 7(b). The introduction of this hypothetical crack would result in crack-face displacements $u_{nA}(a_A, x)$: see Fig. 7(c). Now, consider a second notched plate having a preexisting crack of the same length: see Fig. 8(a). This second notched plate is then loaded by remote stress S (Fig. 8(b)); however, a different set of crack-face displacements $u_{nB}(a_A, x)$ would result: see (Fig. 8 (c)).

FEA¹ was used to calculate $u_{nA}(a_A, x)$ and $u_{nB}(a_A, x)$: see Fig. 9. Figure 10 shows typical exaggerated crack-face displacements $u_{nA}(a_A, x)$ and $u_{nB}(a_A, x)$ obtained from FEA. The NPS as a function of the distance from the notch root (x) is:

$$\frac{NPS(x)}{2} = u_{nB}(a_A, x) - u_{nA}(a_A, x) \quad (4.1)$$

¹The commercial software PATRAN was used to generate the finite element mesh, and ABAQUS was used for the elastic-plastic FEA. The plate was 100 mm wide and had a circular notch with radius $r = 5$ mm. The constant strain triangle element was chosen, and the mesh around the notch is shown in Fig. 9. The material was assumed to have an elastic-perfectly plastic stress-strain relationship with a flow stress $\sigma_0 = 400$ MPa. The Young's modulus was 200 GPa. The isotropic hardening rule and the Von Mises criteria were employed in the calculations. The crack-face displacements $u_{nA}(a_A, x)$ and $u_{nB}(a_A, x)$ were calculated at load levels of $S/\sigma_0 = 0.38, 0.5$, and 0.63 for both plane stress and plane strain conditions. Since the hypothetical crack coincided with the boundary conditions (no displacement in the loading direction), which were located at the symmetrical line of the plate, the hypothetical crack in the first plate was introduced by releasing the constrained nodes up to an arbitrary chosen node which was located beyond the monotonic notch plastic zone.

Since the $u_{nA}(a_A, x)$ and $u_{nB}(a_A, x)$ are the one-half of paired crack-face displacements, the calculated results of Eq. 4.1 are half the total value of the NPS.

4.1.2 Comparison of the Magnitude of the NPS with the Magnitude of the CTPS

As discussed in Sec. 3.3, both the NPS and the CTPS are the sources of the plastic wake left on the crack faces as cracks propagate from notches. To understand how these two types of stretches might contribute to the plastic wake, the size of the CTPS at any crack length (a) was compared with that of the NPS at a corresponding distance² (x) from the notch root $NPS(x = a)$.

Consider a moving coordinate system with its origin located at the crack tip. The magnitude of the CTPS at any distance x_c from the crack tip³ is $CTPS(x_c)$. Figure 11 shows the CTPS as a function of distance from the crack tip. The NPS as a function of distance from the notch root is also shown in Fig. 11. The $CTPS(x_c = 0)$ was chosen as an index of the size of CTPS for a crack of length (a) and is compared with the value of the NPS at $x = a$, that is, $NPS(x = a)$, in Fig. 12.

The strip-yield model was used to calculate the values of $CTPS(x_c)$ for a crack emanating from the 5 mm radius circular notch discussed previously⁴. The ratios of $CTPS(x_c = 0)$ to $NPS(x = a)$, that is $CTPS/NPS$, are plotted versus the ratio of the crack length to the notch plastic zone size⁵ (a/ρ_n) in Fig. 12. All the curves show a similar trend. The values of the ratio $CTPS/NPS$ vary from 10^{-2} at $a/\rho_n \approx 0$ to over⁶ 10 at $a/\rho_n = 1$. The value of the ratio $CTPS/NPS$ becomes unity for crack lengths about 15~30% of notch plastic zone size. When crack length is less 10% of the notch plastic zone size, the ratio decreases drastically; and the CTPS becomes insignificant.

From these results, it is evident that for very small cracks ($a/\rho_n < 0.05$), the entire crack-tip plastic zone is embedded within the notch plastic zone; and the CTPS are much smaller than the NPS. Hence, the plastic wake left behind the crack tip is mainly due to the NPS at this stage. As the crack becomes larger, the size of CTPS becomes comparable to that of the NPS; and the CTPS also contribute an important part of the plastic wake. Finally, when the crack propagates beyond the notch plastic zone, the CTPS control the plastic wake.

²Note that the $NPS(x = a)$ is a quantity which is not related to the crack length.

³Note that x_c is confined to the crack-tip plastic zone, i.e., $0 < x_c < \rho_c$.

⁴A plate thickness of 2.5 mm was assumed for the plane-stress cases. Hence, the constraint factor $\alpha = 1$ for the ordinary plane stress conditions was not employed (see Fig. A.2, the values of α_p for plate thickness of 2.5 mm).

⁵The notch plastic zone sizes at load levels $S/\sigma_0 = 0.38, 0.5$, and 0.63 are 0.5, 1.6, 3.2 mm for plane stress and are 0, 0.8, and 1.5 mm for plane strain, respectively. The case of $S/\sigma_0 = 0.38$ under the plane-strain condition produced no notch plastic zone; therefore, no curve is shown for this case.

⁶The values of the ratio $CTPS/NPS$ should be infinite when $a/\rho_n = 1$, but the numerical errors in the FEA have yielded finite values.

4.1.3 Incorporating the NPS into the Strip-Yield Model

Although there is no direct proof that this is a correct procedure, it seems reasonable to linearly superpose the calculated CTPS (from the theory of Dugdale-type crack) and the NPS (from the results of FEA) together to form the total plastic stretches (TPS) in the plastic zone⁷:

$$\text{TPS}(x_c) = \text{NPS}(a+x_c) + \text{CTPS}(x_c) \quad (4.2)$$

Figure 13 shows three cases which are encountered in the strip-yield model for a crack propagating in a notch plastic zone. Figure 13(a) is the case in which the calculated crack-tip plastic zone (ρ_c) is fully embedded in the notch plastic zone (ρ_n). The NPS and the CTPS located behind the crack-tip have become the plastic wake, hence, the "proper" plastic zone size should be $\rho_n - a$. Figure 13(b) shows the case that part of the two plastic zones overlap. Since the boundary of the crack-tip plastic zone is located beyond the notch plastic zone⁸, the proper plastic zone size for this case is ρ_c . Figure 13(c) shows the case when the crack propagates out of the notch plastic zone. In this case, the plastic zone size is ρ_c and the $\text{TPS}(x_c) = \text{CTPS}(x_c)$ because the $\text{NPS}(a+x_c)$ equals zero.

The model incorporating the NPS into the strip-yield model is termed strip-yield model for notched components (SYMNC model). This new model was created to strengthen the weakness of Newman's strip-yield model when it is applied to notched components. This improved model is expected to give more rational results in predicting the crack-closure behavior in a notch plastic zone. The model is also expected to offer an efficient alternative to the elastic-plastic FEA when the crack-closure concept is used for the fatigue design of notched components.

⁷ Note that the NPS shown in Eq. 4.2 is calculated based on the coordinate system located at the notch root and the TPS and the CTPS are based on the moving crack-tip coordinate system.

⁸ It is evident that $\text{NPS}(a+x_c) = 0$ when x_c is located out of the notch plastic zone.

4.2 COMPARISON OF PREDICTED RESULTS WITH EXPERIMENTAL DATA

In following sections, the reported experimental data⁹ are compared with the results predicted¹⁰ using the developed SYMNC model. Figure 14 and Table 1 through 3 show the considered notch geometries, material properties and the required information for predictions¹¹. For all the cases studied, the $U(a)$ was calculated starting from an initial crack length of 0.01 mm. All the calculations were performed in HP-UX workstations. The CPU time was 5-25 minutes for an entire $U(a)$ curve excluding the analysis of the NPS.

4.2.1 Sharp, Single-Edge Notch in a BS4360 50B Steel Plate

Shin and Smith [28] measured a series of U values for cracks propagating in various sharp, single-edge notched plates. They tested three materials (BS4360 50B steel, BS1470 S1C aluminum, and AISI 316 stainless steel) and reported that the measured crack closure most favorably explained the anomalous crack growth behavior in BS4360 50B steel. In current study, two single-edge notched specimens made of BS4360 50B steel (see Fig. 14 and Table 1) were chosen to compare the tested and predicted results. Both specimens had notch depth (D) of 35 mm and the notch radii (r) of 0.4 and 1.4 mm, respectively. These notch geometries induced stress concentration factors of 29, and 16.8. Remote stress range of 90 MPa was applied at stress ratio $R = 0.05$. Because large plastic zones were produced around the notch root at such high stress concentration notches, the crack-closure behavior was affected by notch plasticity. A notch-free crack with an initial crack length of 35 mm was also tested. It is obvious that the tested crack closure of this notch-free crack was affected only by the crack-tip plasticity.

⁹Many crack closure experiments gave good correlations between the measured closure quantities and crack growth rate, however, not every experimental result reported in literature shows this favorable conclusion for crack closure. Since using a crack-closure model implicitly assumes that crack closure is the only factor which influences the crack growth in notched components, it is important to note that all the notch fatigue testing cases chosen for comparison are those which good correlation have been reported between measured crack growth rate and measured crack-closure quantities.

¹⁰As stated in Appendix A, the required crack-tip plastic zone sizes and the crack-face displacements in the strip-yield model were based on the formulations of single-edge cracks in this study. Therefore, the calculated $U(a)$ was entirely based on this specific crack geometry. For cases other than cracks emanating from a single-edge notched plate (such as center notched plate or double-edge notched plate), the single-edge crack formulations are only valid for a crack length which is smaller than the transition crack length (l_t). For simplicity, when predicting U values of other types of crack, the single-edge crack formulations were still used for crack length larger than l_t based on an assumption that no large differences occur in the predicted U values for various crack geometry formulations. However, when predicting the crack growth rate using the modified Paris equation (Eq. 2.5), large errors might be introduced if the single-edge crack stress-intensity factor range was still used for other types of cracks. Therefore, for a crack length which is larger than l_t , the stress-intensity factor for any type of crack was estimated using Eq. 2.3 with the proper correction factor $f(a+D)$.

¹¹All the C' and m values in Table 2 were obtained from da/dN versus ΔK_{eff} plots given in the literature.

Since the monotonic strain hardening properties of the BS4360 50B steel were given in Shin and Smith's paper¹², these properties were adopted in FEA for the NPS. The results of FEA based on plane-stress condition gave the notch plastic zone sizes approximately 5.2 mm for both notches. The calculated NPS are shown in Fig. 15(a).

Figure 15(b) shows the measured U values and the predicted results. The test data of radius 1.4 mm notch and those of notch-free crack cluster together and were given by a scatter band. The test data of smaller root radius notch ($r = 0.4$ mm) showed a significant "dip" and merged with the scatter band at a crack length of approximate 8 mm.

Miller et al. [23] estimated the transition crack length l_t as $0.13\sqrt{Dr}$. The transition crack lengths of the two notches using Miller's equation were approximate 0.9 and 0.5 mm for a notch radius of 1.4 and 0.4 mm, respectively. Based on these estimates, cracks (propagating in the notched or notch-free specimens) exhibited the same crack-tip stress-intensity factor for $a > 0.9$ mm. Since the strip-yield model (without considering the NPS) calculates the CTPS based on the stress-intensity factor, the predicted crack-closure level should be the same for all specimens when $a > 0.9$ mm. Hence, though not shown in Fig. 15(b), the predicted $U(a)$ curves of notched plates would be close to the notch-free crack curve when the crack length is larger than 0.9 mm if the NPS are not considered. In Fig. 15(b), it is obvious that the $U(a)$ curves for the notched specimens predicted by the SYMNC model extending the deviations from the predicted notch-free crack curve in a crack length range approximately equals the notch plastic zone size. Despite the fact that the predicted "dip" for the $r = 0.4$ mm notched specimen is not as pronounced as the one observed in the test results, it is apparent that this model successfully predicted a similar crack-closure effect as the observed in the test data for all cases.

The curves for $r = 0.4$ and 1.4 mm exhibited almost the same predicted notch crack-closure behavior due to the fact that the calculated NPS and notch plastic zone sizes were close for these two notches: see Fig. 15(a). Figure 15(c) shows the predicted crack growth rate and the test data. It is apparent that the anomalous crack growth behavior of short crack is predicted by the crack-closure concepts.

4.2.2 Blunt Center Notch in a 1020 Steel Plate

Sehitoglu [29] studied the behavior of cracks emanating from a blunt center notch ($K_t = 4$, see Fig. 14). The material considered was 1020 steel with a flow stress of 325 MPa. Four stress levels ($S_{\max} = 96, 117, 146$, and 166 MPa) tested at $R = -1$ were chosen to compare the predicted crack growth rate with the experimental results.

¹²Strain hardening exponent $n = 0.2$ and strength coefficient $K = 1042$ MPa.

For simplicity, the plane-stress condition was used in the FEA despite the fact that the plate thickness was 5.7 mm. The results showed that no notch plastic zone was developed at notch root for the cases of $S_{\max} = 96$ and 117 MPa. The notch plastic zone sizes were 0.7 and 1.2 mm for the other two stress levels. The calculated NPS is shown in Fig. 16(a).

The predicted $U(a)$ curves are shown in Fig. 16(b). For all load levels, the $U(a)$ curves first decreased and then increased as crack length became longer. It seems that this trend is a notch-plastic-zone-induced dip. However, there are two reasons to reject this proposition: (1) the minimum values of $U(a)$ of all load levels take place beyond the notch plastic zones and (2) if an infinite plate ($W = \infty$) was used in the calculations, the $U(a)$ would stabilize. Since the predicted U curves showed no "dip" induced by notch plastic zone, it seems that the crack closure levels are not affected by notch plastic zone for the cases considered. The reason for this lack of a dip will be discussed in Sec. 6.1. Figure 16(c) shows the predicted anomalous crack growth rate which compared favorably with the test data.

4.2.3 Sharp, Double-Edge Notch in a 1070 Steel Plate

Sehitoglu [29] tested another type of specimens made of 1070 steel. Sharp, double-edge notches ($K_t = 11$, see Fig. 14) were machined in the specimens. Four load levels ($S_{\max} = 172, 207, 276$, and 345 MPa) at $R = -1$ were chosen to compare the predicted crack growth rate with the experimental results.

FEA results show the monotonic notch plastic zone sizes were 0.03, 0.04, 0.13, and 0.22 mm corresponding to the maximum stress levels considered. The calculated NPS are shown in Fig. 17(a).

Again, no notch plastic zone induced dip is shown in the predicted $U(a)$ curves: see Fig. 17(b). Figure 17(c) shows that the predicted crack growth rates were much higher than the experimental data for crack length range $a/D < 0.5$ (or $a < 0.3$ mm). However, for longer crack lengths, the predictions fit the test data well. Because of the inaccurate predictions in the early crack growth stage, the predicted U values at that stage are doubtful. Since the measured U values were not presented in Sehitoglu's paper, these values were recalculated based on the given measured S_{open} for the case of $S_{\max} = 172$ MPa in his paper. The results showed that the measured U values for early crack growth ranged from 0.25 to 0.3. The predicted values ranged from 0.4 to 1 and were much higher than the measured values (see Fig. 17(b)).

Based on the test results of 1020 plates and 1070 plates, Sehitoglu concluded that the anomalous crack growth behavior was observed in blunt notches but increasing crack growth rate with increasing crack length was observed in sharp notches. Apparently, the SYMNC

model predicts the anomalous crack growth behavior for both types of notches. To verify the validity of the strip-yield model for sharp notches, another set of experimental data were compared.

4.2.4 Sharp Center Notch in a JIS SM41B Steel Plate

Tanaka and his coworkers [52] fatigued notched specimens to investigate the threshold stresses of various notches. One of the notches was center notch (see Fig. 14) with a stress concentration factor of 8.48. The material was JIS SM41B steel with a flow stress of 309 MPa. Because determining the notch threshold stresses was the object of this study, low stress levels ($S_{\max} = 40, 45, 55$, and 65 MPa) at stress ratio $R = -1$ were applied. At such stress levels, crack growth rates between 10^{-6} to 10^{-9} mm/cycle, i.e., Stage I crack propagation, were observed. To predict the crack growth rate at Stage I and Stage II, two sets of material constants for modified Paris law ($C' = 2.02 \times 10^{-21}$, 5.37×10^{-9} and $m = 24.8$, 3.2 for Stage I and Stage II, respectively) were used. These constants were obtained from the tested da/dN versus ΔK_{eff} curve of long crack propagation which is given in Ref. 52. The intersection of the two straight lines defined by these two pairs of material constants (in the $\log da/dN$ versus $\log \Delta K_{\text{eff}}$ axes) was used as the transition ΔK_{eff} value above which cracks propagate from Stage I to Stage II, i.e., $\Delta K_{\text{eff,tran}} = 3.7 \text{ MPa}\sqrt{\text{m}}$.

Figure 18 shows the Tanaka's test data and the predicted results of the SYMNC model. Cracks which started from notch root may arrest when the ΔK_{eff} is less than the effective threshold stress-intensity range $\Delta K_{\text{eff,th}}$. The reported value of long crack $\Delta K_{\text{eff,th}}$ was $3.06 \text{ MPa}\sqrt{\text{m}}$. Experimental data in Fig. 18(a) show that ΔK_{eff} decreased as crack length increased and became less than $\Delta K_{\text{eff,th}}$ for the cases of $S_{\max} = 40, 45$, and 55 MPa. Apparently, the model predicts the existence of a non-propagating crack only for the case $S_{\max} = 40$ MPa. The anomalous crack growth behavior was shown both in the test data and in the model predictions: see Fig. 18(b). The predicted crack growth rate compared well with the experimental data despite the fact that the model gave poor predictions for the threshold stresses. Based on the predicted crack growth rate of these cases, it is obvious that the SYMNC model can still be used for sharp notch problems.

4.3 SUMMARY

Analyses of notch plastic stretch (NPS) show that the plastic wake left on crack faces is mainly attributed to notch plasticity when crack length is much smaller than the notch plastic zone size. As cracks become longer, crack-tip plasticity controls crack-closure behavior.

By considering the notch plastic stretches, the strip-yield model is capable of correctly predicting the crack-closure behavior of a small crack in a notch plastic zone. The predictions made using the SYMNC model were verified by experimental data reported in the literature. It appears that the SYMNC model is an efficient and useful tool for calculating the fatigue crack-closure behavior for a crack emanating from a notch.

CHAPTER V: THE PREDICTION OF THE PLASTICITY-INDUCED CRACK CLOSURE IN WELDMENTS USING THE STRIP-YIELD MODEL FOR A NOTCHED COMPONENT (SYMNC)

5.1 STRESS-RELIEVED WELDMENTS

5.1.1 A Special Finite Element Mesh for Determining the Notch Plastic Stretches at Weld Toes

To account for the influence of the weld toe plastic deformations on crack closure, the procedure of the two notched plates used in notch problems can be used to calculate the weld toe NPS. However, unlike a symmetrically notched plate discussed in the previous chapter, the path of a crack which starts from weld toe is not a line of symmetry, i.e., a line on which the finite element boundary condition nodes are located (see Fig. 19, the normal mesh). Hence, the hypothetical crack of the first notched plate cannot be introduced by releasing boundary condition nodes in the weldment FEA.

Modifications have been made in the finite element mesh to make the procedure for the analysis of the NPS applicable to weldments. Figure 19(a) shows a normal finite element mesh around a weld toe. Assume that the hypothetical crack lies on the mesh line denoted as 0. Mesh lines on the right side of the crack line are denoted by ascending numbers and by descending numbers on the opposite side. An elastic-plastic FEA of this mesh can only give plastic strains around the weld toe. To obtain the NPS, a mesh line (0⁺) (see Fig. 19(b), the special mesh) is inserted between line 0 and line 1. One of the ends of line 0⁺ is located at the hypothetical crack tip which is an arbitrarily chosen element node on line 0 and is located beyond the weld toe plastic zone. The other end is located at the nominal line of base plate and has a very small distance from the corresponding end of line 0. Every node on line 0 has a corresponding node on line 0⁺. A series of very slender elements formed by the nodes on line 0 and line 0⁺ are inserted. After being loaded to produce the weld toe plastic zone, the hypothetical crack is introduced by removing these slender elements to produce a pair of crack-face displacements $u_{A0}(a_A, x)$ and $u_{A0^+}(a_A, x)$. The other weldment mesh with no element inserted between line 0 and line 0⁺ is loaded to obtain another pair of crack-face displacements $u_{B0}(a_A, x)$ and $u_{B0^+}(a_A, x)$. Then the differences between $u_{A0}(a_A, x)$ and $u_{B0}(a_A, x)$, and the differences between $u_{A0^+}(a_A, x)$ and $u_{B0^+}(a_A, x)$ are the weld toe NPS.

Crack-closure behavior at a weld toe can be calculated by the strip-yield model with the calculated weld toe NPS. It is important to note that the formulations of the strip-yield model and the current technique for weld toe NPS are based on 2-D through-width cracks.

The use of the 2-D crack to estimate crack closure in weldments is a simplified approach since 3-D surface cracks are commonly observed in weldment fatigue tests.

5.1.2 Comparison of Predicted Results with the Experimental Data of Cruciform

Weldments

Verreman and his coworkers [47,53,54] used strain gages to measure the crack lengths and crack-opening stresses of non-load carrying, automatic welded cruciform joints. Uniform through-width cracks were observed in their tests, therefore, the experimental results can be used to verify the validity of the current 2-D SYMNC model for weldments. Since the residual stresses of the tested specimens were released by heat treatment, residual stress effects on crack propagation were not considered in the predictions.

The base plate was ASTM A36 steel and the geometry of the weld is shown in Fig. 20(a). Table 4 shows the required material properties in the predictions. Four-node quadrilateral elements were used for the FEA of weld toe NPS. The element formed between line 0 and line 0⁺ at the hypothetical crack tip is not a quadrilateral element but is a constant strain triangle element (see Fig. 19(b)). For simplicity, the lack of penetration was not modeled in the meshes. Figure 20(b) shows the meshes around the weld toe which was 50 μm ¹. The line 0 and line 0⁺ are so close (the distance between the top ends of these two lines was 0.1 μm) that they cannot be distinguished in the mesh.

It is apparent that the special mesh is a substitution of the normal mesh for the NPS at weld toe. Since the NPS are related to loading direction plastic strains, the monotonically loaded weld toe plastic strains calculated from the special mesh without removing slender elements were compared with those obtained from the normal mesh to check the validity of the special mesh. The isotropic hardening rule and the von Mises yielding criterion were used in the elastic-plastic FEA. Because the slender elements in the special mesh caused divergent solutions if they behaved elastic-plastically, all the slender elements were assumed to behave elastically. Axial load levels of $S_{\text{max}} = 147$ and 177 MPa were applied. Loading direction plastic strains at the intersections of mesh lines (line -4 to line 2) and the horizontal dash lines (AA', BB', CC') were calculated by interpolation of the plastic strain values at element nodes (see Fig. 19). Line AA' was coincident with the nominal line of base plate. Lines BB' and CC' were 0.05 and 0.1 mm below line AA', respectively. The node strains on line 0 of the normal mesh are presented by the corresponding node strains on line 0 and 0⁺ in the special mesh, therefore, the average of the node plastic strains along line 0 and line 0⁺

¹The weld toe radius was reported to be 50 μm or less. Verreman et al. also performed FEA for the weld toe plastic zone based on both the cyclic and monotonic properties of base plate. They concluded that the crack-closure behavior was strongly affected by the size of the monotonic weld toe plastic zone.

were compared with the corresponding plastic strains along line 0 calculated from the normal mesh.

Figure 21(a) and (b) show the ratios of loading direction plastic strain from the special mesh ($\epsilon_{p,spe}$) to those from the normal mesh ($\epsilon_{p,nor}$) of the two load levels. Almost all of the points where the plastic strains were recorded had ratio values of approximately unity except for a sudden drop along line 0. This result indicates that the presence of the slender elements in the special mesh caused a strain field discontinuity. Although the strain-field disturbance exists, the special mesh can still be used to calculate the plastic stretches at weld toe. This assertion can be explained as follows:

Figure 22 shows that the plastic stretch on a horizontal line crossing the weld toe plastic zone can be obtained by a simple integration. The differences of the plastic stretch obtained by these two meshes can be written as:

$$\Delta NPS(x) = \int_{y_1}^{y_2} (\epsilon_{p,spe}(x,y) - \epsilon_{p,nor}(x,y)) dy \quad (5.1)$$

It is obvious that $\Delta NPS(x)$ depends both on the $\epsilon_{p,spe}(x,y) - \epsilon_{p,nor}(x,y)$ and the small interval (dy) where the two strain values differ. Since the disturbance of strain field in the special mesh only occurs in a small range around line 0 and line 0⁺, it is believed that the NPS calculated from the special mesh will be close to the NPS in the normal mesh.

Figure 23(a) and (b) show the calculated $u_{A0}(a_A, x)$, $u_{B0}(a_A, x)$, $u_{A0^+}(a_A, x)$ and $u_{B0^+}(a_A, x)$. The shaded area between $u_{A0}(a_A, x)$ and $u_{B0}(a_A, x)$, and the area between $u_{A0^+}(a_A, x)$ and $u_{B0^+}(a_A, x)$ are the weld toe NPS on the both sides of the hypothetical crack. It is obvious that the calculated sizes of the two sets of NPS are different². Since the plastic stretches considered in the strip-yield model are symmetric about the crack line, the average of the calculated NPS on two sides of the hypothetical crack was adopted in the model for estimating crack closure in a weld.

Figure 24 shows the predicted $U(a)$ curves of the two stress levels ($S_{max} = 147$ and 177 MPa) at stress ratio $R = 0$. The crack closure caused by the weld toe plastic zone causes the dips in the predictions. Apparently, the experimental data also show these dips. For stress ratio $R = -1$, the $U(a)$ curves of three stress levels ($S_{max} = 118, 137$, and 177 MPa) were

²This difference is due to the weld toe plastic zone which is not symmetric about the hypothetical crack line. Since the weld toe plastic zone is divided into two parts by line 0 and line 0⁺, the calculated NPS on each side of the hypothetical crack is dependent on the magnitude of plastic strains and the size of the divided plastic zones. Because the divided plastic zone sizes depend on the location of the hypothetical crack, the calculated NPS on each side will be different if another mesh line (such as line -1 to -4) is chosen as the crack line. However, the calculated total NPS of the two sides will not change because the weld toe plastic zone size does not change when different mesh lines are chosen as the crack line.

calculated. The predicted results and the measured data are shown in Fig. 25(a). Despite the fact that the weld toe NPS were considered in the calculations, no plastic-zone dip is shown in the predicted $U(a)$ curves. Experimental data for all stress levels decreased first and then slightly increased. These dips are not as significant as those observed in the $R = 0$ cases.

From the experiment data, it is obvious that the dips of $U(a)$ curves are of different types for $R = 0$ and $R = -1$ cases. For the cases of $R = 0$, the U values reach the stable state at crack length $a \approx 0.3$ mm and 0.5 mm for the two considered load levels. These two values are close to the calculated weld toe plastic zone sizes; see Fig. 23 for the extent of the weld toe NPS. For the cases of $R = -1$, it seems that the tested $U(a)$ curves show, though insignificant, larger crack length to reach the stable state. It is worth noting that the applied maximum load levels for $R = -1$ cases are close to those of $R = 0$ cases, hence, the monotonic weld toe plastic zone sizes should be also close to $R = 0$ cases. If the dips of $R = -1$ cases are mainly due to the weld toe plastic zone, the U values should stabilize before cracks propagate to 0.5 mm. Therefore, it seems that the occurrence of the insignificant dip in $R = -1$ cases is not likely entirely due to the weld toe plastic zone. These phenomena have been discussed in the notch cases of previous chapter and will be discussed further in Sec. 6.1. Figure 25(b) shows the predicted and the measured crack growth rate.

5.2 AS-WELDED WELDMENTS

5.2.1 The Development of Strip-Yield Model Including Residual Stress Effects

The fatigue behavior of as-welded weldments reflects residual stress effects. Since the role played by residual stresses is the same as the role of mean stress (which can be explained by the crack closure), the strip-yield model for crack closure is capable of predicting the crack propagation behavior in a residual stress field.

The model for residual stress used in this study is shown in Appendix B. In Sec. 5.2.2 and 5.2.3 this model was used to predict the crack-closure behavior of center cracks in smooth plates containing residual stresses. In Sec. 5.2.4, crack closure in a weld toe plastic zone in a residual stress fields was considered when the $U(a)$ curve of an as-welded T-joint was predicted using the SYMNC model.

5.2.2 Comparison of Predicted Results with the Test Data: Case I

Kang et al. [38] studied crack propagation in a tensile residual stress field and focused on the effects of negative R ratios. The cracks were oriented perpendicular to the weld. Because the initial crack tip (initial crack length $a_i = 8$ mm) was beyond the HAZ, the crack propagation behavior was not affected by the microstructural differences between the base

metal and the HAZ and was only affected by the residual stresses. The specimen, the crack geometries, and the shape of the measured residual stress distribution are shown in Fig. 26. The $K_{res}(a)$ was calculated using the following equation with the residual stress distribution given in their paper:

$$K_{res}(a) = \int_{-a}^a \sigma_{res}(x) \left[\frac{2 \sin \frac{\pi(a+x)}{W}}{W \sin \frac{2\pi a}{W} \sin \frac{\pi(a-x)}{W}} \right]^{1/2} dx \quad (5.2)$$

The base metal was JIS SM50A steel. The thickness of the specimen was 6 mm. The mechanical properties and the constants for the modified Paris equation of this steel are listed in Table 5. The applied stress ratio ranged from $R = 0$ to $R = -\infty$. Because the applied stress levels were not given explicitly in the paper, this information was obtained by converting the given $K_{max} + K_{res}$ versus crack length relationship to the applied stress levels. The results showed that S_{max} was 50, 33.3, 25, and 16.7 MPa for stress ratio $R = 0, -0.5, -1$, and -2 , respectively.

The calculated R' using Eq. 2.8 is shown in Fig. 26(a). Initially, cracks propagate in tensile residual stress region. The values of R' are strongly affected by the residual stress field, and all the values cluster at 0.65 to 0.75 despite the fact that the nominal R values ranged from -2 to 0 . At these high effective stress ratios, little crack closure or even no crack closure should be expected since it is well known that cracks tested at high nominal stress ratios (without residual stresses) exhibit no crack-closure effects. As cracks become longer, the effects of residual stresses decrease and the values of R' approach their nominal R values. Figure 26(b) shows the predicted $U(a)$ curves. Note that the U values are initially unity which correspond to high R' values, that is, i.e., no crack closure occurs. As cracks propagate a distance, the U values start to decrease indicating the occurrence of crack closure. This distance is dependent on the nominal R values. For more negative nominal R values, crack closure takes place at a shorter crack length. Figure 26(c) shows the predicted and observed crack growth rate at various nominal R ratios. The test data cluster when nominal $\Delta K < 13 \text{ MPa}\sqrt{\text{m}}$ indicating that the crack growth rate is independent of the nominal R values. This trend indicates that no crack closure exists, i.e., no crack-tip driving forces reduction occurs at the crack tip. Therefore, all cracks tested at various R values are subjected to the same ΔK_{eff} (which equals the nominal ΔK) and show the same crack growth rate. As the cracks become longer and crack closure takes place, the crack growth rates separate and show the

known effects of stress ratio (R) on da/dN versus ΔK . Apparently, the predicted crack growth rate shows the same trend as the experimental data.

5.2.3 Comparison of Predicted Results with the Test Data: Case II

Glinka [33] tested three types of welded specimens to study crack propagation in various residual stress fields. Figure 27 shows the geometries of those welded specimens. Specimen U was a smooth plate with a center crack. Specimen L and Specimen P were welded plates with center cracks propagating in directions perpendicular and parallel to the weld, respectively. The shape of the residual stress fields along the path of crack propagation are also shown. The measured maximum magnitude of the residual stresses were 200 MPa and 90 MPa, and the tensile residual stress regions extended approximate 20 mm and 40 mm away from the center line of the weld for Specimen L and Specimen P, respectively. Figure 28 shows the calculated $K_{res}(a)$ using Eq. 5.2. It is obvious that the residual stresses of Specimens L and P still cause stress intensity despite the fact that the crack tips are in a compressive residual stress field.

The base plate was 18G2AV steel: see Table 6 for material properties. The thickness of specimens was assumed to be 2.5 mm since the actual value was not given. The applied stress range was 111 MPa at stress ratio $R = 0.35$ and 107 MPa at $R = 0.5$.

Because of the different residual stress fields in Specimens L and P, cracks propagating in these two types of specimens showed different behavior. In Specimen P, cracks propagated in a tensile residual stress field throughout the crack length range considered ($a < 40 \sim 45$ mm). However, cracks in Specimen L propagated in a tensile residual stress field first and then in a compressive field. The experimental results showed that the measured crack growth rate of Specimen L was initially close to those of Specimen P and then merged with test data of Specimen U³: see Fig. 29. Using Forman's equation (Eq. 2.9) for the crack growth rate, Glinka concluded that the test data of Specimen L merged with those of Specimen U because the crack propagated into the compressive residual stress field. However, the tested crack growth rate of the Specimen L started to deviate at $\Delta K \approx 25$ MPa \sqrt{m} which corresponds to a crack length of approximate 15 mm. At this crack length, the crack tip was still in the tensile residual stress field. Furthermore, the $K_{res}(a)$ curves in Fig. 28 show that the cracks in Specimen L experience larger residual stress-intensity when $a = 15$ mm. This finding indicates a larger R' value, i.e., higher mean stress effects, which implies that a higher crack growth rate should be observed in Specimen L. This behavior is

³This phenomenon is similar to the Case I studied in the previous section: the test data cluster for all nominal stress ratios.

not observed in the test data. Therefore, the LEFM approach based on the concept of R' can not explain the observed crack growth rate in Specimen L.

Nelson [34] used the crack-closure concept to explain crack propagation behavior in Specimen L. Without the entire $U(a)$ curve, he assumed that the value of U for cracks propagating in tensile residual stresses was unity, i.e., no crack closure. A stable U value obtained from Newman's calculations was used for cracks propagating in the compressive stress field. For the transition region from tensile stresses to compressive residual stresses, an ambiguous region was postulated because the U values were not available. In a subsequent publication, Keyvanfar and Nelson [55] were able to calculate the crack-closure effects of Specimens L and P with a ligament model. In their results, the ligament model predicted the cracks remained open over the whole range of crack lengths for the case of $R = 0.5$.

The entire $U(a)$ can be predicted using the current strip-yield model. The predicted U values were unity throughout the entire crack length range considered for Specimen P. The model also predicted that the cracks in Specimen L experienced no crack closure ($U(a) = 1$). Since no crack closure was predicted, the da/dN versus ΔK curves⁴ of Specimen P and L coincide: see Fig. 29. However, little crack-closure effect was predicted in Specimen L as the crack propagates deeply into the compressive residual stress field for the case of $R = 0.35$. This crack-closure effect is shown in Fig. 29(a) in which the predicted crack growth rates start to deviate from the predicted curve of Specimen P when $\Delta K \approx 45 \text{ MPa}\sqrt{\text{m}}$.

Since neither crack-closure models are capable of giving good explanations of the crack growth behavior in Specimen L, it seems that crack closure in Specimen L was affected by other factors. Lawrence et al. [30] modeled the mean stress (due to the residual stress) relaxation resulting from plastic deformation at weld toe. Pang and Pukas [56] used a hole drilling strain gage method to measure the residual stresses in a cruciform welded joint. Pang [57] concluded that the residual stresses "shake down" when $S_{\text{max}}/S_y > 0.25$. In Glinka's tests, S_{max}/S_y was 0.24 and 0.30 for $R = 0.35$ and 0.5, respectively. According to Pang's conclusions, these applied stresses are the stress levels at which the residual stresses begin to relax. In Fig. 28, it is apparent that Specimen L experienced larger residual stress-intensity when $a < 22 \text{ mm}$. Therefore, despite the fact that the two types of specimens are subjected to the same nominal stress-intensity factor, cracks in Specimen L experienced more serious plastic deformations at its crack tip. This result indicates that the residual stresses in Specimen L are more likely to relax. Hence, the actual $K_{\text{res}}(a)$ of Specimen L might gradually decrease due to stress relaxation and finally becomes zero. Stress relaxation must

⁴With the tested da/dN versus ΔK relationship of Specimen P at $R = 0.5$ as a base line, the values of C' and m were calculated. This operation is based on the facts that little crack closure takes place at such high R ratios and that the da/dN versus ΔK is similar to the da/dN versus ΔK_{eff} .

cause the crack growth rate to approach that of Specimen U much earlier than the crack-closure model predicts. This argument can also explain a phenomenon exhibited by the measured crack growth rate of Specimen L tested at the two different stress ratios. It seems that in Fig. 29 the crack growth rate approaches Specimen U faster in the case of $R = 0.5$. This phenomenon might be explained by the fact that the value of S_{\max}/S_y for $R = 0.5$ is larger than that of $R = 0.35$. Thus, larger crack-tip plastic deformation is expected for $R = 0.5$, that is, faster residual stress relaxation.

To incorporate residual stress relaxation in the strip-yield model requires a detailed understanding that how the residual stresses relax under the crack tip-plastic deformation. Unfortunately, to author's knowledge, it seems that information is scarce.

5.2.4 Comparison of Predicted Results with the Test Data of an As-Welded T-Joint

Unlike a well-defined notch, the measurement of crack closure in a welded joint is much more difficult because the locations where surface cracks start are unknown. Furthermore, some accurate techniques for crack closure measurement, such as crack-tip strain gauge and crack-tip clip gauge, are not applicable to welded joints.

It has been shown in previous sections that crack closure in a weld is affected by both the weld toe plastic zone and the residual stresses. The numerical techniques to solve these weld toe plastic zone and residual stress problems have been developed separately and will be combined to predict crack closure in an as-welded joint. Note that the developed strip-yield model is not capable of predicting the crack closure of a surface crack. Therefore, the predicted through-width crack closure is assumed to be the same as that of a surface crack of same crack depth.

Otegui, Mohaupt and Burns [58] placed ten strain gauges close to the weld toe of a welded T-joint to detect crack initiation and early crack growth. These strain gauges were also used to measure the crack closure. The geometry of the T-joint is shown in Fig. 30. The average flank angle and weld toe radius were reported to be 40° and 0.5 mm. The mechanical properties of base plate are listed in Table 7 and were used in the predictions. The applied bending stress range was 305 MPa at stress ratio $R = 0.1$.

Because the residual stress distribution is complex in a weld, a simple shape of the residual stress along the base plate thickness direction was assumed:

$$\sigma_{\text{res}}(x) = S_y \cos\left(\frac{2\pi x}{t}\right) \quad (5.3)$$

Although tensile residual stress as large as the yield strength of the base plate was assumed as the worst case for weldments, Otegui et al. stated that the maximum tensile residual stress at weld toe should range from one third to one half of the base metal yield strength. Therefore, 42% of S_y was used in Eq. 5.3 instead of S_y .

FEA results showed that the weld toe monotonic plastic zone size was approximate 0.45 mm.

Both crack closure with and without residual stress were calculated. Figure 30 shows that no crack closure was predicted when the residual stresses were considered. The "big dip" of the results in the absence of residual stresses was due to the large crack length compared with the plate thickness⁵. The scatter in the measured data shows the nature of the difficulties in measuring the crack closure in a weld. It is obvious that most of the measured crack closure data were bounded by the two predicted curves.

5.3 SUMMARY

A special finite element mesh was used to calculate the NPS around a weld toe. The calculated weld toe NPS were incorporated into the strip-yield model for the crack-closure behavior in a stress-relieved cruciform weldment. The predicted crack closure results show the model accurately captures the crack-closure phenomenon and compared favorably with the experimental data.

The predicted results of strip-yield model show that the tensile residual stresses in a weld increase the effective stress ratio R' and eliminate crack closure. The relaxation of residual stresses due to the crack-tip plasticity may be significant but is not considered in this study.

Most of the measured crack-closure levels of a T-joint are bounded by the predicted results of the SYMNC model for the case of: (1) no residual stress, and (2) $U(a) = 1$.

⁵This is the same situation as for the predicted $U(a)$ curves in Sec. 4.2.2.

CHAPTER VI: DISCUSSION

6.1 EFFECTS OF STRESS RATIO R ON CRACK CLOSURE IN THE VICINITY OF A NOTCH

For some notched specimens studied in Chapter IV and the stress-relieved cruciform weldment mentioned in Chapter V, it was seen that the experimentally observed crack-closure "dip" in a notch or a weld toe plastic zone was not predicted by the SYMNC model for $R = -1$ (see Fig. 16(b) and Fig. 25(a)). Studies were made to understand the reason for this unexpected result, and the findings are discussed below.

As detailed in Chapter III, the strip-yield model predicts the crack-closure effects from the contact stresses along the crack faces at minimum load of a loading cycle. The cruciform weld studied in Sec. 5.1.2 was used to compare the contact stresses calculated from the model with and without the NPS incorporated. Figure 31 shows the contact stress distributions¹ on crack faces at minimum stress for the case of $R = 0$. The magnitude of contact stresses near the crack tip are approximately the same for both cases. This fact indicates that the addition of the NPS to the CTPS causes no significant change in the stress state near the crack tip. However, the contact stresses at a distance away from the crack tip are higher for the case with the NPS incorporated. This increase is a result of the fact that the addition of the NPS to the CTPS produces a larger size of plastic wake. Since larger contact stresses result, the calculated $U(a)$ curve in Fig. 24 shows the value of U at that crack length is 0.68. Recalculation of the $U(a)$ curve without the NPS incorporated shows the value of U is 0.77 at that crack length. Since the value of U is smaller when the NPS is incorporated, the "dip" appears in the predicted $U(a)$ curve.

For the case of $R = -1$, the calculated results of both the strip-yield model and the SYMNC model show that the plastic wake always yields at minimum load. Because elastic-perfectly plastic material properties are assumed, the contact stress distributions calculated by both models are the same, i.e., $\sigma_{c,wNPS}(x) = \sigma_{c,w/oNPS}(x) = -\sigma_0$. Therefore, the calculated $U(a)$ curve of the strip-yield model curves are not influenced by incorporating the NPS in the calculations, and hence, the "dip" of $U(a)$ predicted for $R = 0$ cases is not observed for the $R = -1$ case.

The above discussion leads to the conclusion that the notch plastic deformations should not increase crack-closure effects for $R = -1$ or more negative values. Many researchers measured the U values for cracks emanating from notches. Those measured U values show significant "dip" are always those tests performed at $R \geq 0$ [28,53,59]. There are

¹These results correspond to the case of $S_{max} = 147$ MPa and a crack length of 0.15 mm (entirely embedded in the monotonic weld toe plastic zone).

also measured data that showed no "dip". When one checks the loading conditions of these experiments, it is not surprising that the applied stress ratios are always $R = -1$ or more negative values [46,53,64].

Obviously, the effects of load ratio on the crack-closure behavior in notch plastic zones are similar to the crack-growth retardation caused by a tensile single overload. Most research work on the overload effects was performed for an overload followed by $R = 0$ constant amplitude loadings. This condition is similar to the discussed notch components subjected to $R = 0$ loadings and the "dip" of $U(a)$ curves is related. However, when the tensile single overload is followed by constant amplitude loads with $R \leq -1$, no larger crack-closure effect is expected to be caused by the overload crack-tip plastic zone. Hence, crack growth retardation effects should be insignificant for this condition. This observation may explain the experimental results of Stephens et al. [60] which showed negative stress ratios reduce crack retardation effects.

6.2 GENERAL DISCUSSION OF THE SYMNC MODEL FOR FATIGUE LIFE PREDICTIONS

It is well known that using of the LEFM approach may overestimate the crack propagation life of notched components since the anomalous crack growth behavior at notches cannot be explained by LEFM. Crack-closure concepts explain the anomalous crack growth behavior, and hence, using the SYMNC model with the modified Paris law may give more rational fatigue life predictions for notched components and welded joints.

There are two main steps in using the SYMNC model for fatigue life predictions:

- Find the NPS using the elastic-plastic FEA procedure proposed in Sec. 4.1.1.
- Determine crack-closure load using the strip-yield model and determine the values of NPS using the procedure proposed in Sec. 4.1.4.

Thereafter, the calculated $U(a)$ curves can be used to predict the crack growth rate using the modified Paris equation.

The required information for the SYMNC model includes:

- Notch and plate geometries: notch depth (D), notch radius (r), plate width (W) and plate thickness (t).
- Material properties: "flow stress" (the average of the yield and ultimate strengths - σ_0), Young's modulus (E), modified Paris equation constants (C' , m).
- Loading conditions: applied maximum and minimum stresses (S_{\max} , S_{\min}).

As discussed in the previous section, the NPS have no effect on the predicted $U(a)$ curves for $R = -1$ cases. This observation indicates that it is unnecessary to perform the NPS analyses for the cases of $R = -1$ or more negative values. For $R = 0$ cases, the NPS are not important at the threshold stress range since the notch plastic zone is insignificant. At high stress levels or high stress concentration notches in which the notch plastic zone effects are significant, the estimated U values with the NPS considered may range from 75% to 100% of the estimated U values without considering the NPS². Assuming that $m = 3$ for the modified Paris law and assuming that the U values considering the NPS are always 75% of the U values without the NPS, the ratio of the estimated crack propagation lives is:

$$N_{F,wNPS} / N_{F,w/oNPS} \approx 1/(0.75)^3 \approx 2.37 \quad (6.1)$$

This number is an overestimate because the ratio of the U values should be larger than or equal to 0.75 for any crack length. Hence, the effect of including the NPS or the ratio of $N_{F,wNPS} / N_{F,w/oNPS}$ should be 2 or less.

Since determining the NPS is quite difficult and involves an elastic-plastic FEA, this step for the SYMNC is unnecessary if the inaccuracy resulting from ignoring the NPS is tolerable. However, it is worth noting that when a notched component is subjected to variable amplitude load, the need for an analysis of NPS is inevitable because an overload may induce a huge notch plastic deformation which will significantly affect the crack-closure behavior, and hence, the fatigue life.

It should also be noted that the SYMNC model considers PICC only. At the threshold stress level, OICC and RICC become more important and should be considered. Therefore, care must be exercised when the model is used near the threshold stress level.

Since crack closure alone cannot entirely explain the microstructurally small crack propagation, the initial crack length used in the integration of modified Paris law is still controversial and arbitrary. In this study, as will be seen, the crack length used was 0.1 mm which corresponds the size of one to several grains. Smaller initial crack lengths are not recommended for estimating fatigue life since the application of fracture mechanics to microstructurally small cracks is probably inappropriate.

²Estimated from the results of the cases studied in Sec. 4.2.1 and Sec. 5.1.2.

6.3 COMPARISON OF VARIOUS MODEL PREDICTIONS FOR WELDMENT FATIGUE LIFE

6.3.1 Crack Propagation Life:

Many efforts have been made in last twenty years to apply the LEFM approach to estimate the N_{P2} of weldments, or to estimate N_T if the crack initiation stage is neglected. The straight-front crack is always assumed for calculations of stress-intensity factors in this approach: see Fig. 32(a). Since multiple crack initiation and coalescence of surface semi-elliptical cracks (see Fig. 32(b)) are commonly observed in the fatigue of shielded metal arc weldments, many researchers have measured the crack-shape development in weldments by the ink-staining technique. Bell and Vosikovsky [61] gave an empirical forcing function to account for the crack-shape development:

$$a/c = e^{-ka} \quad (6.2)$$

where a/c is the aspect ratio (the ratio of minor axis length to the major axis length) of the semi-elliptical crack and $k = 2.09 \times 10^{-6} (K_{IS_{max}})^{1.95}$. The stress-intensity factor at the deepest point of a semi-elliptical crack can be calculated by the weight function procedure proposed by Niu and Glinka [62]. Two models based on the LEFM approach are used in the comparison of model predictions:

- | | | |
|---------|---|-------------------------------------|
| Model A | - | LEFM, straight-front crack assumed. |
| Model B | - | LEFM, with crack-shape development. |

When one applies the crack-closure concept to the fatigue life prediction of weldments, residual stresses must be considered. Figure 33 shows the residual stress distributions parallel and transverse to a weld. It is obvious that if a crack is initiated at weld toe close to the center of the plate (location A), the crack is fully embedded in a tensile residual stress field. As discussed in the Chapter V, the tensile residual stresses easily open the crack, hence, crack closure is unlikely to develop under this condition. Of course, residual stress relaxation could decrease these tensile residual stress and create an environment for the occurrence of crack closure. As the crack propagates into a compressive residual stress field, crack closure is certain. If the crack starts from a location close to the edge of the plate, i.e., location B, which is in the compressive stress field of the residual stress distribution parallel to the weld, the compressive residual stresses reduce the nominal R values and will induce crack closure in the early stage of crack propagation. These observations suggest that crack closure in an as-welded weldment is a complex phenomenon

because the crack initiation sites are unknown and the residual stress distributions are uncertain. To simplify the uncertain effects of residual stresses, two crack propagation models based on the crack-closure concept are used to bound the possible values of N_{P2} :

- | | | |
|---------|---|---|
| Model C | - | Crack-closure model, crack-shape development, $U(a) = 1$ assumed. |
| Model D | - | Crack-closure model, crack-shape development, $\sigma_{res} = 0$ assumed. |

For the crack propagation life predictions, the weld toe radius used in stress-intensity factor calculations is important when the weight function method is applied because the localized unflawed stress state around weld toe is affected by the weld toe radius. In this study, the reported average value of measured weld toe radius (0.5 mm [58]) was used for the weld-toe, crack-free stress distribution and the stress-intensity factor calculations.

Bell et al. [61] performed a series of three-point bending tests on various base plate thickness of T-joints. The tested results of base plate thickness $t = 16$ and 78 mm specimens were chosen for comparison with the model predictions. Using of the strain gage technique, they claimed that cracks of 0.5 mm depth were detected. The fatigue life from this crack size to the final failure and the total fatigue life were both recorded.

An initial crack depth of 0.5 mm was used in Model A to D to estimate N_{P2} of these specimens. Material properties for crack-closure calculations and constants for Paris equation are listed in Table 8. Figure 34(a) and (b) show the predicted³ and experimental results of N_{P2} .

Yagi et al. [63] also tested T-joints and cruciform welded joints to study weldment thickness effects. They measured the crack propagation life from crack size of 1~2 mm to final failure. The S_y and S_u of the base plate are close to the values listed in Table 8. Model predictions for the N_{P2} of T-joints were made for the specimens with base plate thickness of 22 mm. The initial crack length used for N_{P2} predictions was 1.5 mm. Figure 34(c) shows the predicted and experimental results.

In comparing the predicted S-N curves with the observed data, it is evident that Model A predictions are conservative for all three plate thicknesses. Model B in which the crack-shape development is considered still predicts smaller N_{P2} than the observed results. However, it should be noted that using this model and stress-intensity factors calculated

³It should be noted that C and C' listed in Table 8 should be dependent ($C'=C/U^m$). Since these values were obtained from different studies, the listed numbers are not related. This difference causes the predicted lives using the crack-closure concepts to be higher than those obtained by LEFM, which is contradictory to the expected results that the LEFM overestimates the crack propagation life.

using the finite element technique, Bell et al. [61] obtained predictions that agreed well with the test data: see Fig. 34(d). Most experimental data are bounded by the predicted S-N curves of Model C and D except the cases of $t = 22$ mm.

6.3.2 Total Fatigue Life:

Four crack propagation models and the I-P model were used to estimate N_T of the T-joints discussed in the previous section:

Model A'	-	LEFM, straight-front crack and $a_i = 0.1$ mm assumed.
Model B'	-	LEFM, crack-shape development and $a_i = 0.1$ mm assumed.
Model C'	-	Crack-closure model, crack-shape development, $\sigma_{res} = 0$, linear modified Paris law and $a_i = 0.1$ mm assumed.
Model D'	-	Crack-closure model, crack-shape development, $\sigma_{res} = 0$, bilinear modified Paris law, and $a_i = 0.1$ mm assumed.
Model E	-	I-P model, with crack closure, crack-shape development considered for N_{P2} and $a_i = 0.25$ mm assumed.

Because of the bilinear modified Paris law assumed in model D', an additional set of material constants⁴ for the modified Paris equation are listed in Table 8 to account for the Stage I crack propagation. The required material properties for estimating N_I using the I-P model are also listed in Table 8.

Figures 35(a) to (c) show the model predictions and the observed data obtained from Bell et al. and Yagi et al.. Again, Model A' predicts much lower fatigue strengths than the tested data. Model C' to E predicts more favorable results except that they are slightly higher at $10^6 \sim 10^7$ cycles. The results of Model D' deviate from those of Model C' in the long-life regime. This deviation is due to the bilinear modified Paris law employed in Model D'. These deviations increase with decreasing base plate thickness. Model E predicts a same trend as Model D', that is, the slope of the predicted S-N curves becomes less in long-life regime. However, if one doesn't assume a bilinear modified Paris law, Model C' predicts no slope change in the long-life regime. The issue on the change of the slope of S-N curves is very important for predictions at lives larger than 10^7 cycles.

⁴These data are scarce in literature. The values used were obtained from the test data of Verreman et al. [53] for ASTM A36 steel weldments.

6.4 THE IMPORTANCE OF CRACK INITIATION IN WELDMENTS

Improvements of crack length measurement technique have made the measurement of smaller crack lengths in weldments possible. This possibility has stimulated the study of fatigue crack initiation in welded joints. However, even with the current technology, it is difficult to monitor early crack growth in weldments. In Bell's tests, many strain gages were placed close to the weld toe region, and yet the smallest detectable crack size was 0.5 mm. In Yagi's tests, fewer strain gages were used. Yagi defined the end of crack initiation as a 5% drop of strain gage readings, which corresponds to the existence of a crack with size of 1~2 mm. This information, while still too vague for understanding crack initiation, may provide a means of checking the validity of the crack initiation life predictions.

Model C' and Model D' were used to estimate N_I and N_T for this study. The total fatigue life is the calculated crack propagation life from $a_i = 0.1$ mm to $a_f = t/2$, i.e., $N_T = N_F(0.1-t/2)$. Thereafter, $N_I = N_F(0.1-0.5)$ for Bell's cases and $N_I = N_F(0.1-1.5)$ for Yagi's cases, respectively. The I-P model, i.e., Model E, for which N_I is calculated using the Basquin-Morrow equation was also used to estimate the value⁵ of N_I/N_T .

The results of the model predictions on the N_I/N_T for the Bell's tests ($t = 16$ mm) are shown in Fig. 36(a). Model C' predicts an increasing then a decreasing trend as N_T increases. The results of Model D' are close to those of Model C' when the total fatigue life is less than 9×10^5 cycles. For longer fatigue lives, the results of Model D' increase as N_T increases. This increase is due to large portion of Stage I crack propagation being involved in the crack initiation stage. Model E predicts an increasing trend of N_I/N_T as N_T increases which is consistent with the results of Model D' in long-life regime.

The value of N_I/N_T from Bell's test data show that the value of the ratio N_I/N_T is not dependent on the observed total fatigue life. Their values of the ratio ranged from 10% to 40% and the average was 26.6%: see Fig. 36(b) and (c). The calculated values of N_I/N_T from Yagi's test data also showed that no strong relationship exists between the values of the ratio and the total fatigue life. These results are shown in Fig. 36(d).

Figure 36(b) to (d) show the predictions of Model C', E and the test data. Neither of the two different trends shown by Model C' and E are exhibited by the test data. The predicted N_I and N_T based on Model A' (straight-front crack assumed) considering crack closure was also calculated in Yagi's case. The calculated results of N_I/N_T show no

⁵Note that N_I calculated by the I-P model is defined as the existence of a crack with a size of 0.25 mm. To make the definition of the crack initiation consistent with those experimental conditions, the calculated N_{P2} from crack length 0.25 mm to 0.5 mm, and 0.25 mm to 1.5 mm were added to the calculated N_I for the Bell's cases and the Yagi's cases, respectively.

dependence on N_T : see Fig. 36(d). Therefore, the increasing and decreasing trend of N_I/N_T predicted by Model C' was entirely due to crack-shape development.

From the discussion above, it is apparent that a definitive prediction for the value of N_I/N_T is still not possible using the current models. However, both observed data and the predictions showed that the crack initiation of weldments is important and should be considered when estimating the total fatigue life.

CHAPTER VII: CONCLUSIONS AND PROPOSED FUTURE WORK

7.1 CONCLUSIONS

1. Analyses of notch and crack-tip plastic stretches showed that notch plasticity is the main source of the plastic wake when the crack length is small compared with the notch plastic zone. As the crack length increases, crack-tip plasticity increasingly contributes to the plastic wake. A model termed strip-yield model for notched components (SYMNC) was developed to consider the effects of notch plastic deformations on the crack-closure behavior at the vicinity of a notch.
2. A special finite element mesh was developed in this study which can be used to estimate the plastic stretches around an asymmetrical notch such as a weld toe. Using these calculated weld toe plastic stretches, the SYMNC model offers a simple and efficient numerical approach for calculating crack-closure in weldments.
3. The residual stress effects on crack propagation can be explained using the SYMNC model. The weld tensile residual stresses were found to increase the mean stress effect, and hence, reduce the crack-closure levels. The crack-closure behavior of an as-welded joint is complicated by the fact that the crack initiation sites are unknown and the residual stress distributions are uncertain. However, most of the measured U values of an as-welded weldments were bounded by the predicted results of the SYMNC model considering: (1) no residual stress, and (2) $U(a) = 1$.

7.2 PROPOSED FUTURE WORK

1. Because the SYMNC model considers both the notch plasticity and the crack-tip plasticity, this model should be capable of capturing the interaction of a notch plastic zone and a crack-tip plastic zone, and hence, the SYMNC model could be extended to simulate the crack-closure behavior under variable amplitude loads.
2. The importance of OICC and RICC increase when the applied stresses are close to the threshold stress. A thin film of material can be added to the depth of the plastic wake to simulate these two crack-closure mechanisms and, hence, to include environmental and other near-threshold effects in the SYMNC model.

3. As a crack propagates in a residual stress field, residual stress relaxation may occur. Neglecting the residual stress relaxation may overestimate the crack growth rate, and hence, underestimate the crack propagation life. Therefore, understanding how residual stresses relax near a crack tip would allow the effects of residual stresses to be more accurately simulated.

TABLES

Table 1 Notch and plate geometries, all units are in mm.

	Notch depth, D	Notch radius, r	Plate width, W	Plate thickness, t	K_t
Sharp, single-edge notch [28]	35	0.4	140	2	29
	35	1.4	140	2	16.8
Blunt center notch [29]	3.81	1.90	51	5.7	4
					43
Sharp, double-edge notch [29]	0.6	0.025	15.88	2.5	11
Sharp center notch [49]	3	0.16	45	2.5*	8.48

* Not reported in the literature, the value was assumed and was used in the predictions.

Table 2 Material properties for the notched plates considered.

	Material	Flow stress, σ_0 (MPa)	C^*	m
Sharp, single-edge notch [28]	BS4360 50B steel	436	3.88×10^{-8}	2.6
Blunt center notch [29]	1020 steel	325	8.03×10^{-9}	3.2
Sharp, double-edge notch [29]	1070 steel	715	9.86×10^{-10}	4.6
Sharp center notch [49]	JIS SM41B steel	309	$2.02 \times 10^{-21**}$ 5.37×10^{-9}	24.8** 3.2

* The values listed give the unit of da/dN in mm/cycle.

** Stage I crack propagation constants.

Table 3 The correction factors for cracks emanating from various type of notched plates.

Correction factor $f(a+D)$	
Sharp, single-edge notch [28]	$1.12 - 0.231\left(\frac{a+D}{W}\right) + 10.55\left(\frac{a+D}{W}\right)^2 - 21.72\left(\frac{a+D}{W}\right)^3 + 30.39\left(\frac{a+D}{W}\right)^4$
Blunt center notch [29]	$\sqrt{\sec\left(\frac{\pi(a+D)}{W}\right)}$
Sharp, double-edge notch [29]	$1.12 + 0.406\left(\frac{a+D}{W}\right) - 4.788\left(\frac{a+D}{W}\right)^2 + 15.44\left(\frac{a+D}{W}\right)^3$
Sharp center notch [49]	$\sqrt{\sec\left(\frac{\pi(a+D)}{W}\right)}$

Table 4 Material properties of ASTM A36 steel [53].

Yield strength, S_y (MPa)	224
Ultimate strength, S_u (MPa)	414
C'	$8.20 \times 10^{-11}^*$
m	4.56

* The values listed give the unit of da/dN in mm/cycle.

Table 5 Material properties of JIS SM 50A steel [38].

Yield strength, S_y (MPa)	330
Ultimate strength, S_u (MPa)	510
C'	$1.0 \times 10^{-8}^*$
m	3

* The values listed give the unit of da/dN in mm/cycle.

Table 6 Material properties of 18G2AV steel [33].

Yield strength, S_y (MPa)	625
Ultimate strength, S_u (MPa)	784
C'	1.34×10^{-11}
m	4.29

* The values listed give the unit of da/dN in mm/cycle.

Table 7 Material properties of the base plate of the as-welded T-joint [58].

Yield strength, S_y (MPa)	421
Ultimate strength, S_u (MPa)	509

Table 8 The material properties for fatigue life prediction of the T-joints [61].

Yield strength, S_y (MPa)	421
Ultimate strength, S_u (MPa)	509
C^*, m (for LEFM)	$5.36 \times 10^{-9}, 3.2$
$C' *$	1.5×10^{-9} [58]
	$6.1 \times 10^{-12} **$ [53]
m	3.2 [58]
	$6.3 **$ [53]
$\sigma_f' = 1.5S_u + 345$ (MPa) [65]	1109
$b = -\frac{1}{6} \log 2(1 + \frac{345}{1.5S_u})$ [65]	-0.077

* All the C' values listed give the unit of da/dN in mm/cycle.

** Constants for the Stage I crack propagation.

FIGURES

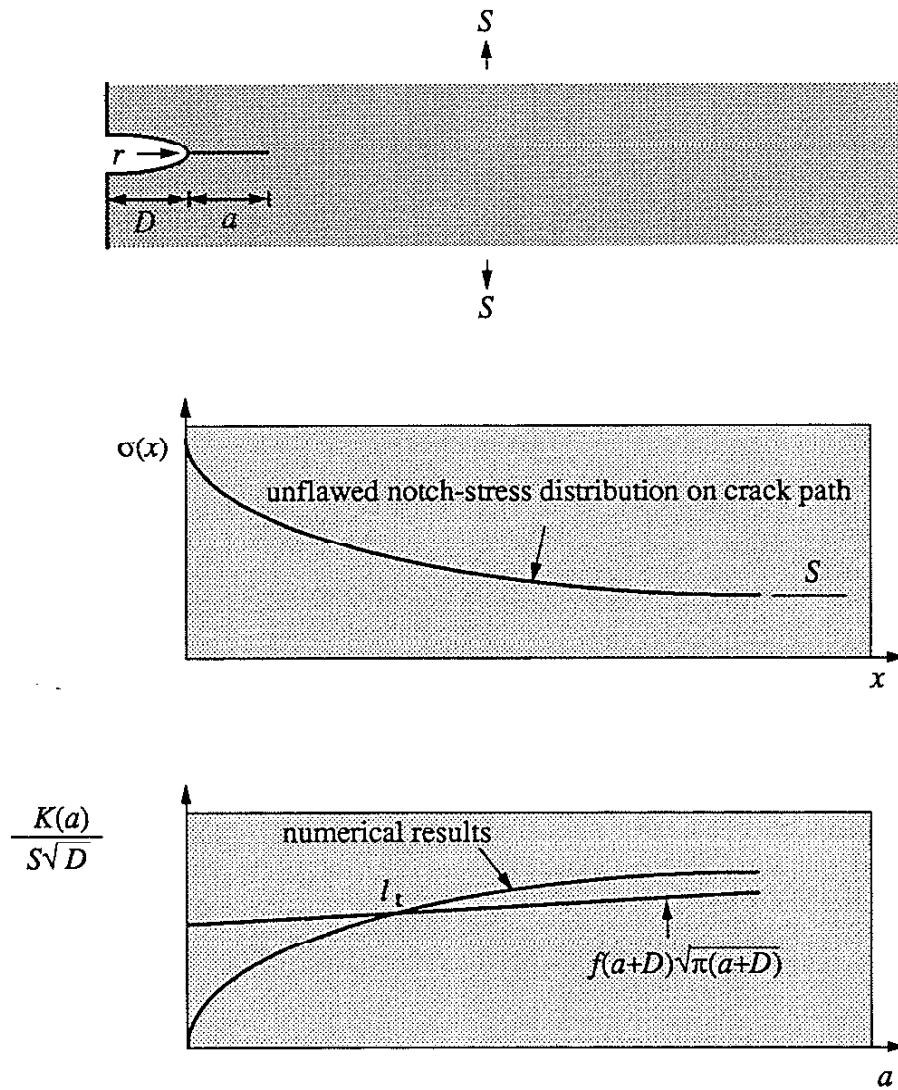


Fig. 1 The unflawed notch-stress distribution and the transition of notch stress-intensity factor to the remote stress-intensity factor.

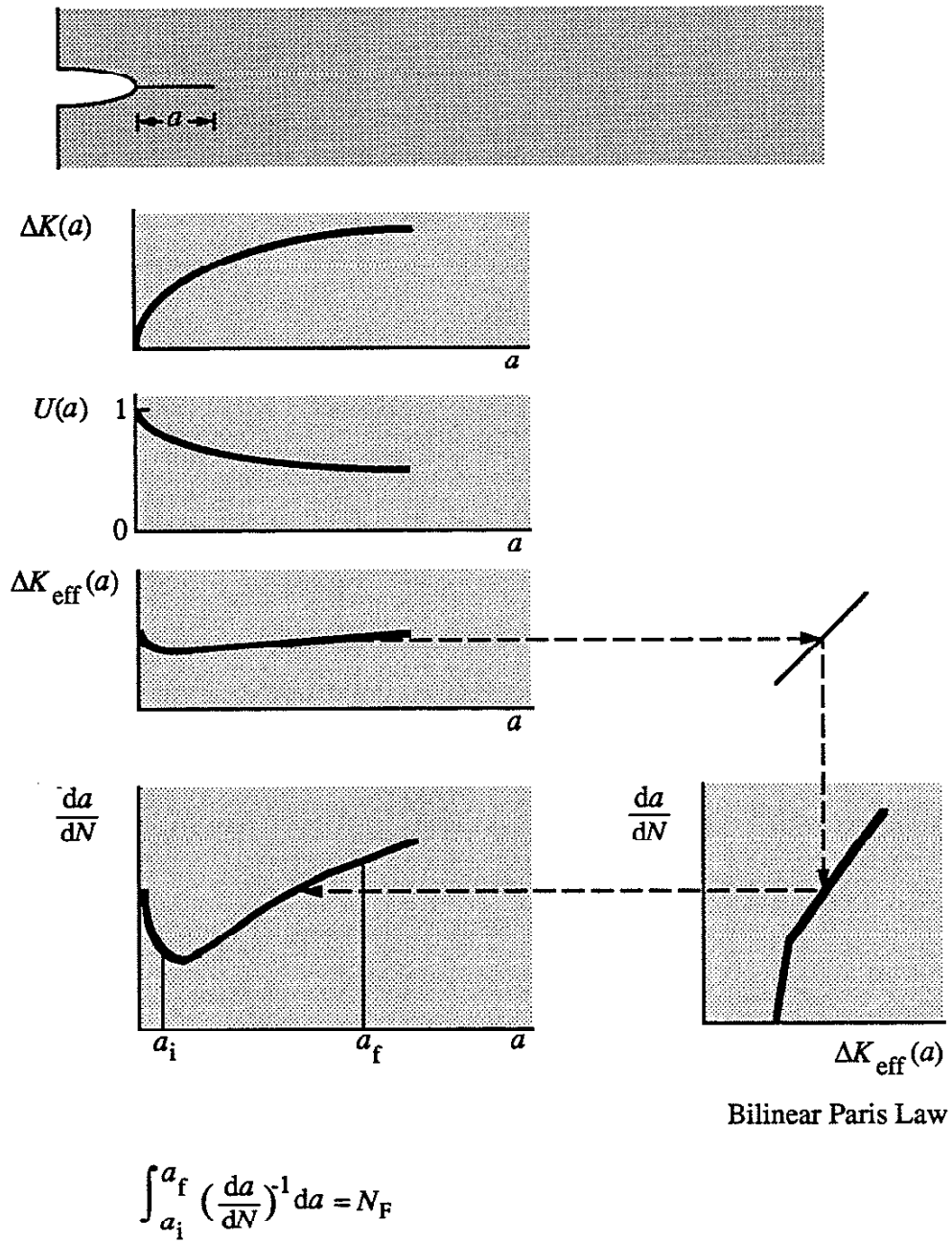


Fig. 2 An illustration of the CCN model .

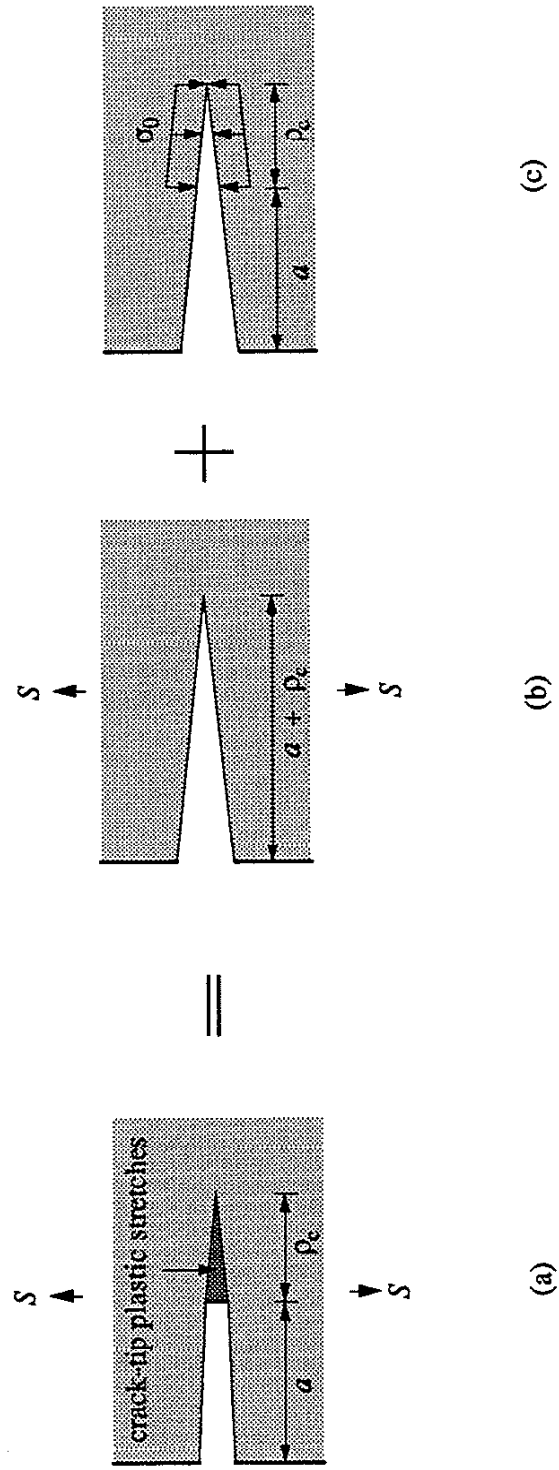


Fig. 3 (a) A Dugdale-type crack is equivalent to the superposition of (b) a fictitious crack of length $a + \rho_c$ subjected to remote load S and (c) a fictitious crack of length $a + \rho_c$ loaded from a to $a + \rho_c$ with flow stress σ_0 .

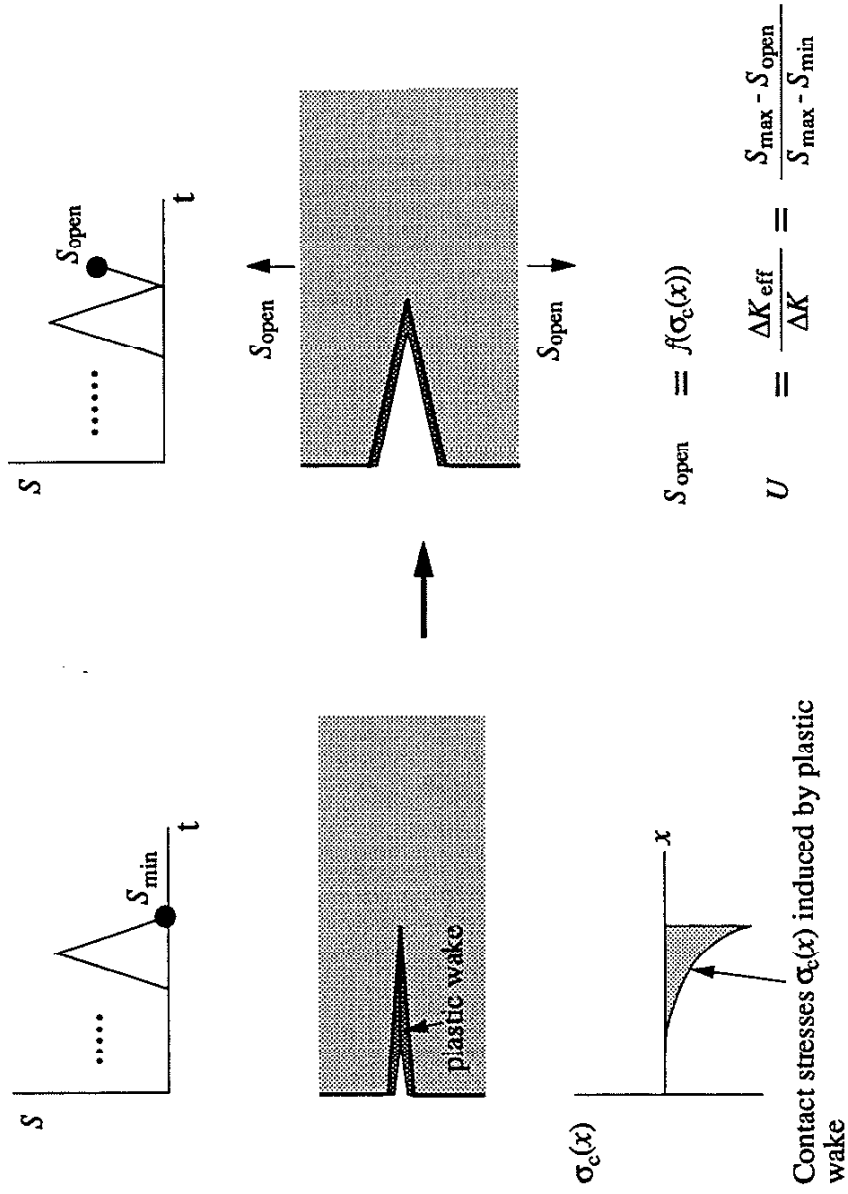
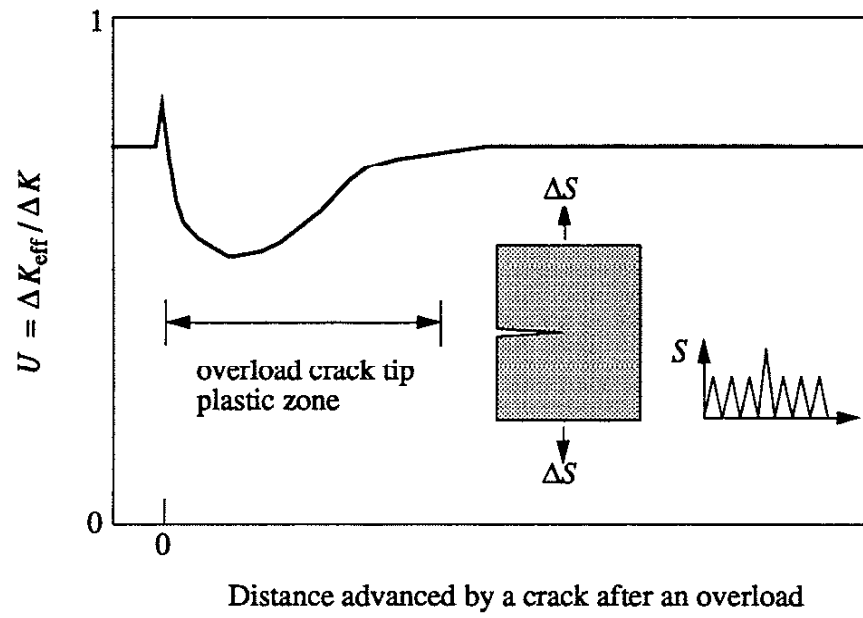
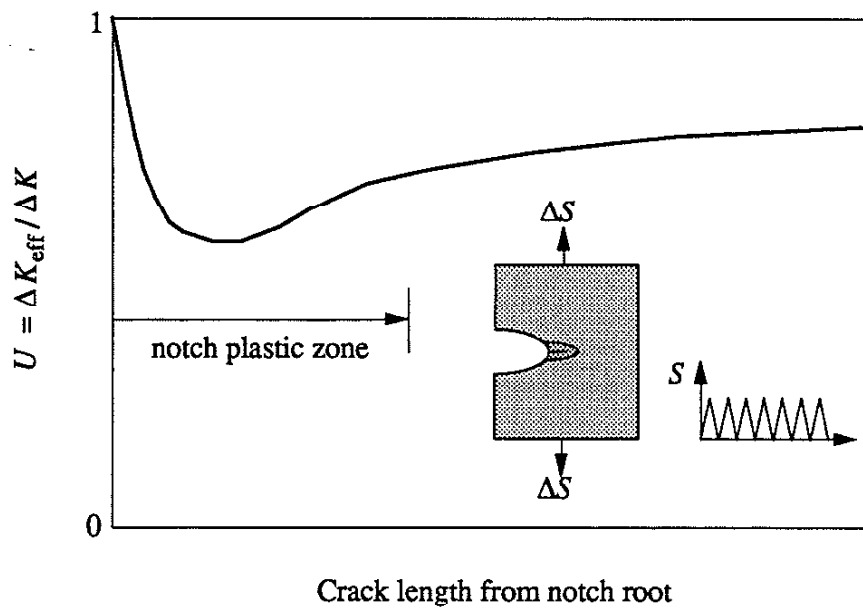


Fig. 4 An illustration of the modified Dugdale strip-yield model for crack closure.



(a)



(b)

Fig. 5 Crack-closure behavior: (a) after an overload (b) of a crack emanating from a notch.

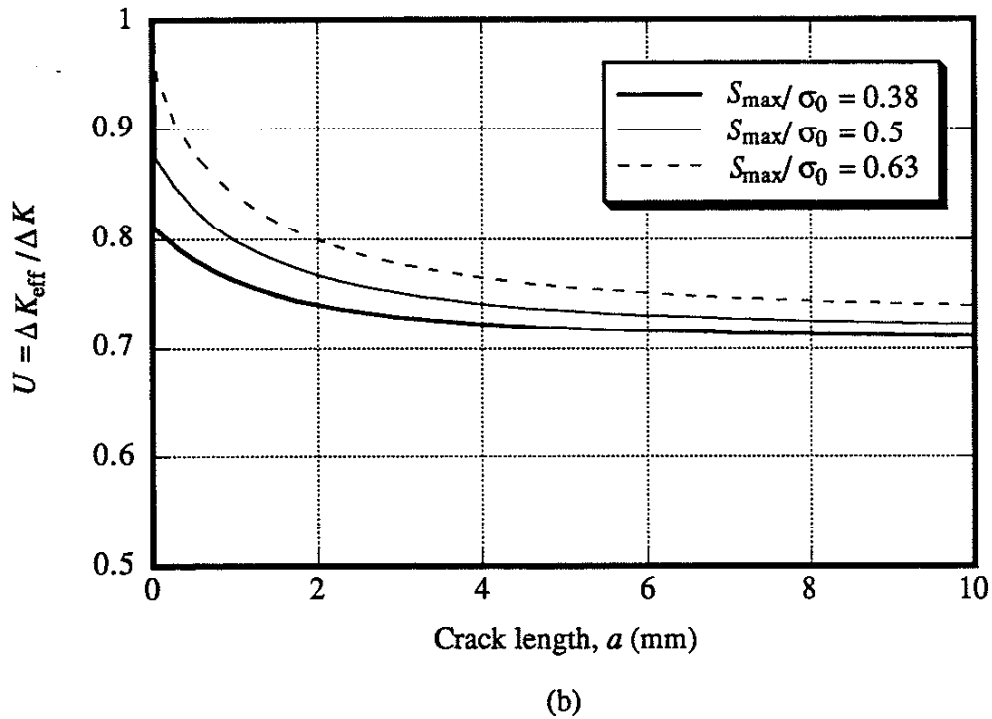
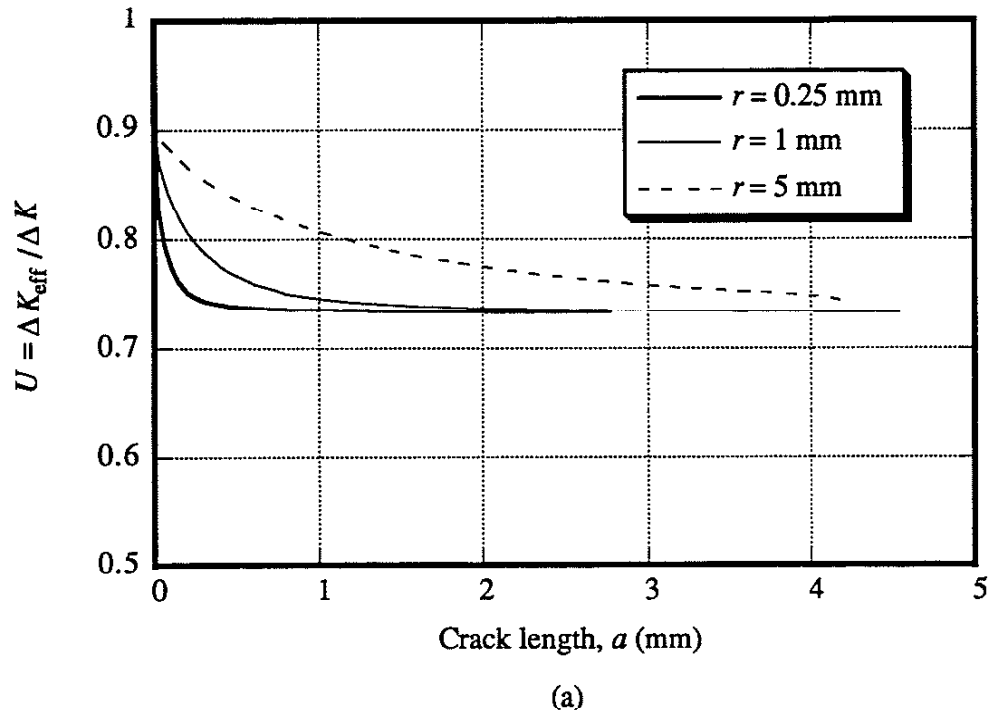


Fig. 6 The calculated $U(a)$ using Newman's strip-yield model ($E = 200$ GPa, $\sigma_0 = 400$ MPa) (a) various notch sizes ($S_{\max}/\sigma_0 = 0.5$, $R = 0$) (b) various load levels ($r = 5$ mm, $R = 0$).

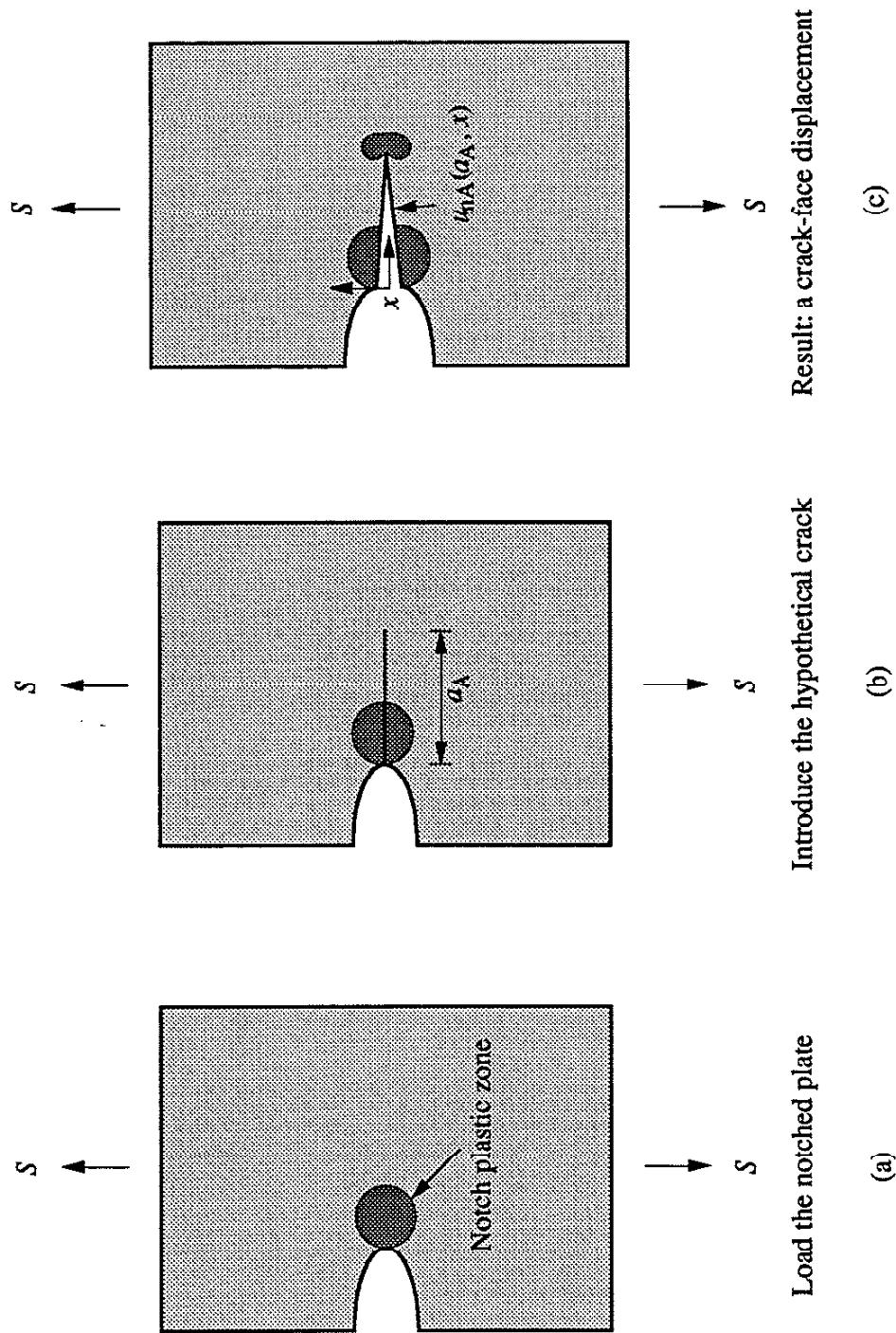


Fig. 7 The notched plate for $u_{nA}(a_A, x)$.

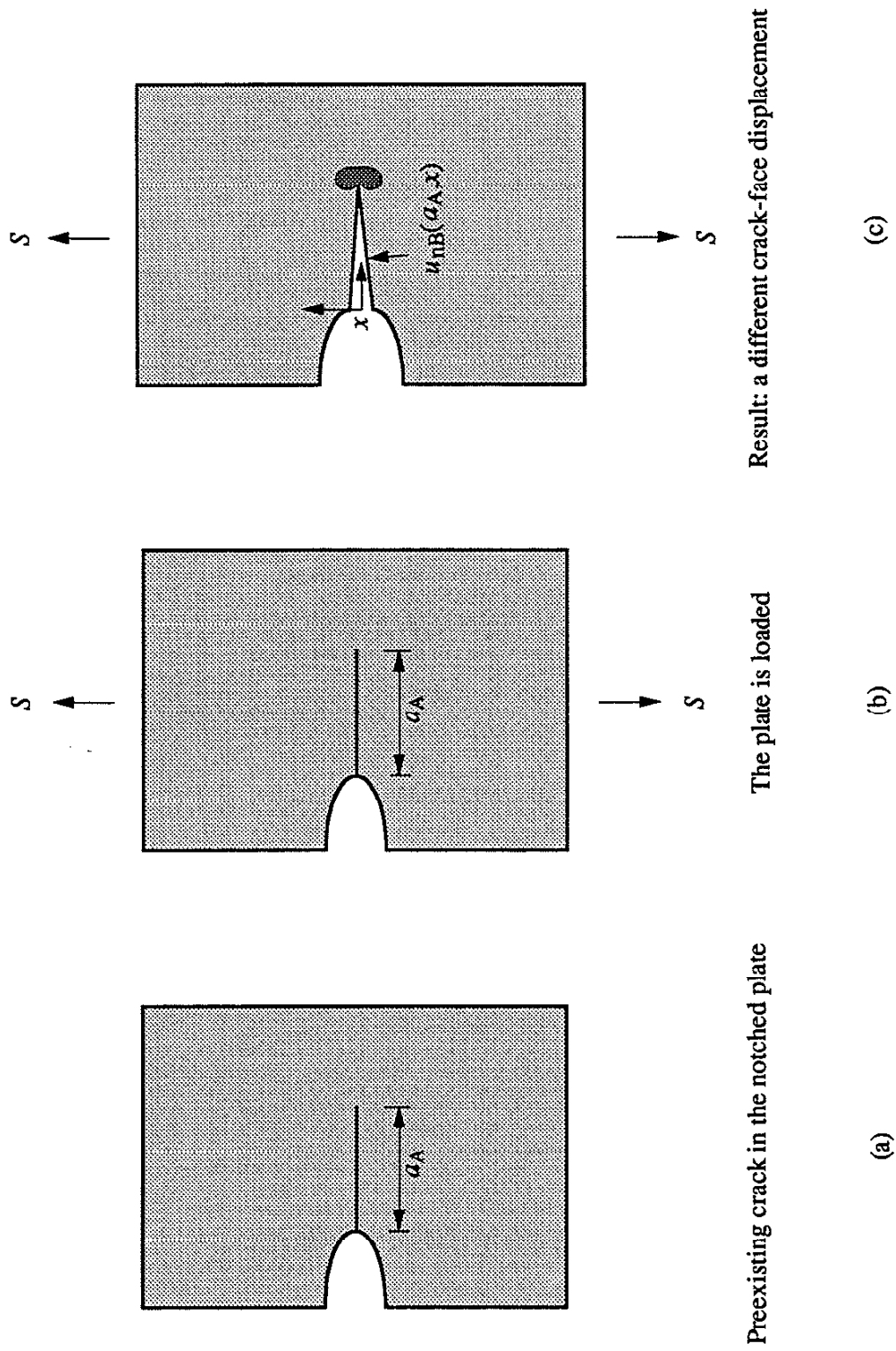


Fig. 8 The notched plate for $u_{nB}(a_A, x)$.

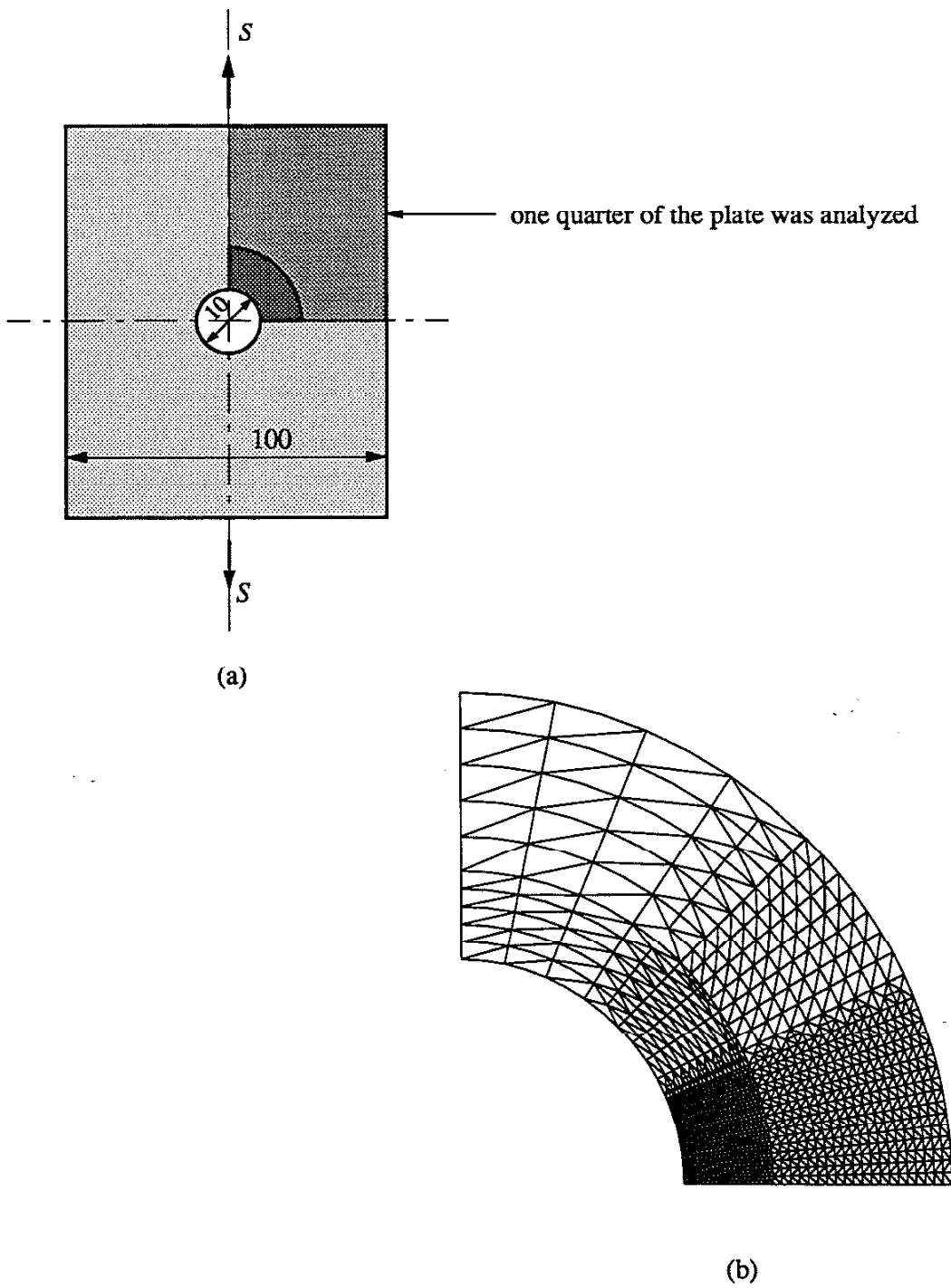


Fig. 9 (a) The geometry of the plate for FEA and, (b) the mesh around the notch. All dimensions are in mm.

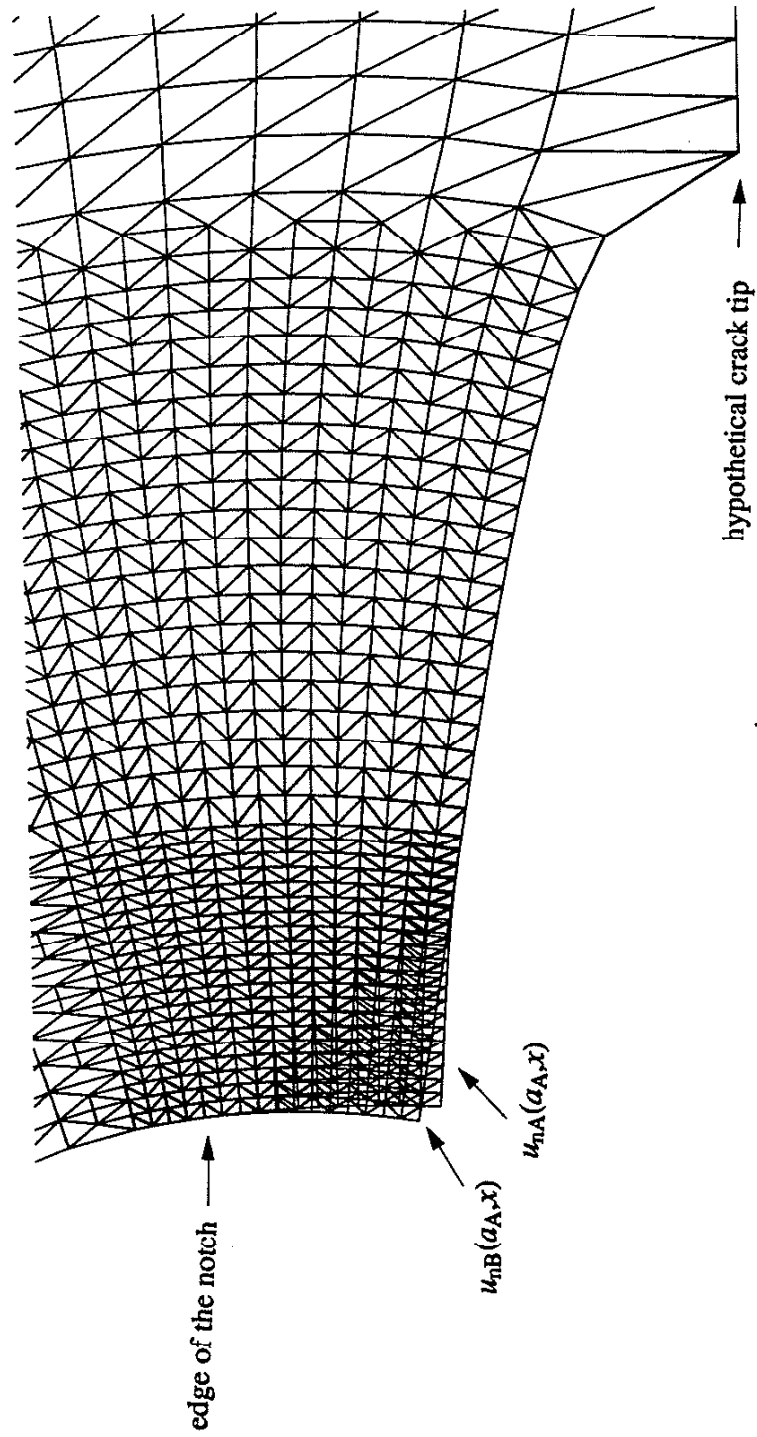


Fig. 10 Exaggerated crack-face displacements of the two notched plates.

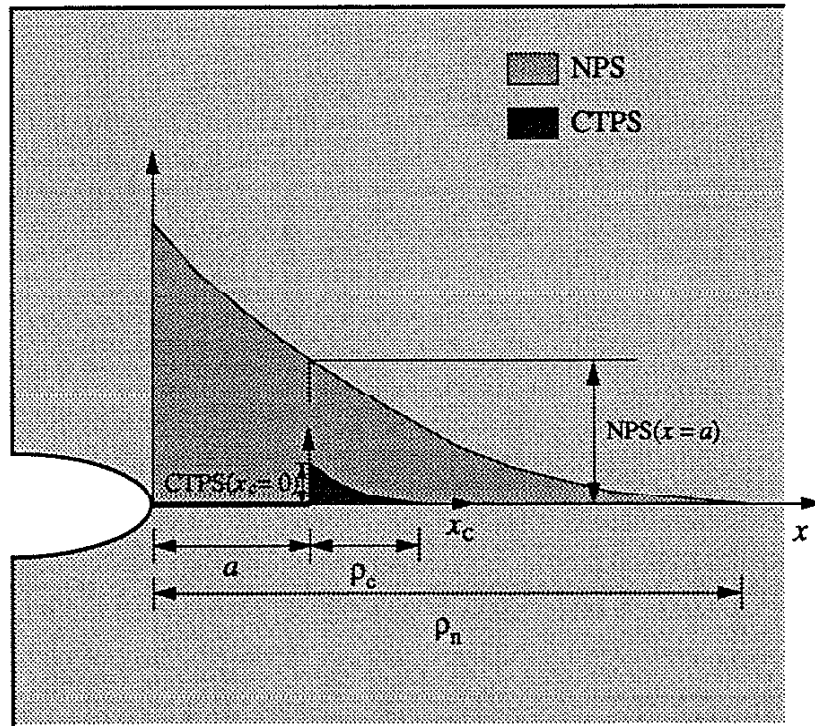
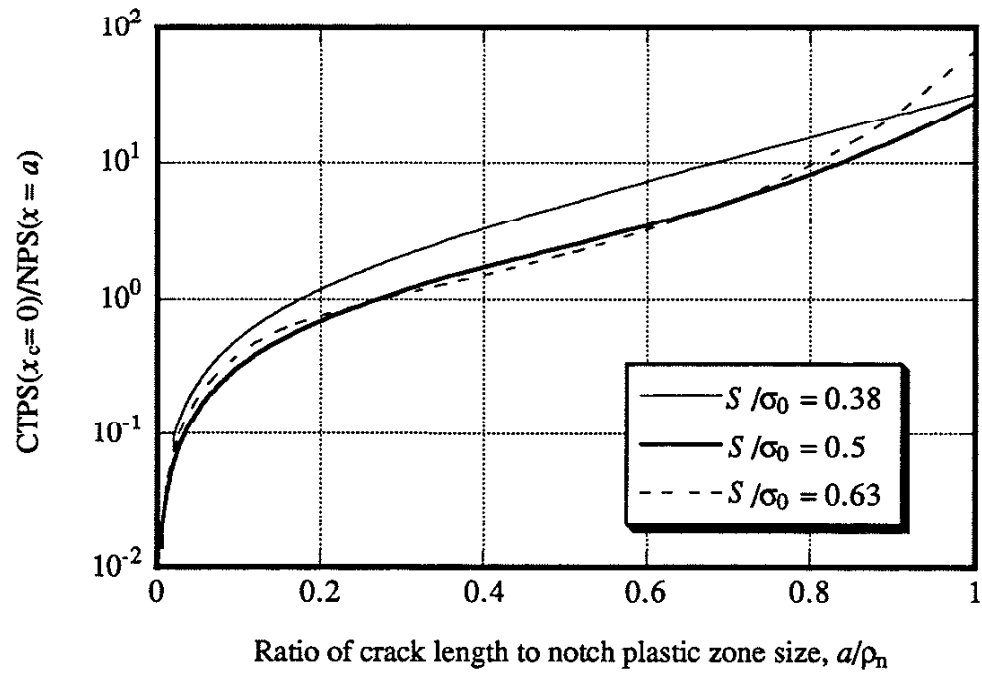
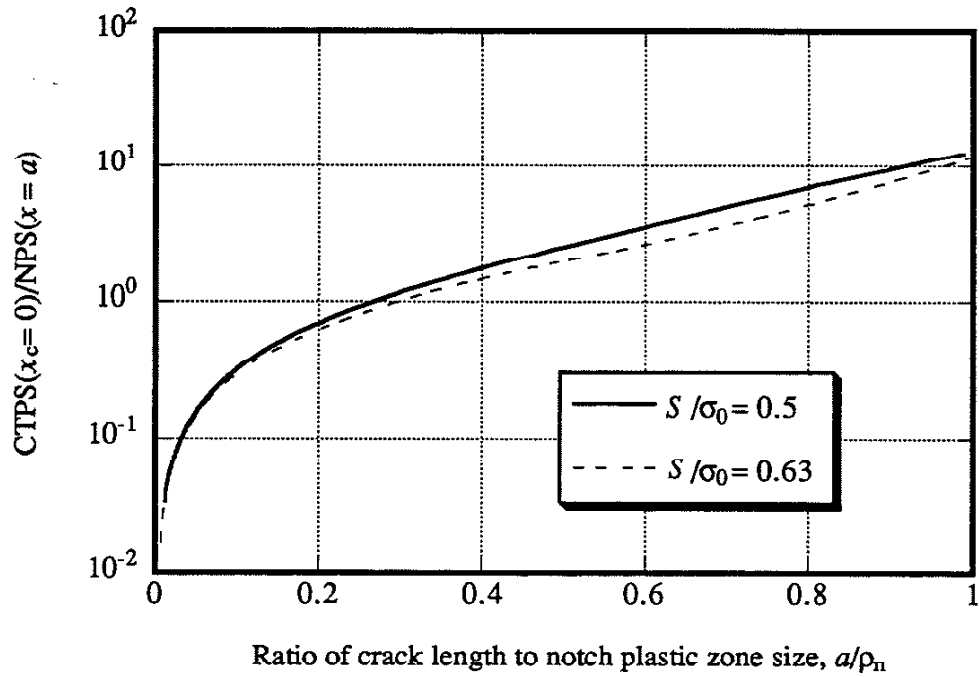


Fig. 11 The notch plastic stretches and the crack-tip plastic stretches.

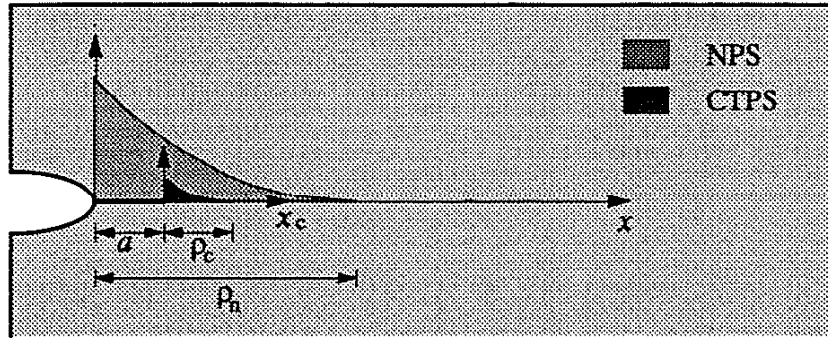


(a)

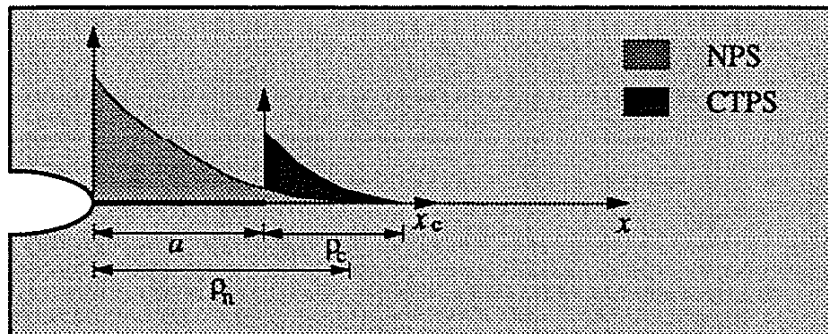


(b)

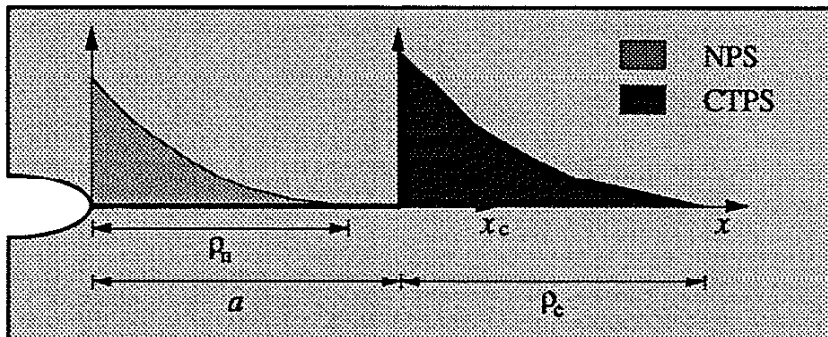
Fig.12 The ratios of the magnitude of the CTPS to that of the NPS:
(a) plane stress (b) plane strain.



(a) $a + \rho_c < \rho_n$



(b) $a + \rho_c > \rho_n$, and $a < \rho_n$



(c) $a + \rho_c > \rho_n$, and $a > \rho_n$

Fig. 13 Incorporating the CTPS with the NPS under various conditions: (a) the crack-tip plastic zone is entirely embedded in the notch plastic zone (b) part of the crack-tip plastic zone is beyond the notch plastic zone (c) the crack tip is located beyond the notch plastic zone.

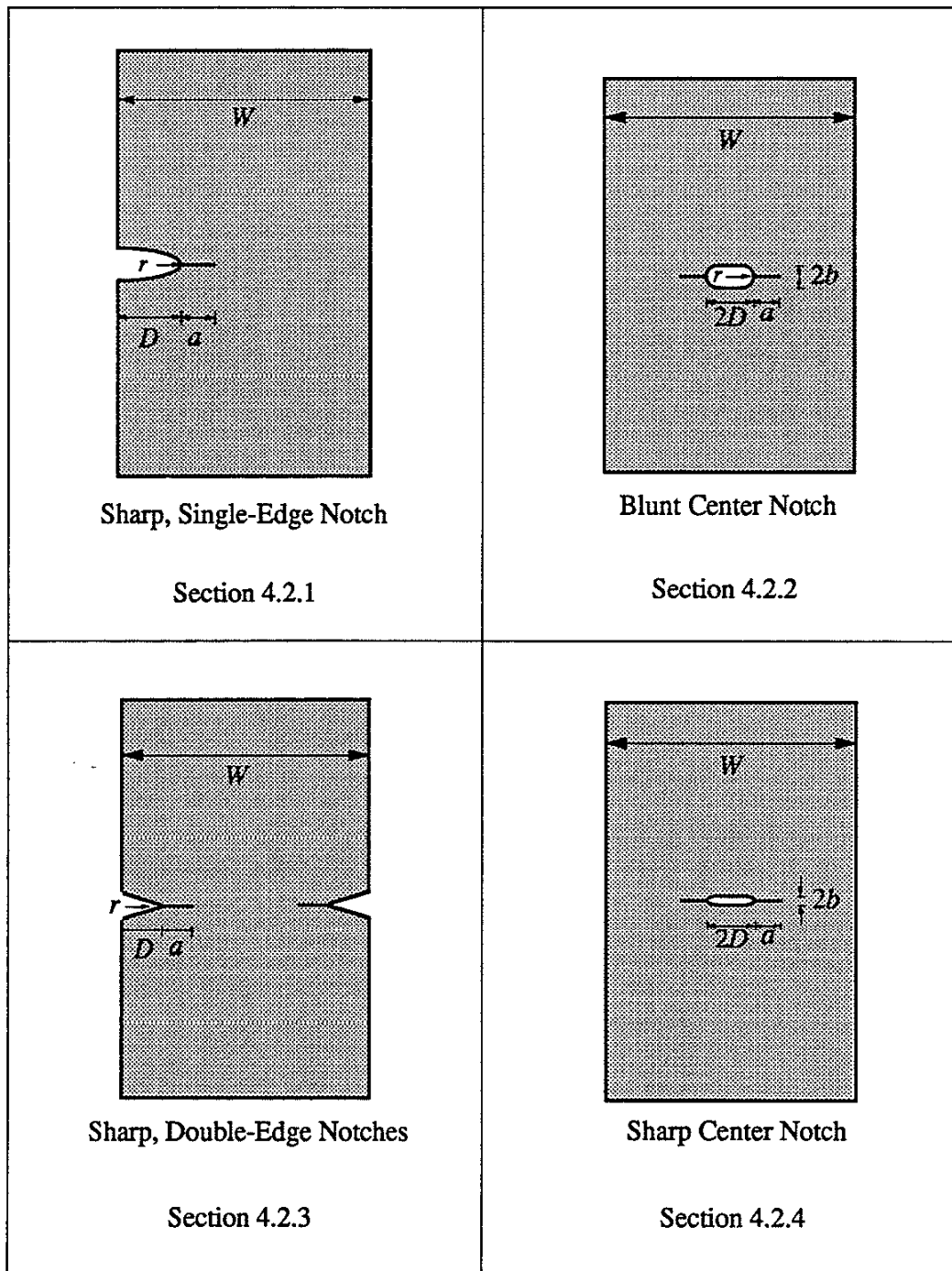


Fig. 14 Notch and specimen geometries considered in predictions.

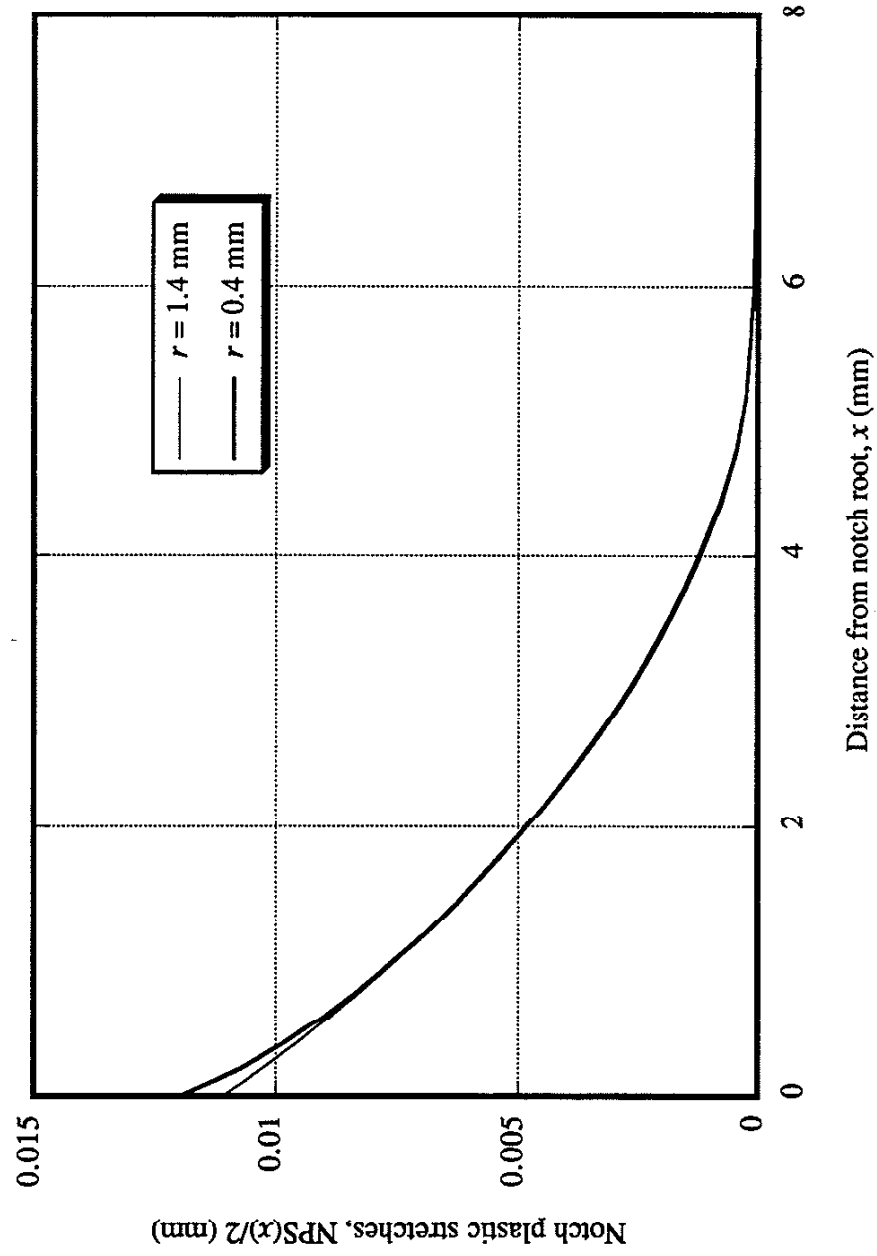


Fig. 15(a) The calculated notch plastic stretches of the sharp, single-edge notches.

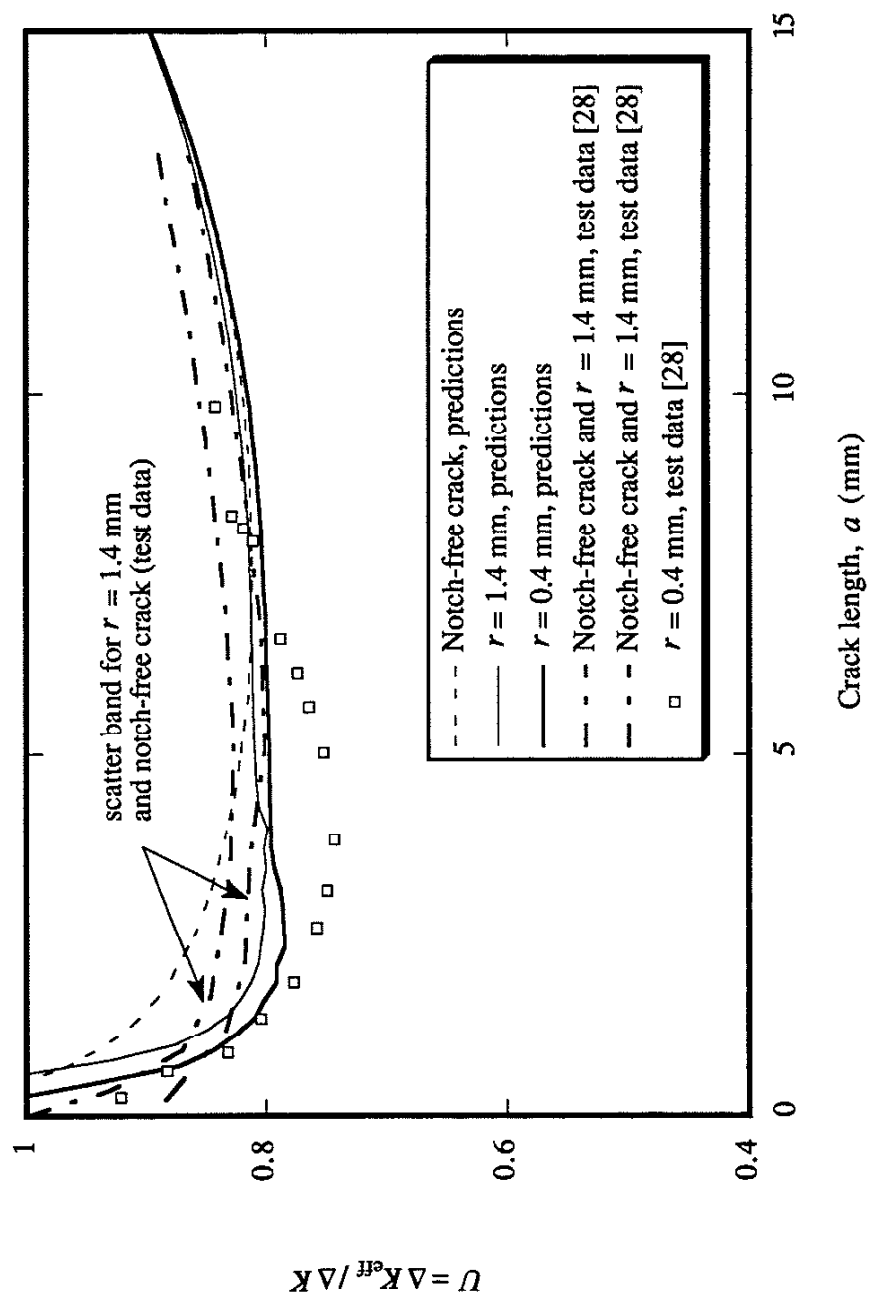


Fig. 15(b) The predicted U values of cracks emanating from sharp, single-edge notches and the test data.

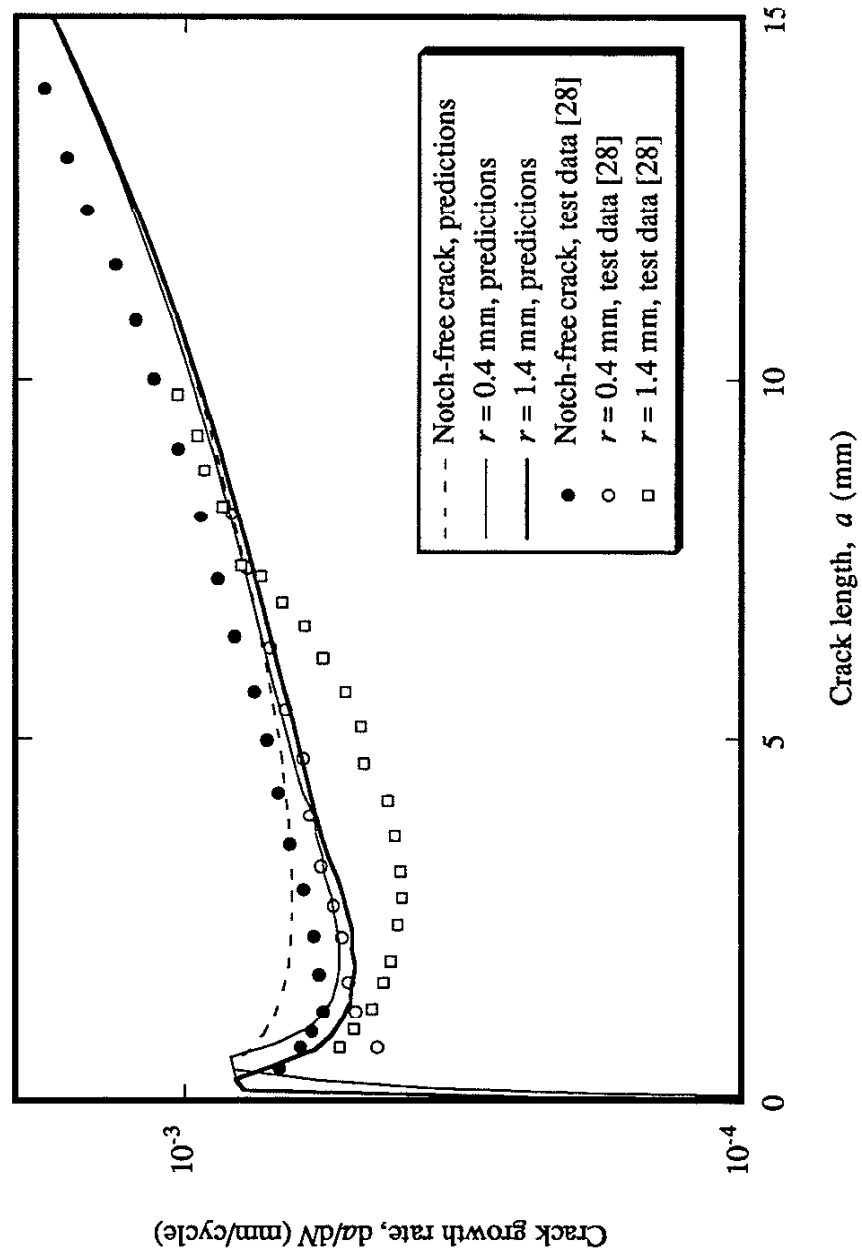
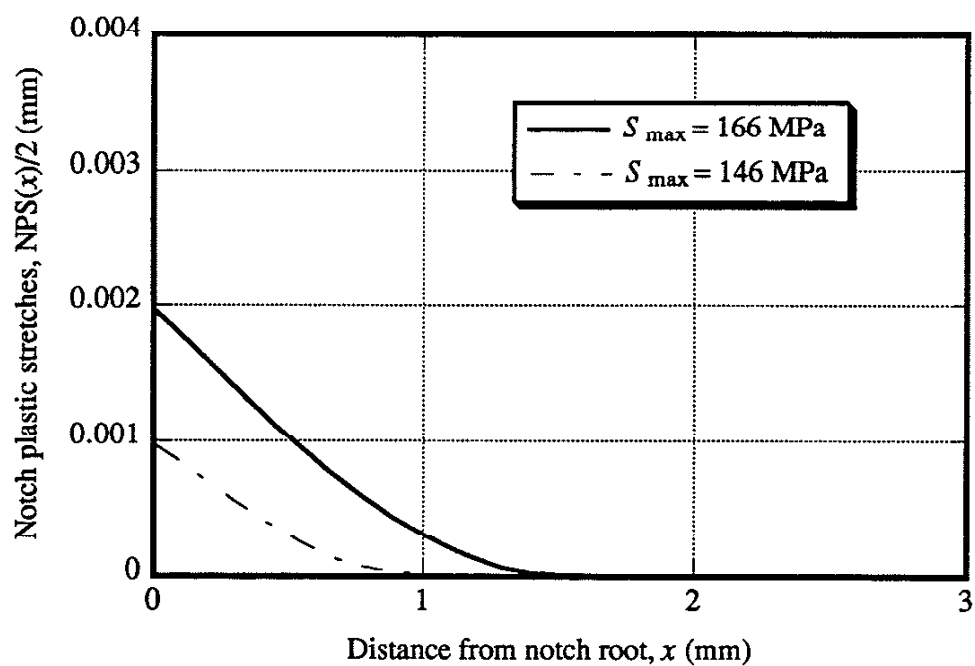
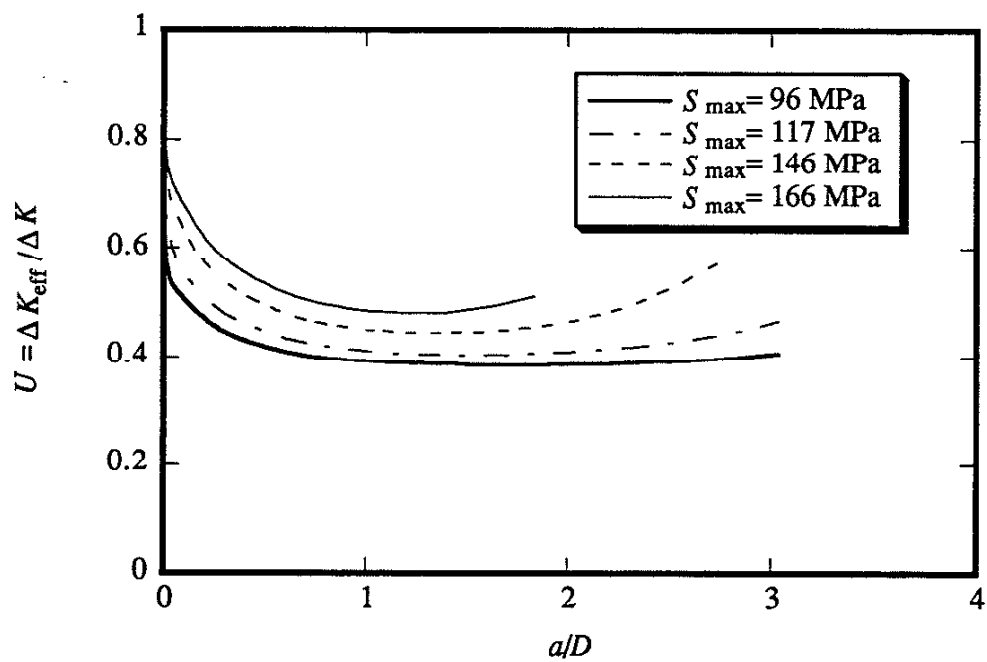


Fig. 15(c) The predicted crack growth rate of cracks emanating from sharp, single-edge notches and the test data.



(a)



(b)

Fig. 16 Blunt center notch: (a) the calculated NPS (b) the predicted U values.

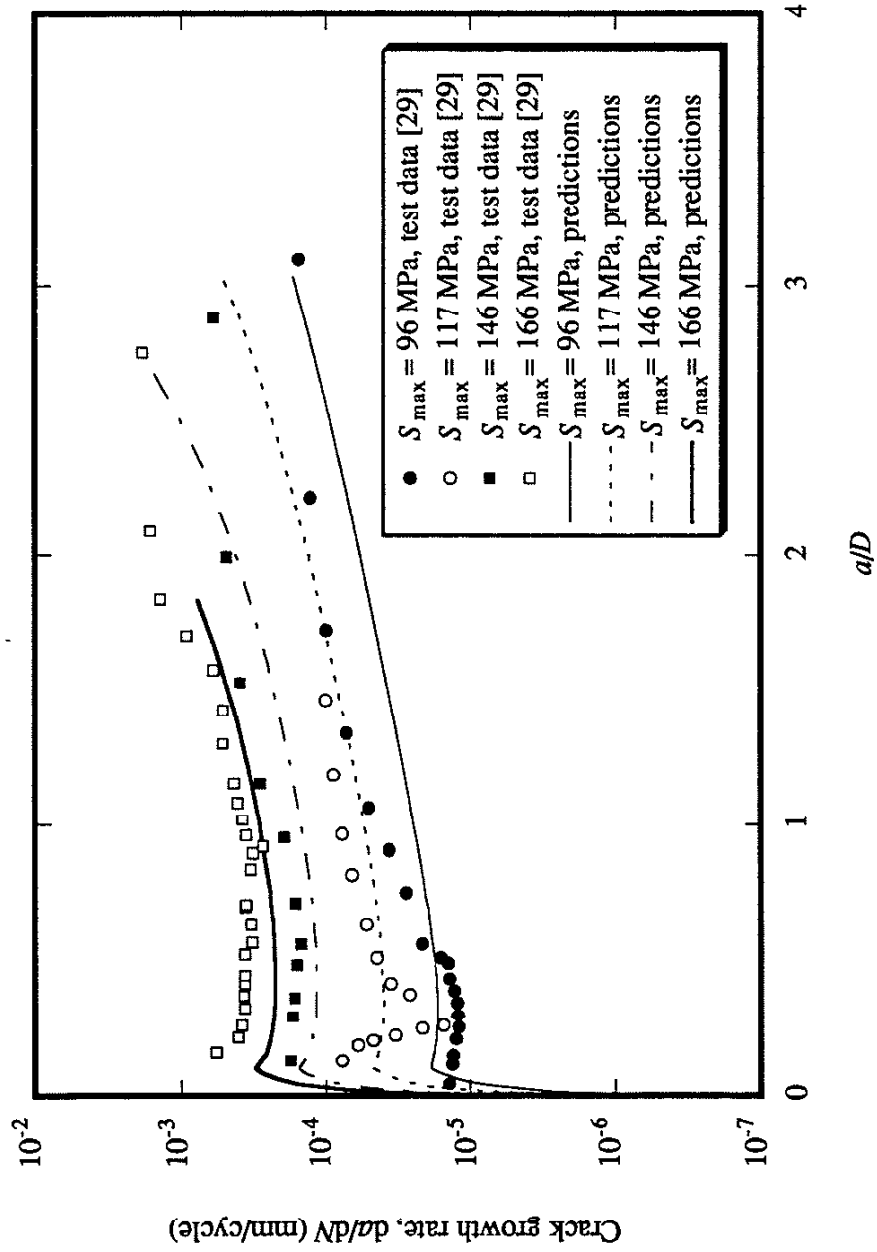
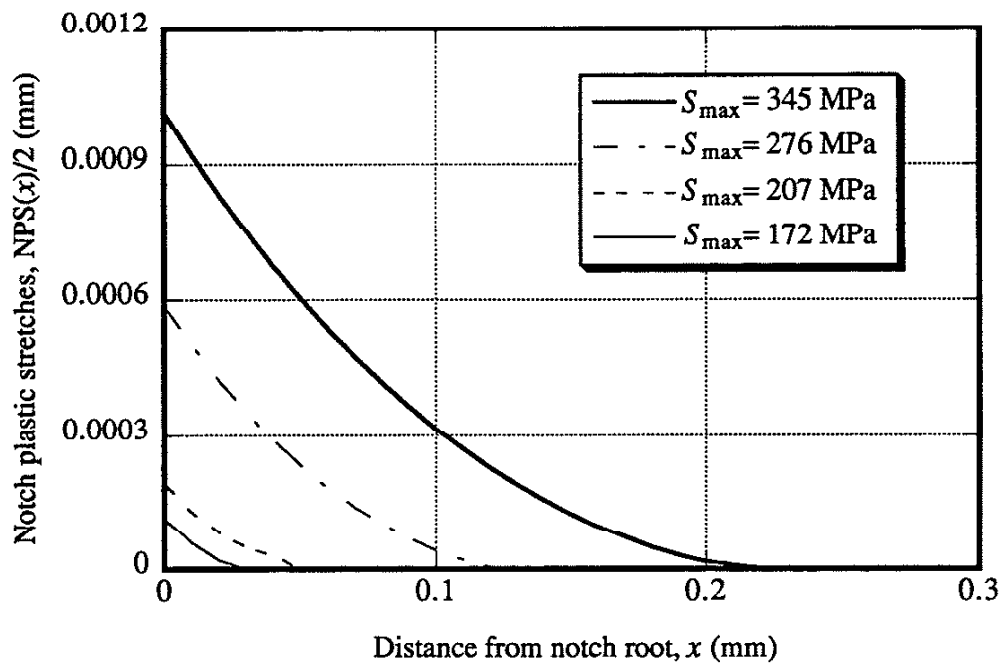
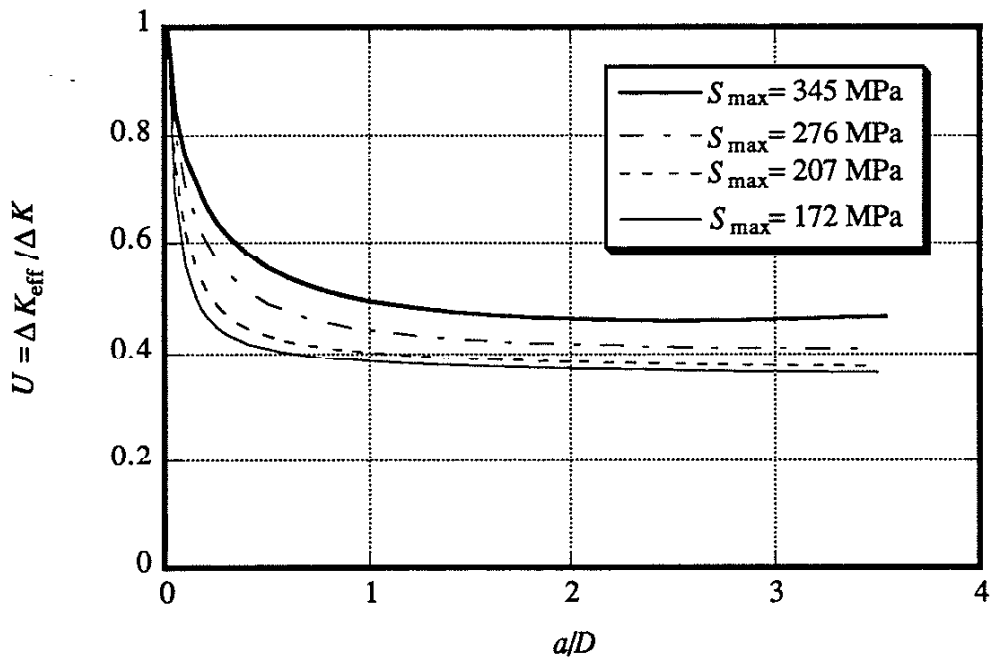


Fig. 16(c) The predicted crack growth rate for cracks emanating from a blunt center notch and the test data.



(a)



(b)

Fig.17 Sharp, double-edge notch: (a) the calculated NPS (b) the predicted U values.

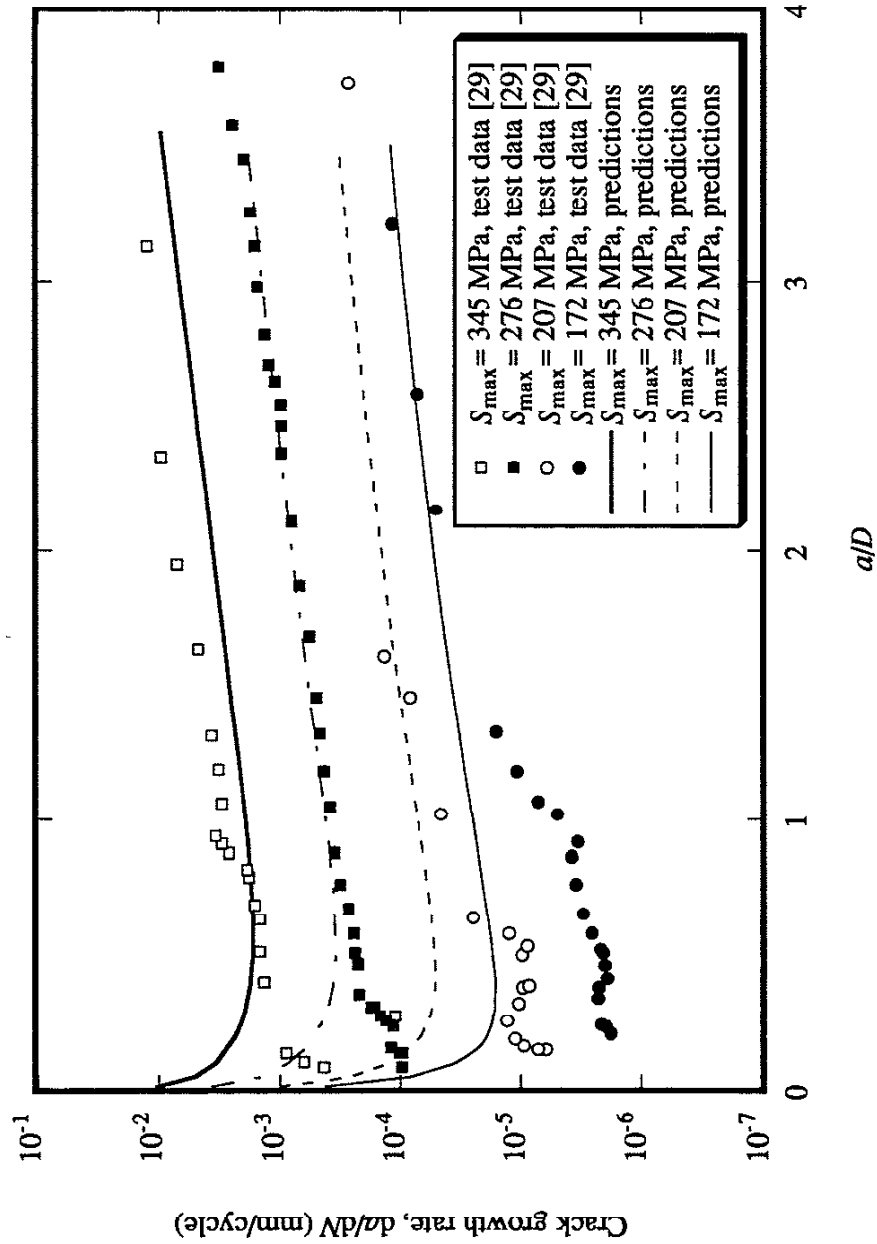


Fig.17(c) The predicted crack growth rate for cracks emanating from sharp, double-edge notch and the test data.

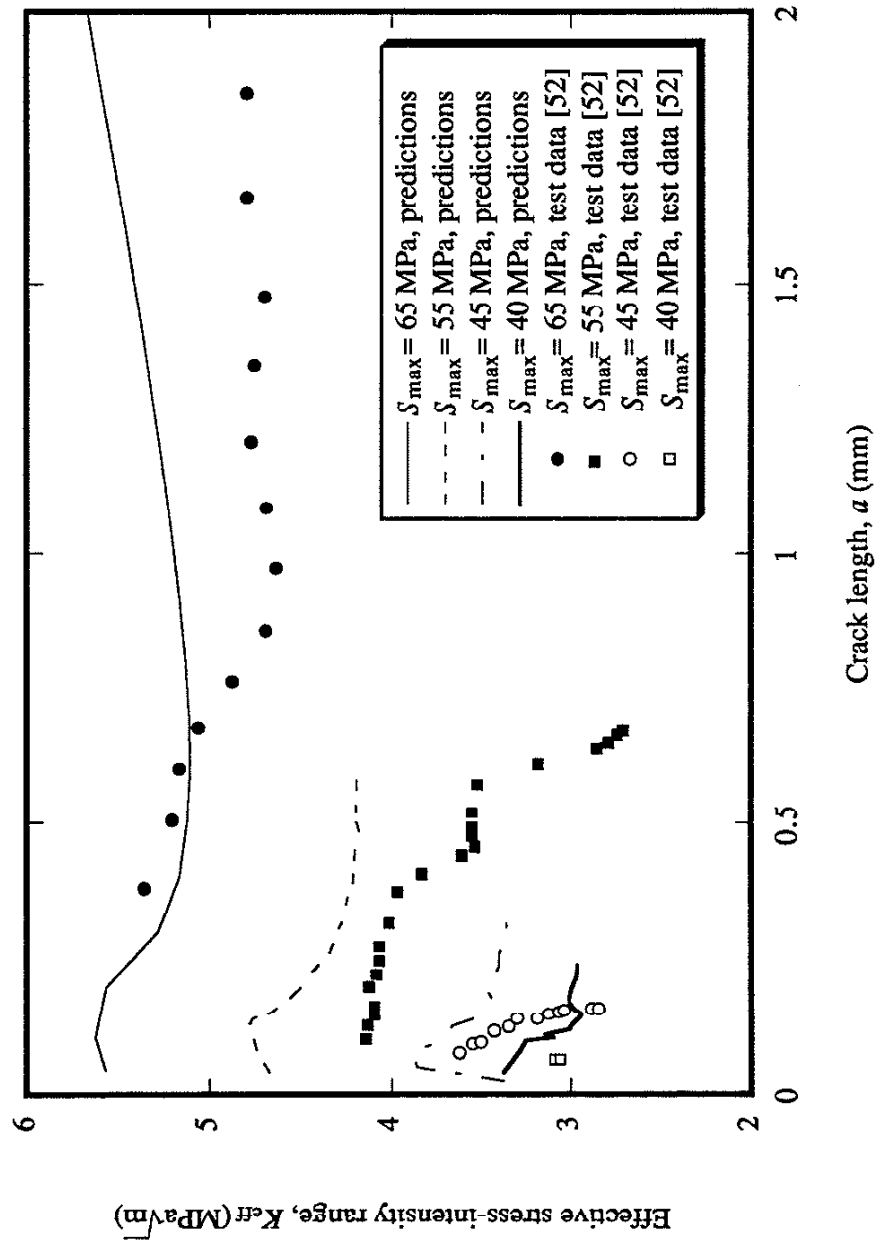


Fig.18 (a) The predicted effective stress-intensity factor for cracks emanating from a sharp center notch and the test data.

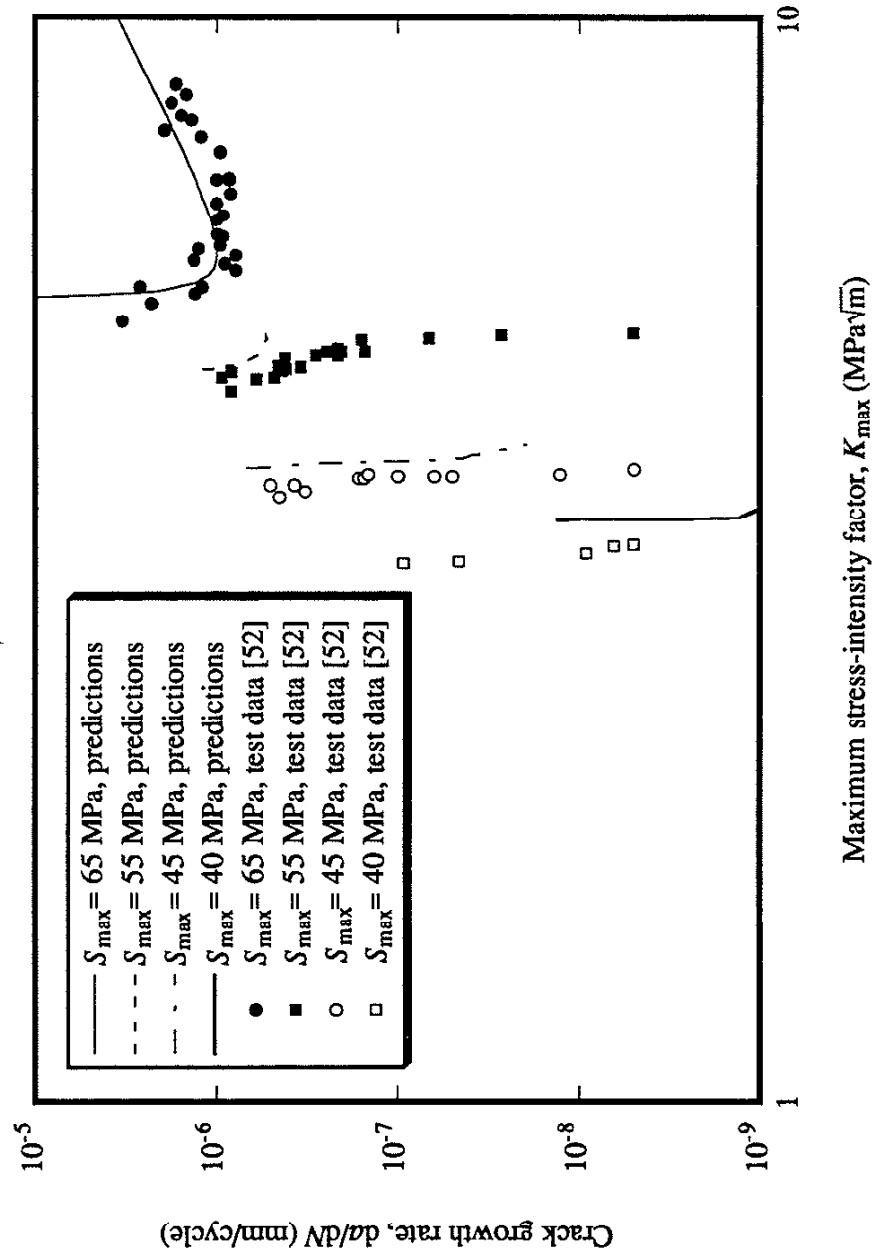
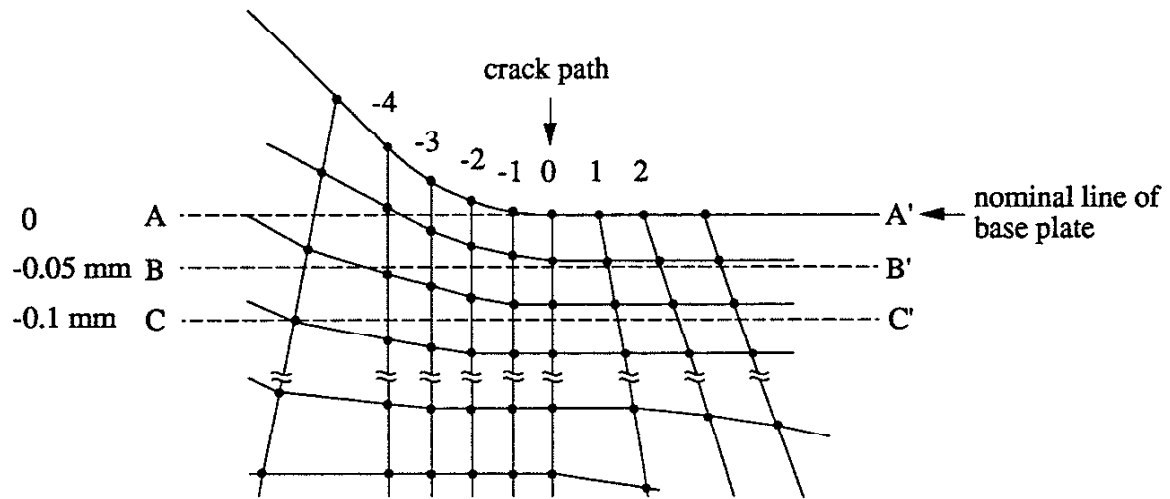


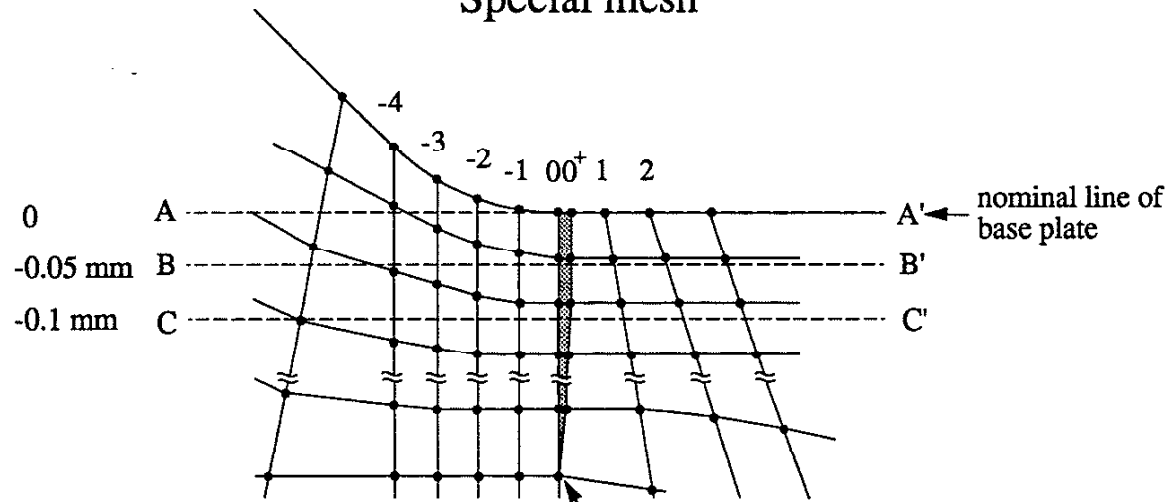
Fig.18(b) The predicted crack growth rate for cracks emanating from a sharp center notch and the test data.

Normal mesh



(a)

Special mesh



shaded elements: very slender elements, behave elastically, removed after the plastic zone formed around weld toe

hypothetical crack-tip node

(b)

Fig. 19 Finite element meshes around a weld toe: (a) the normal mesh
(b) the special mesh.

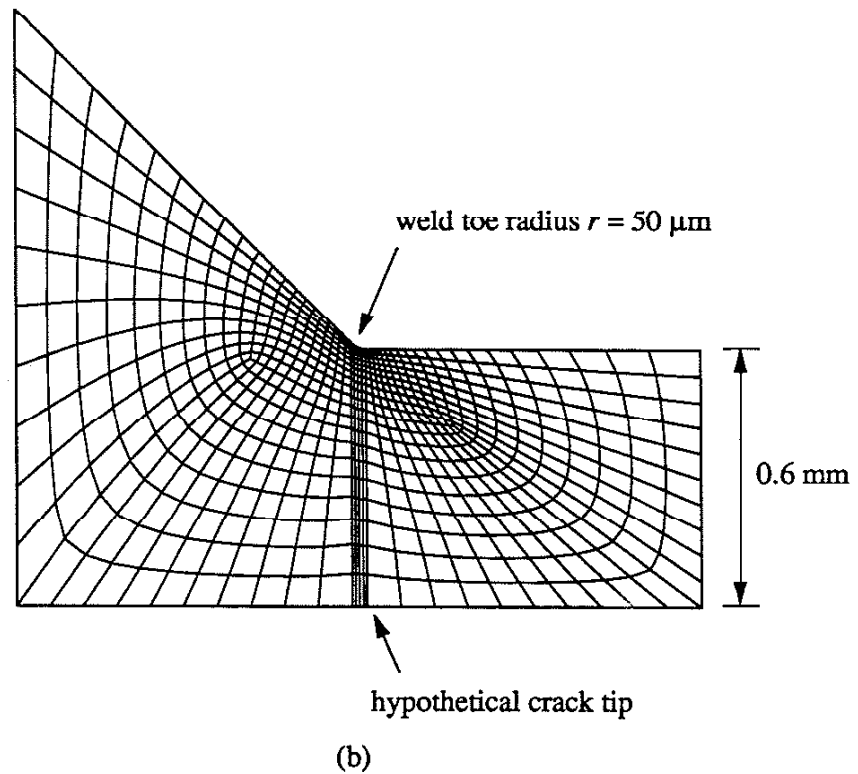
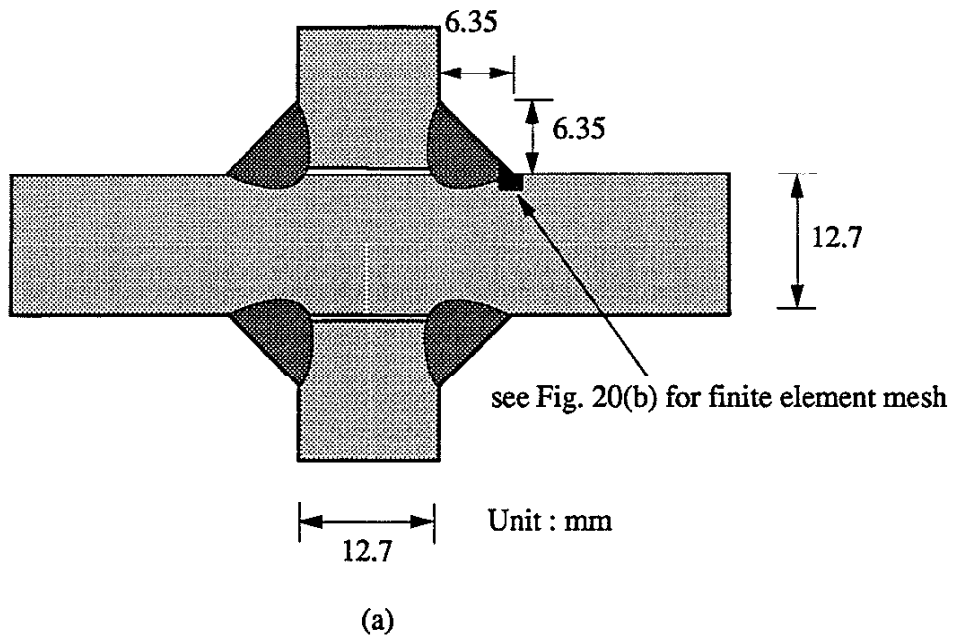
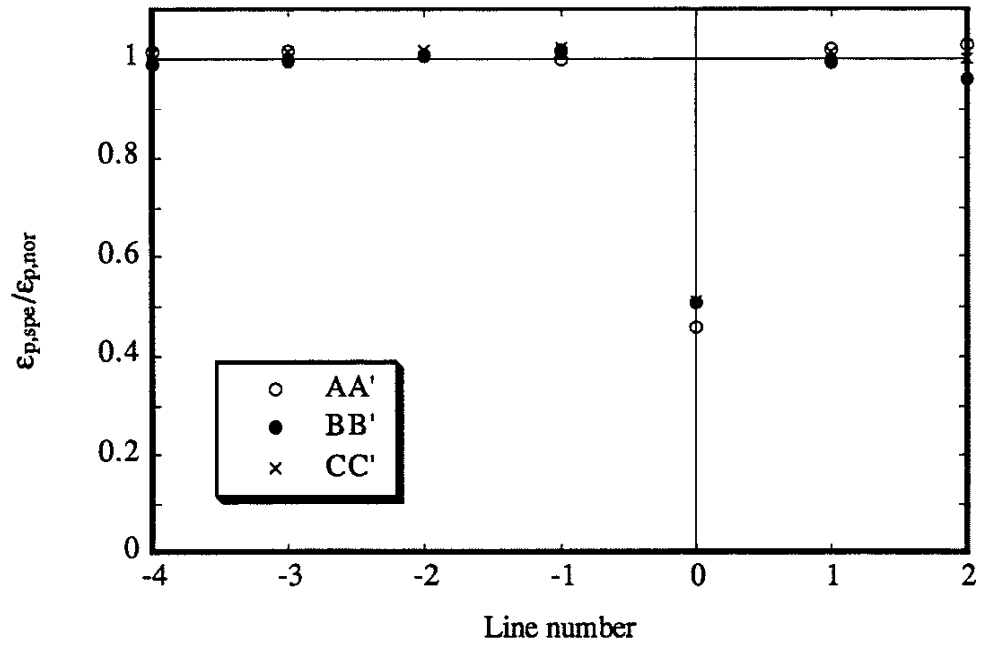
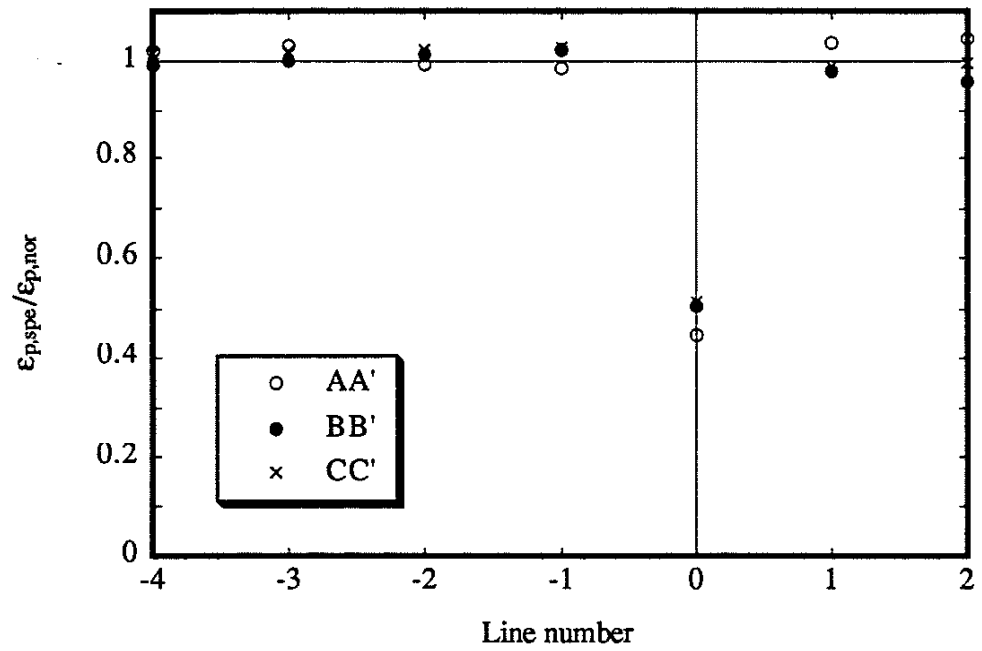


Fig. 20 The crack closure in a stress-relieved weld: (a) the geometry of the cruciform weldment (b) the finite element mesh around the weld toe.



(a)



(b)

Fig. 21 The ratio of plastic strains calculated from normal mesh and special mesh: (a) $S_{\max} = 147$ MPa (b) $S_{\max} = 177$ MPa.

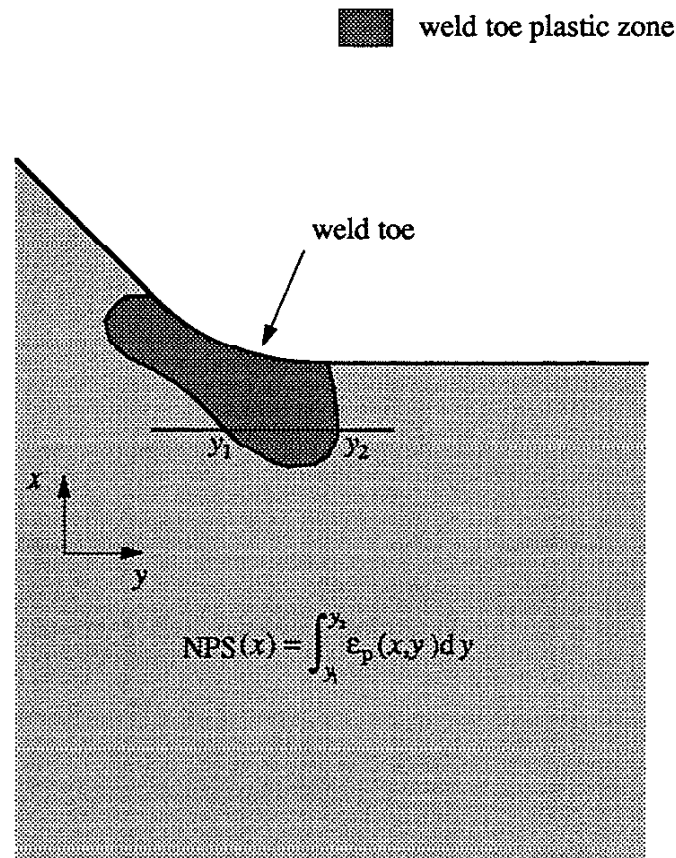
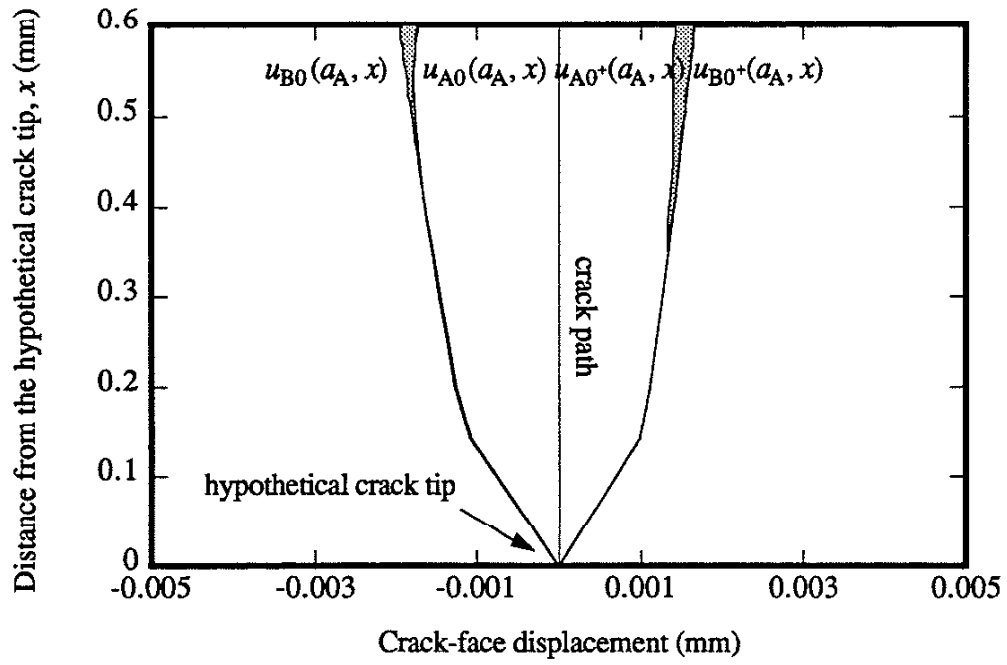
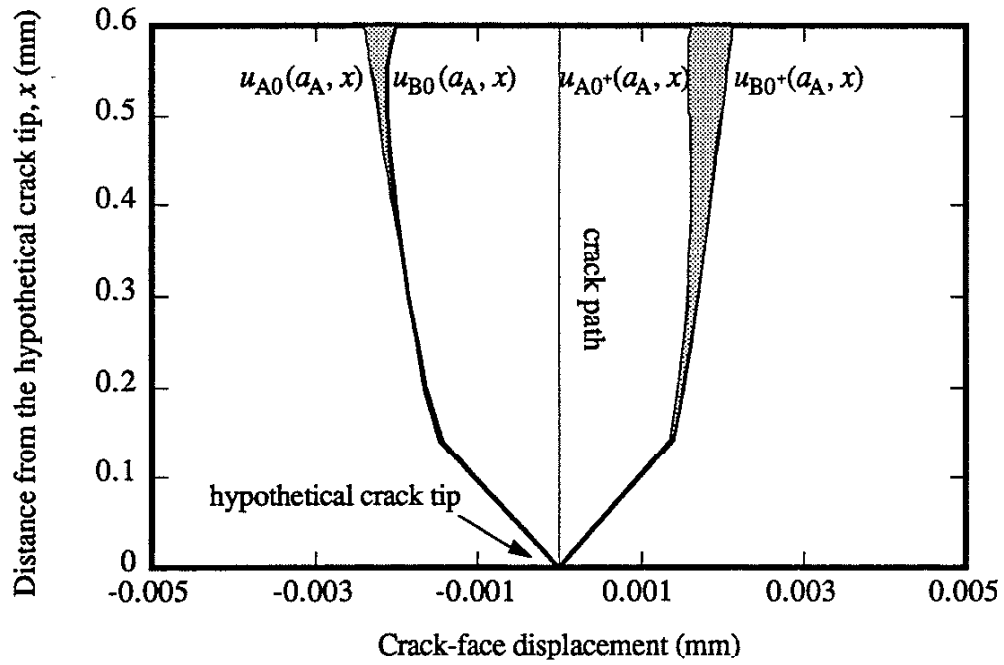


Fig. 22 The integration of weld toe plastic strain for the NPS.



(a)



(b)

Fig. 23 The calculated crack-face displacements: (a) $S_{\max} = 147$ MPa
(b) $S_{\max} = 177$ MPa.

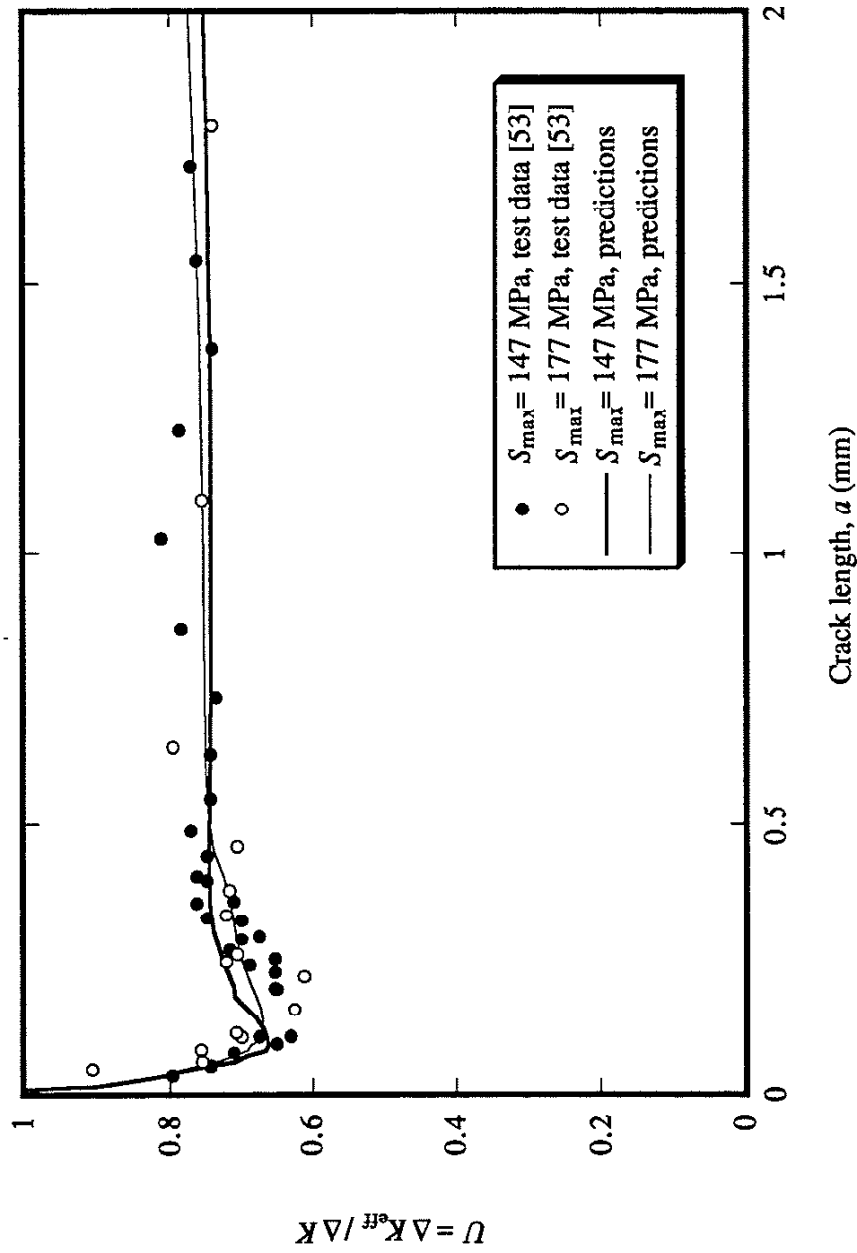


Fig. 24 The comparison of the predicted $U(a)$ curves with the tested results for $R = 0$ cases.

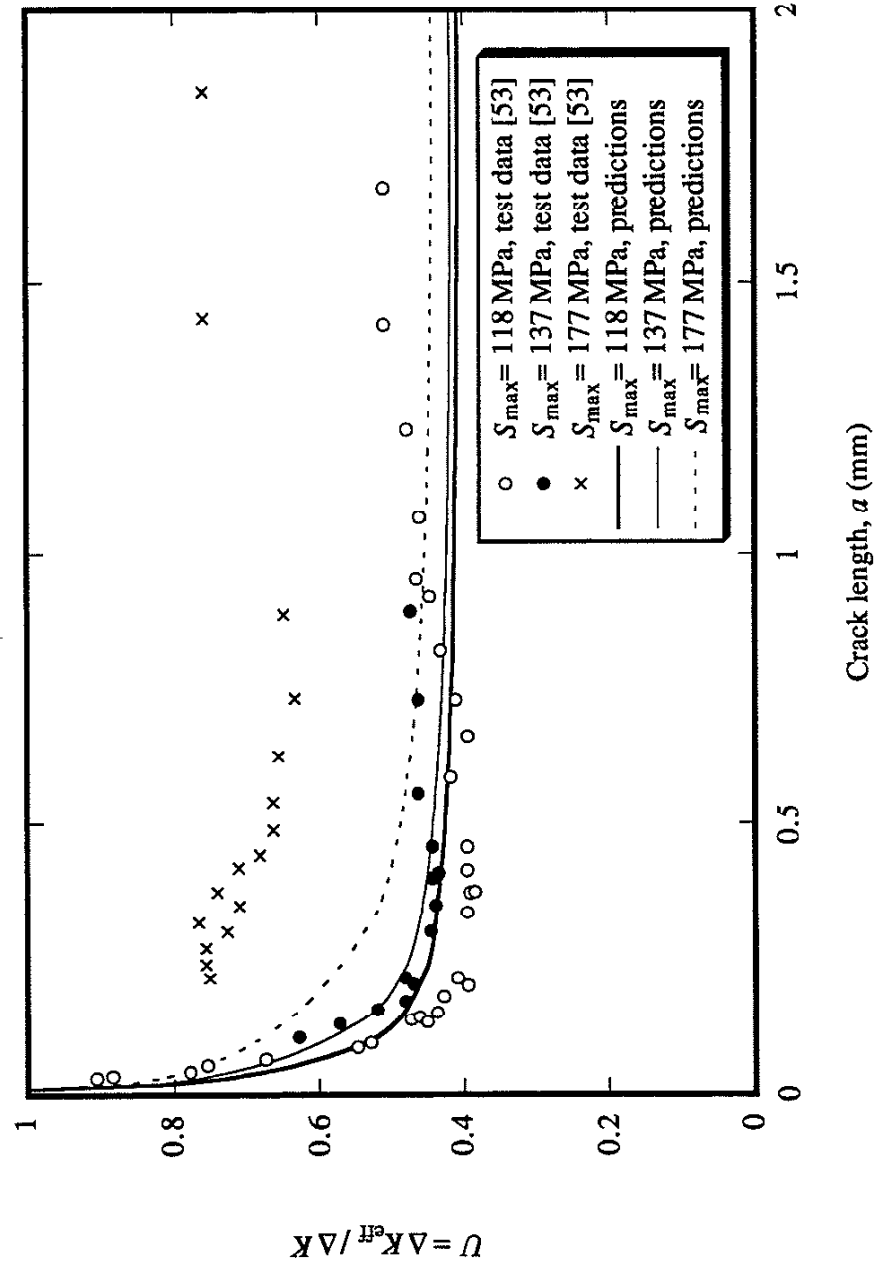


Fig. 25(a) The comparison of the predicted $U(a)$ curves with the tested results for $R = -1$ cases.

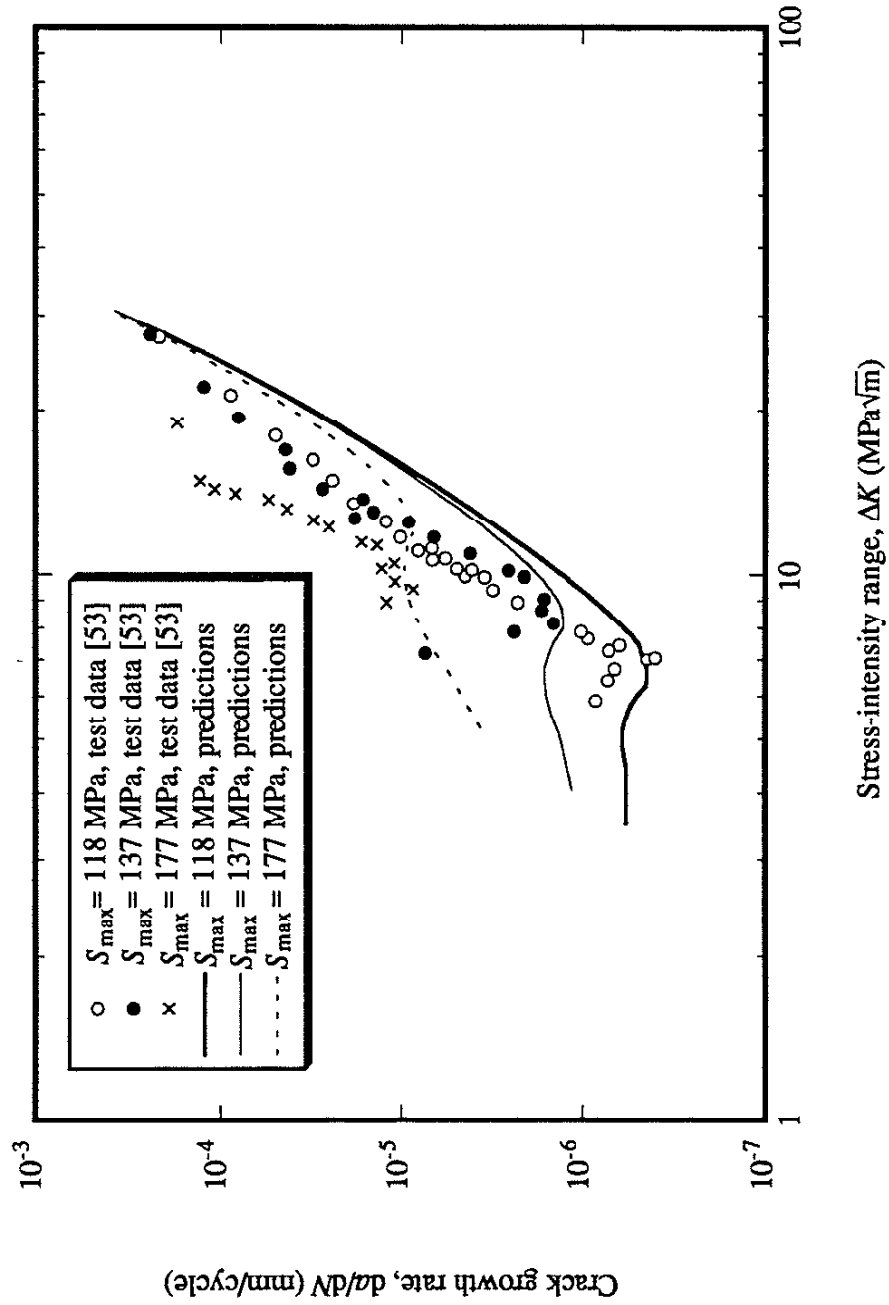


Fig. 25(b) The comparison of the predicted crack growth rate with the tested results for $R = -1$ cases.

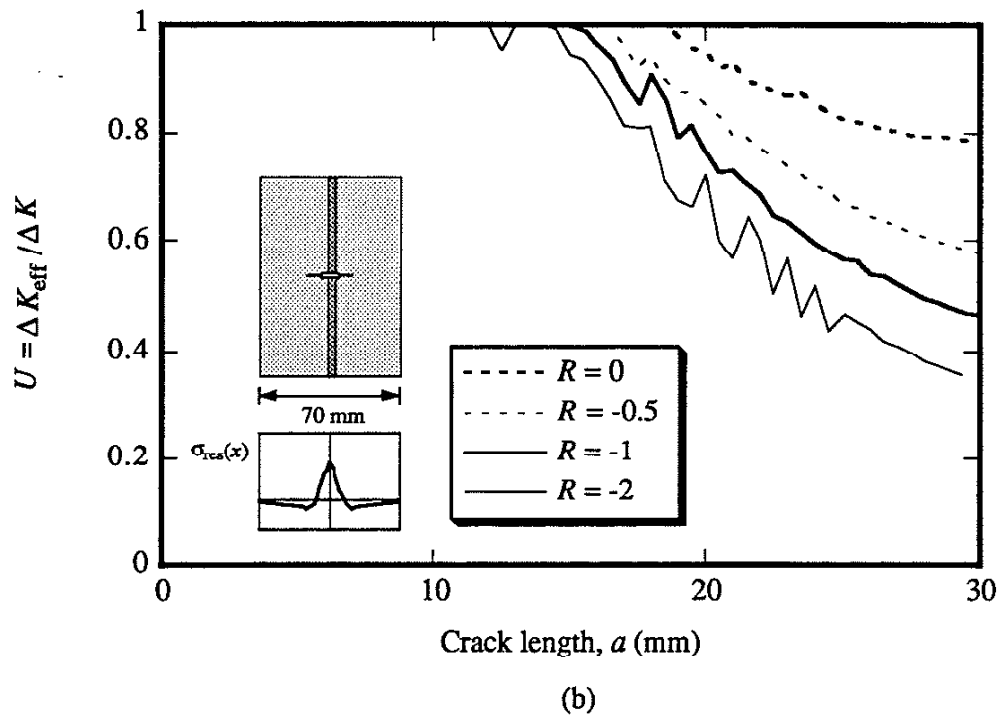
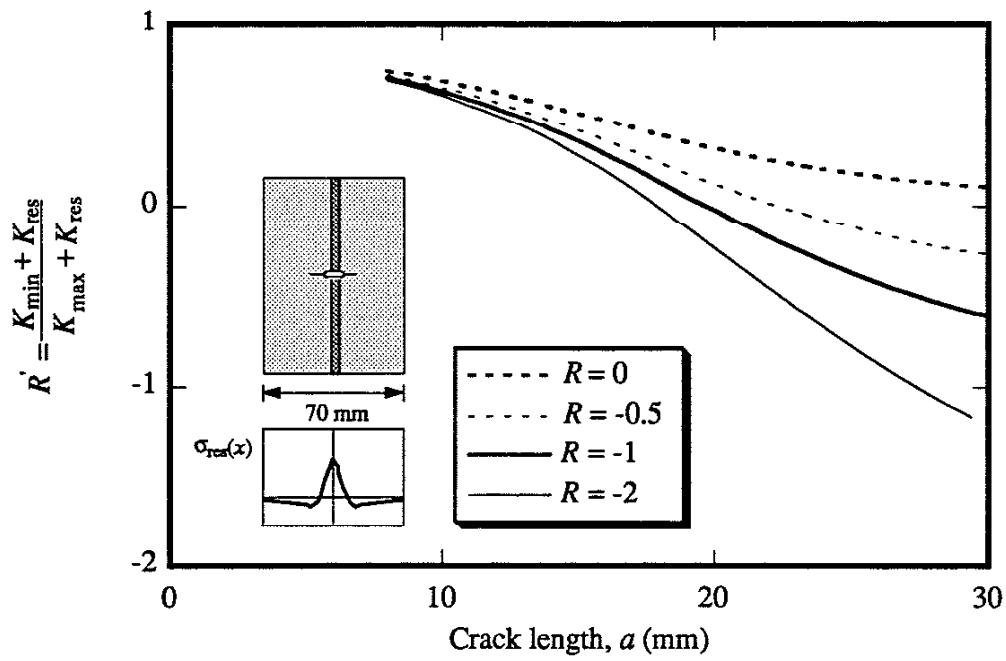


Fig. 26 The crack-closure behavior in a residual stress field: (a) the calculated $R'(a)$ (b) the calculated $U(a)$.

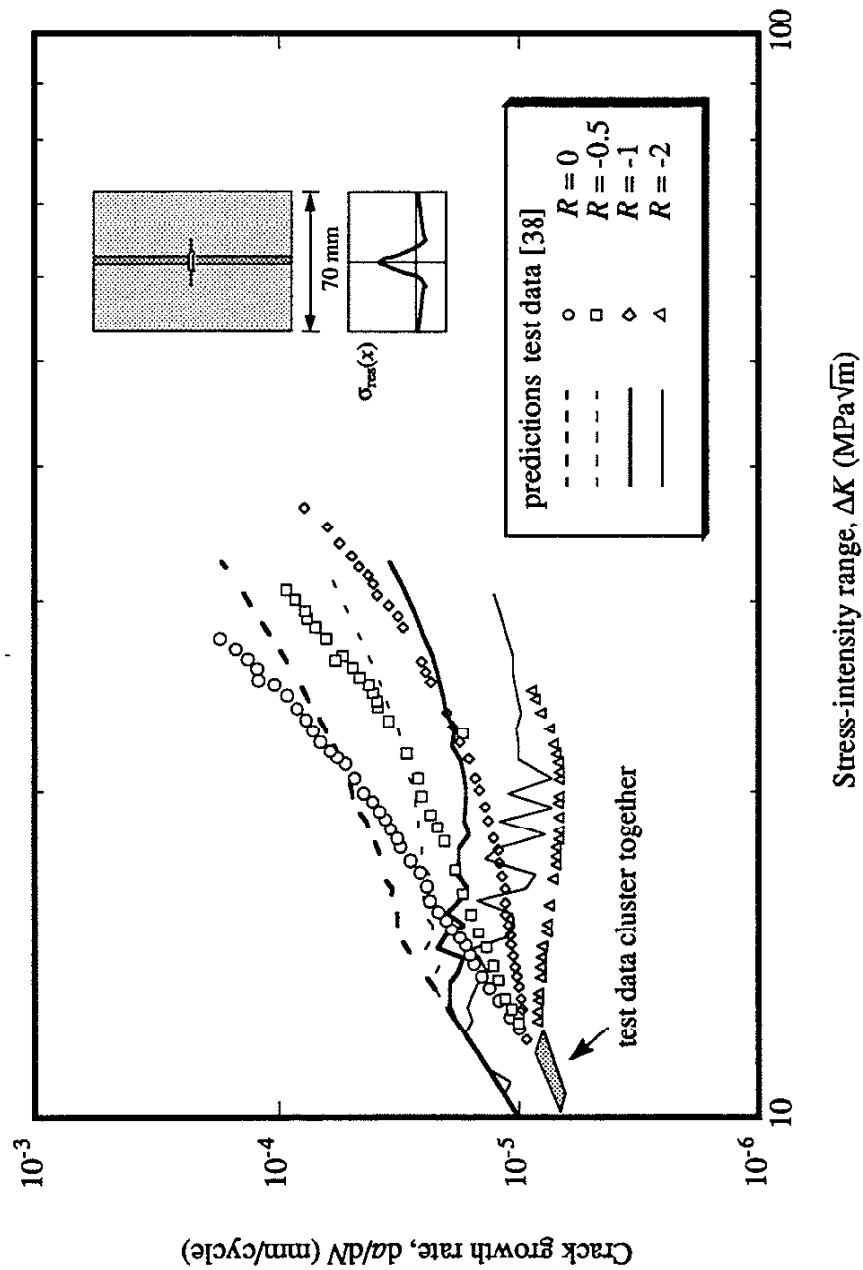


Fig. 26(c) The predicted and the measured crack growth rate in a residual stress field.

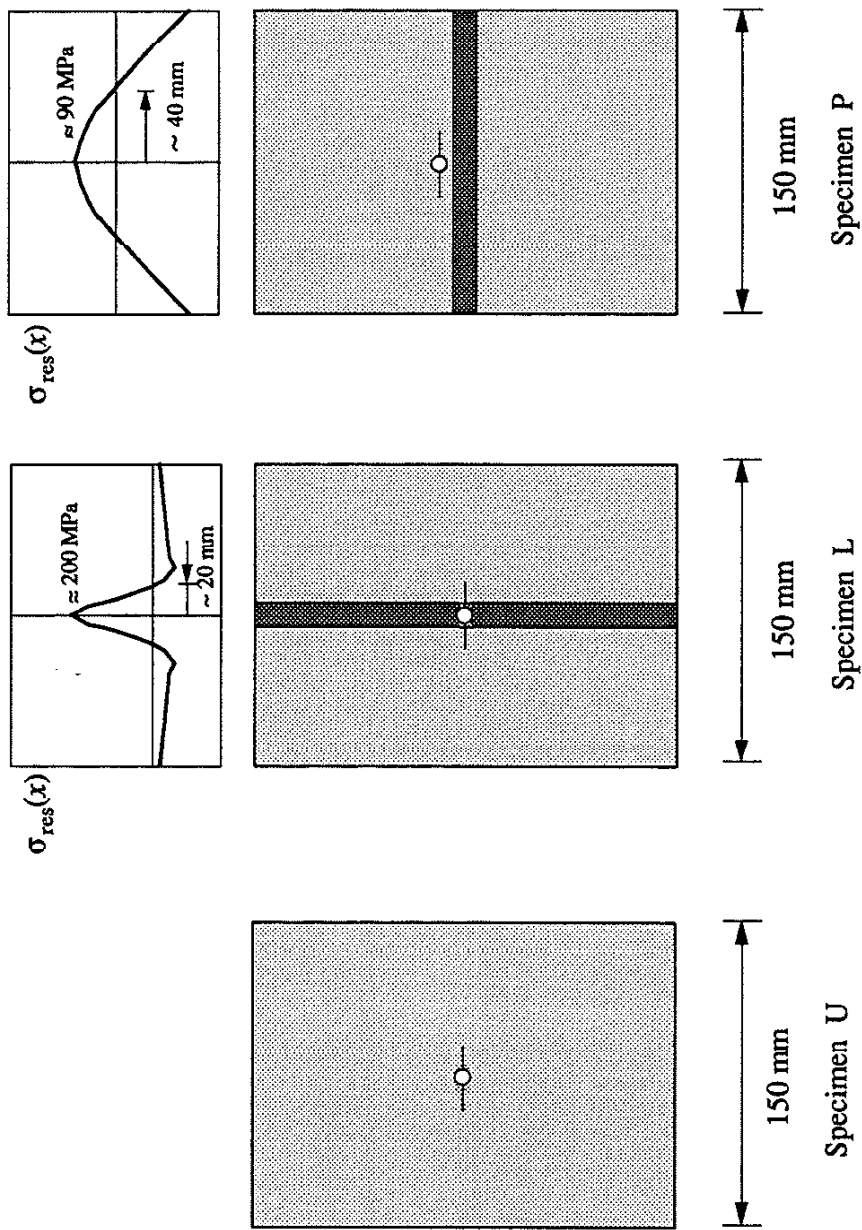


Fig. 27 Three types of specimens used in Glinka's tests [33].

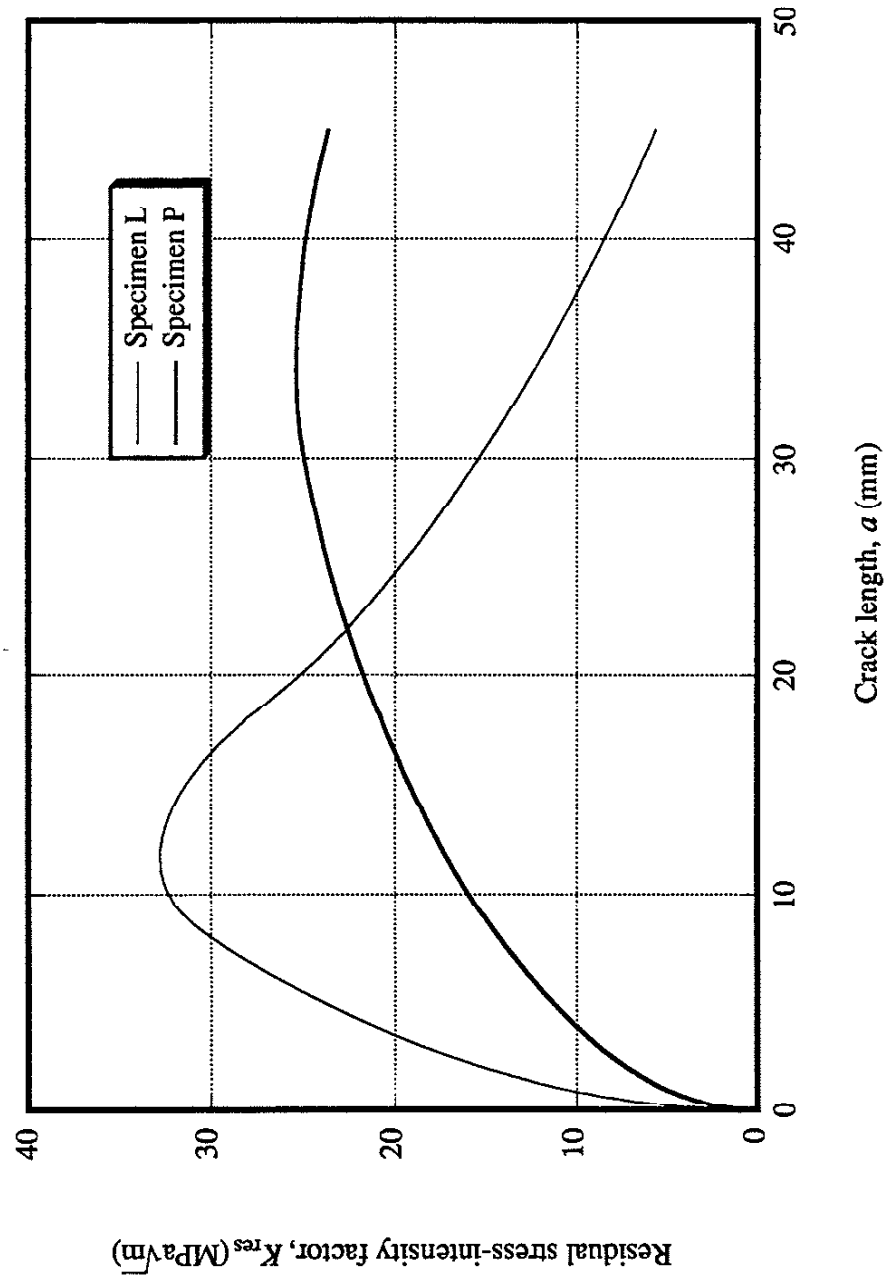
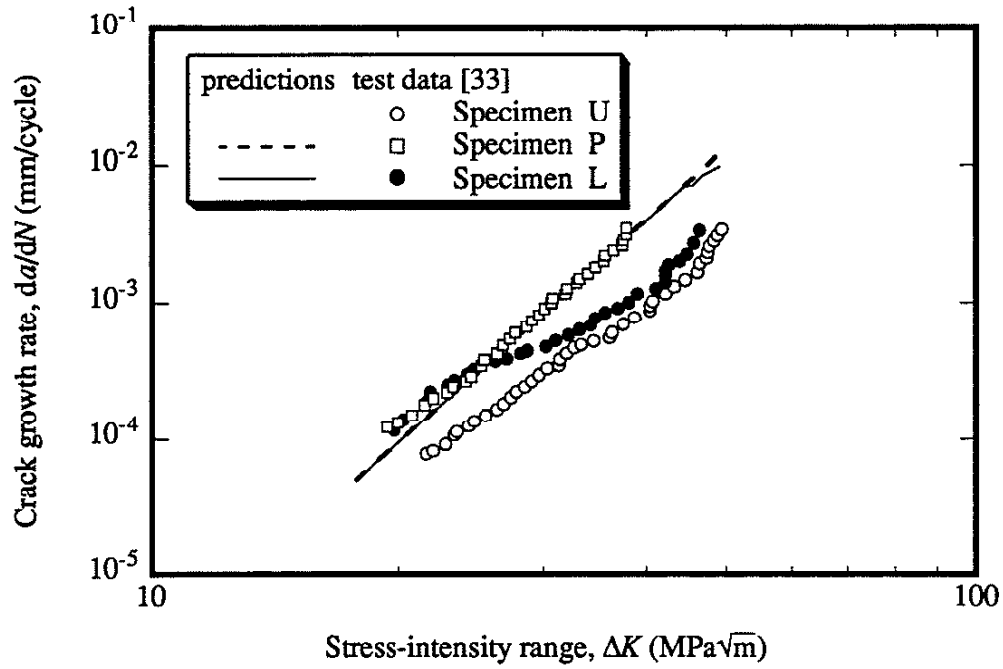
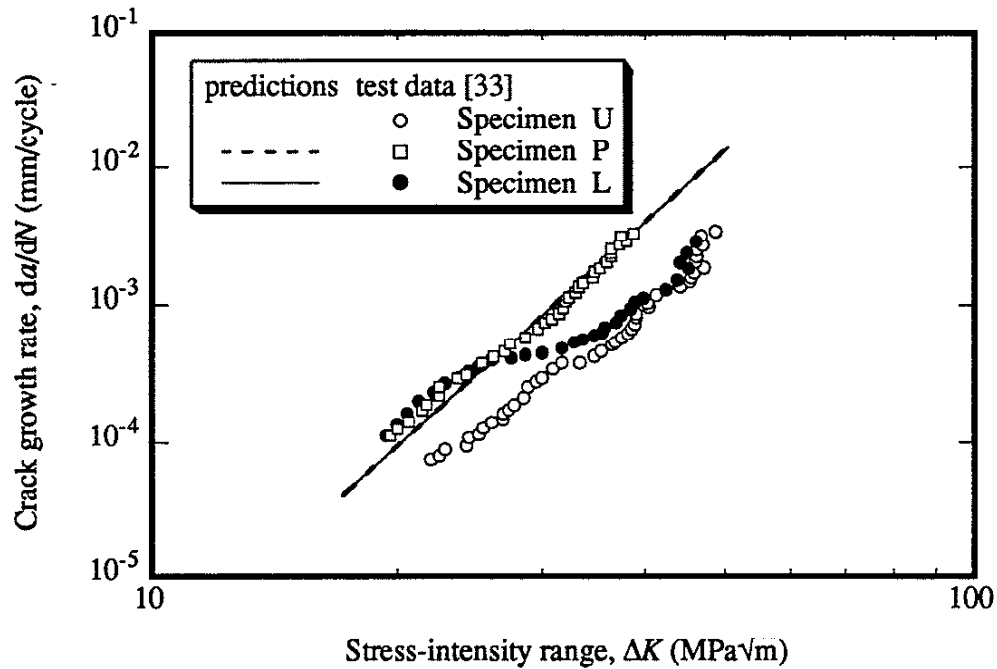


Fig. 28 The calculated K_{res} of Specimen L and Specimen P.



(a)



(b)

Fig. 29 The predicted crack growth rate and the test data in residual stress fields: (a) $\Delta S = 111$ MPa, $R = 0.35$ (b) $\Delta S = 107$ MPa, $R = 0.5$.

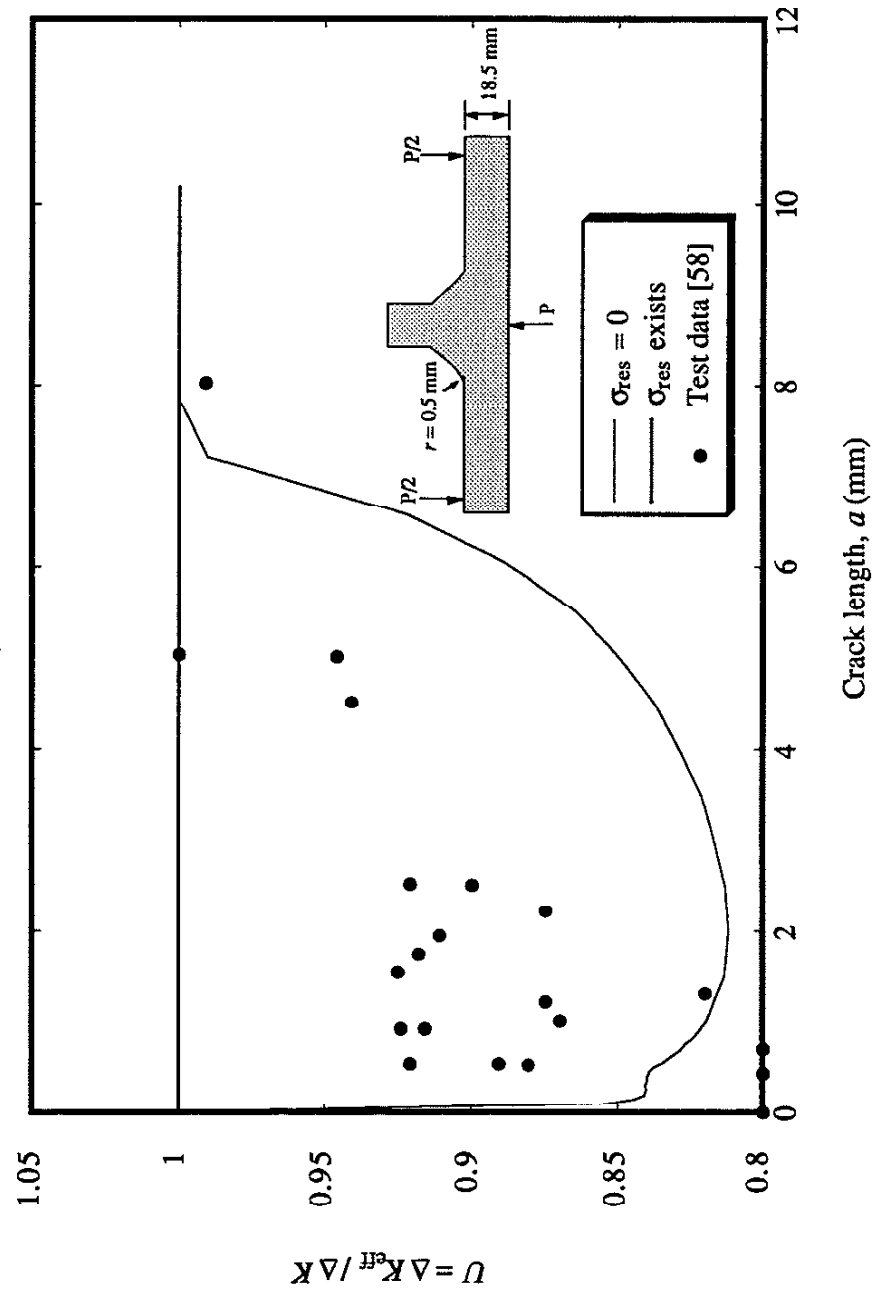


Fig. 30 The measured and the predicted crack closure of a welded T-joint.

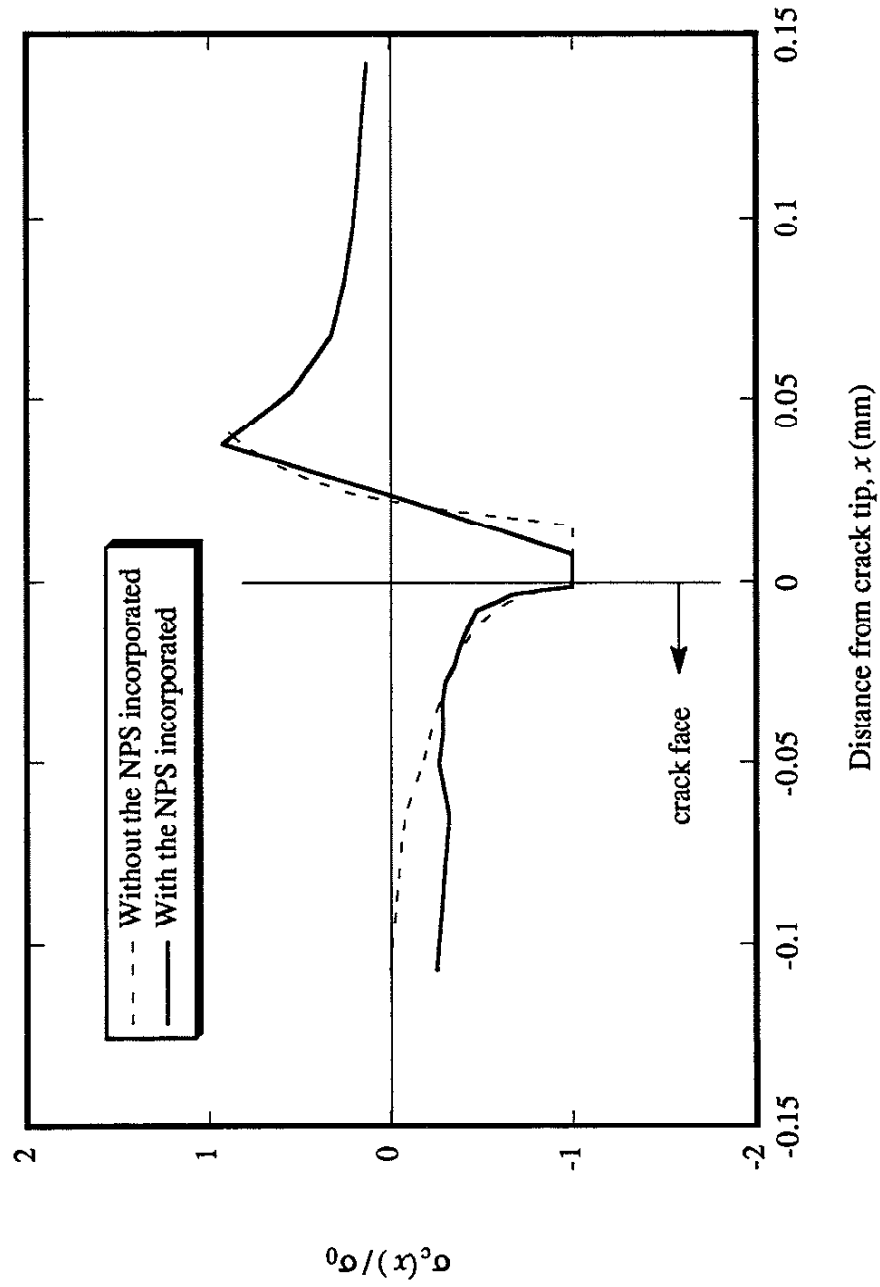


Fig. 31 The calculated crack-face contact-stress distributions with and without the NPS considered for the case of $R = 0$.

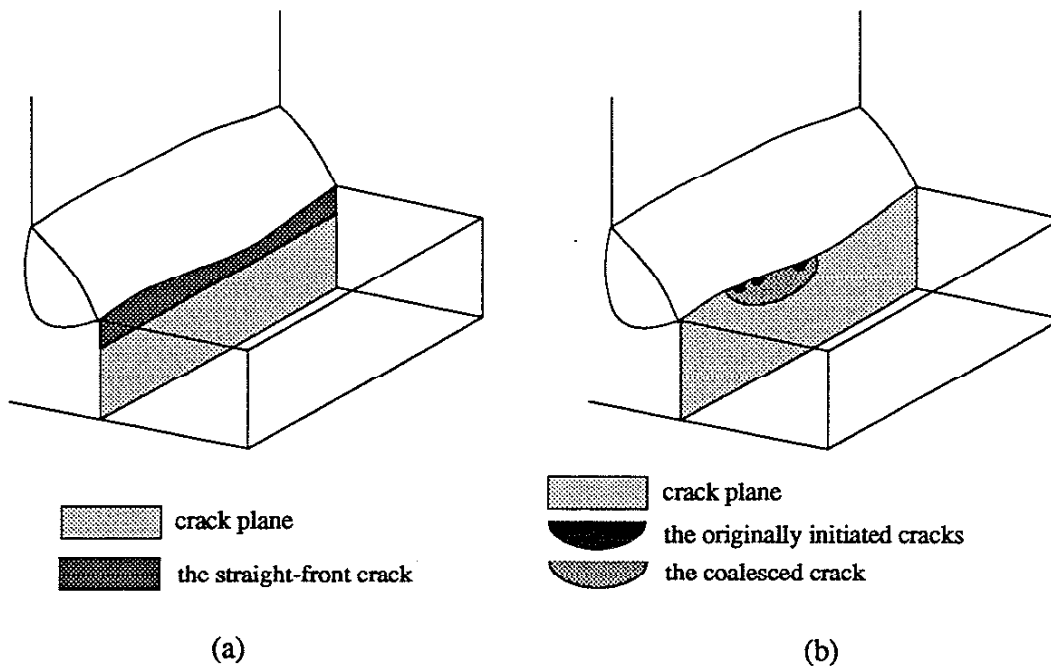


Fig. 32 (a) Straight-front crack in a weld toe, (b) Multiple crack initiation and crack coalescence.

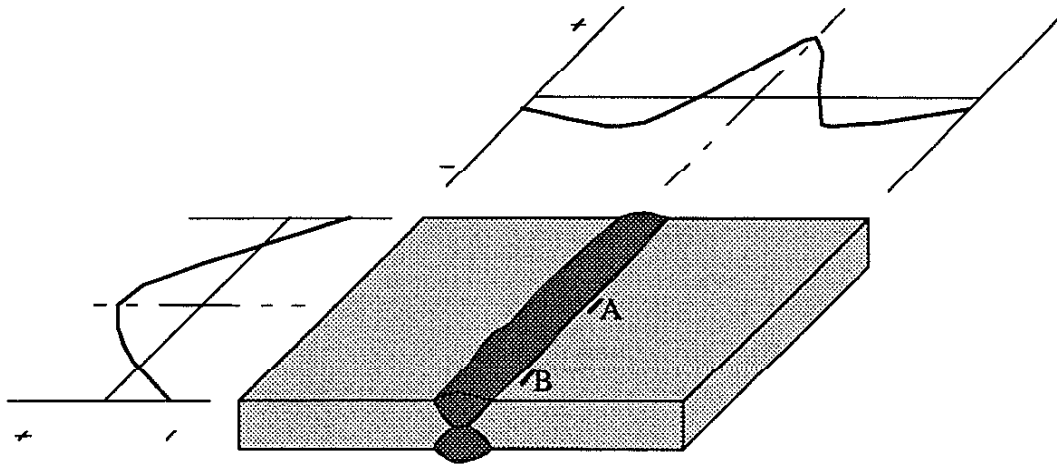
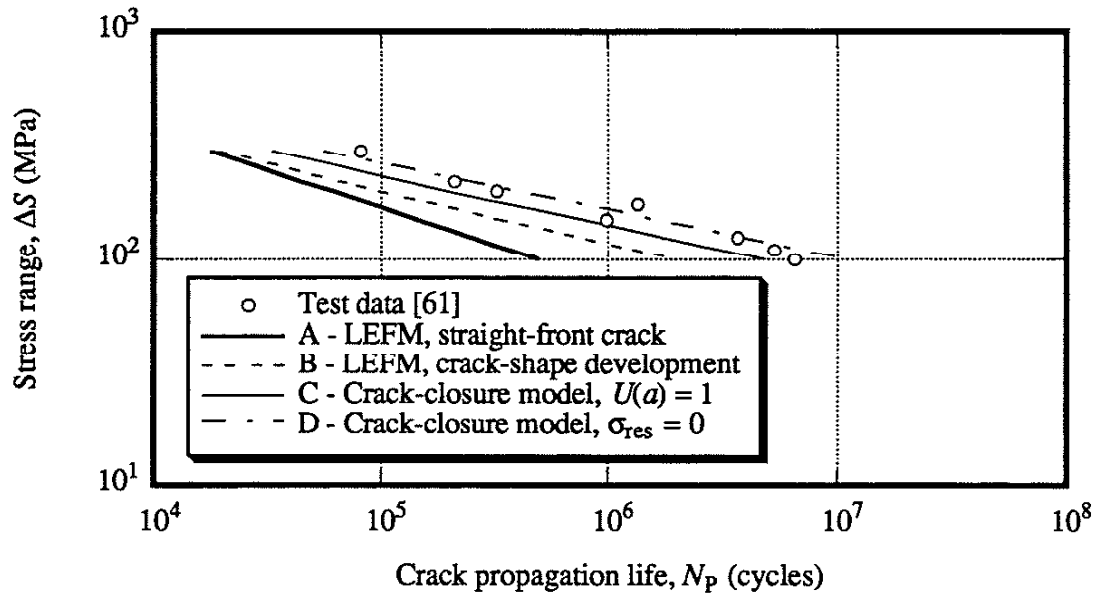
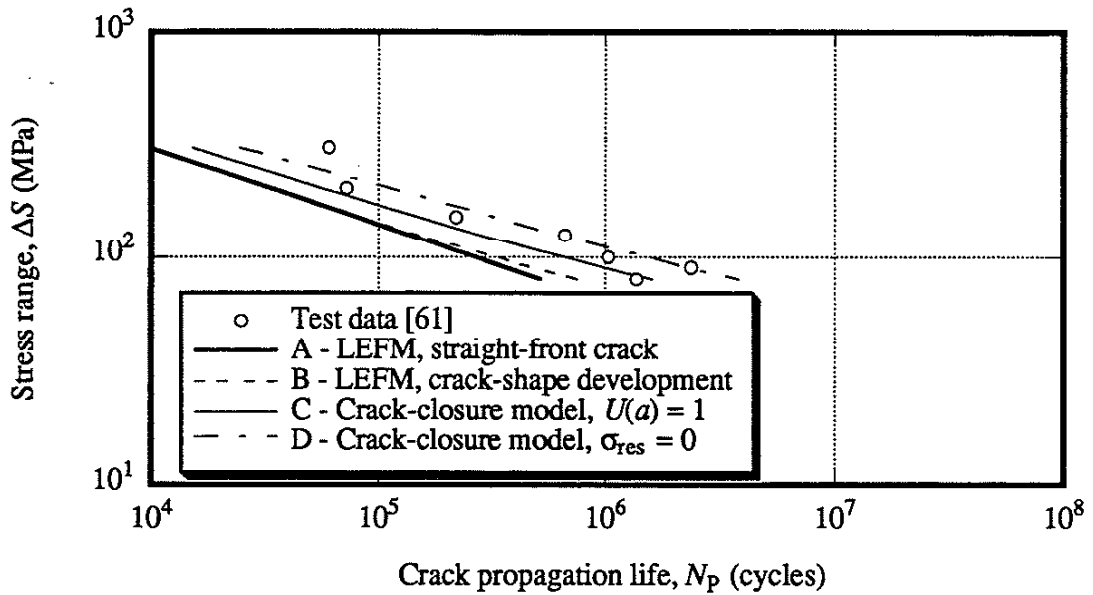


Fig. 33 The residual stress distributions in a welded plate.

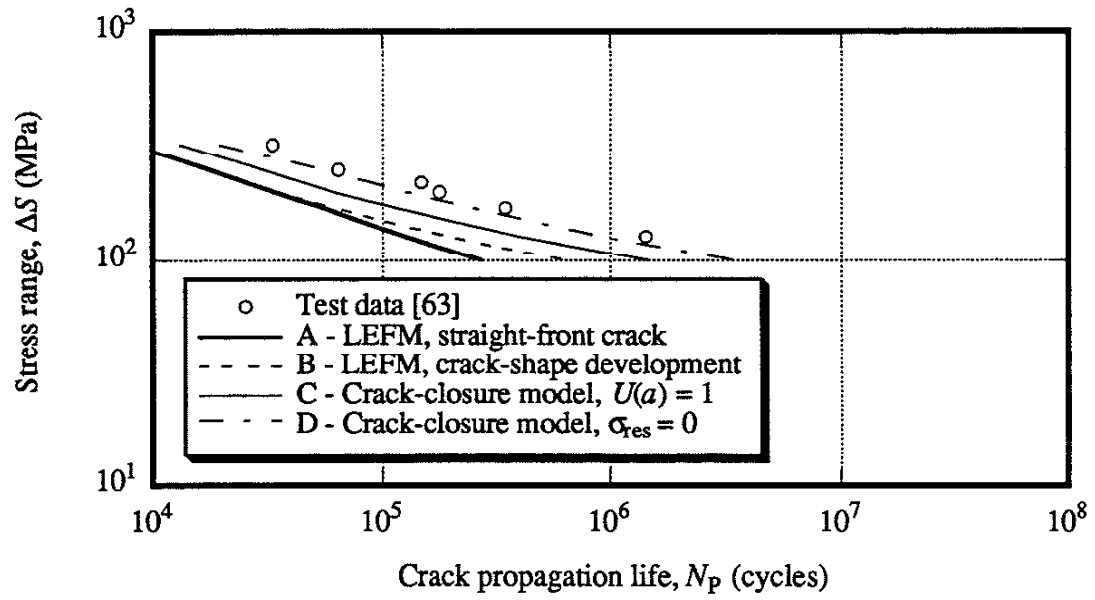


(a)

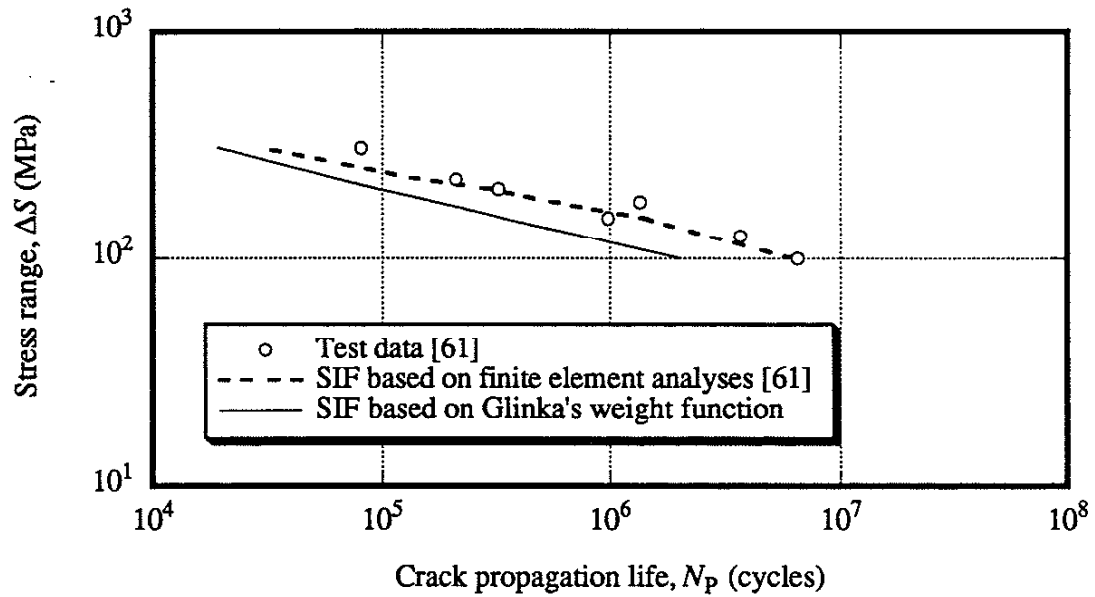


(b)

Fig. 34 Comparison of the model predictions with the observed crack propagation life: (a) $t = 16$ mm (b) $t = 78$ mm.



(c)



(d)

Fig. 34 (cont.) Comparison of the model predictions with the observed crack propagation life (c) $t = 22$ mm (d) comparison of the results between different approaches for the SIF calculations for the case of $t = 16$ mm.

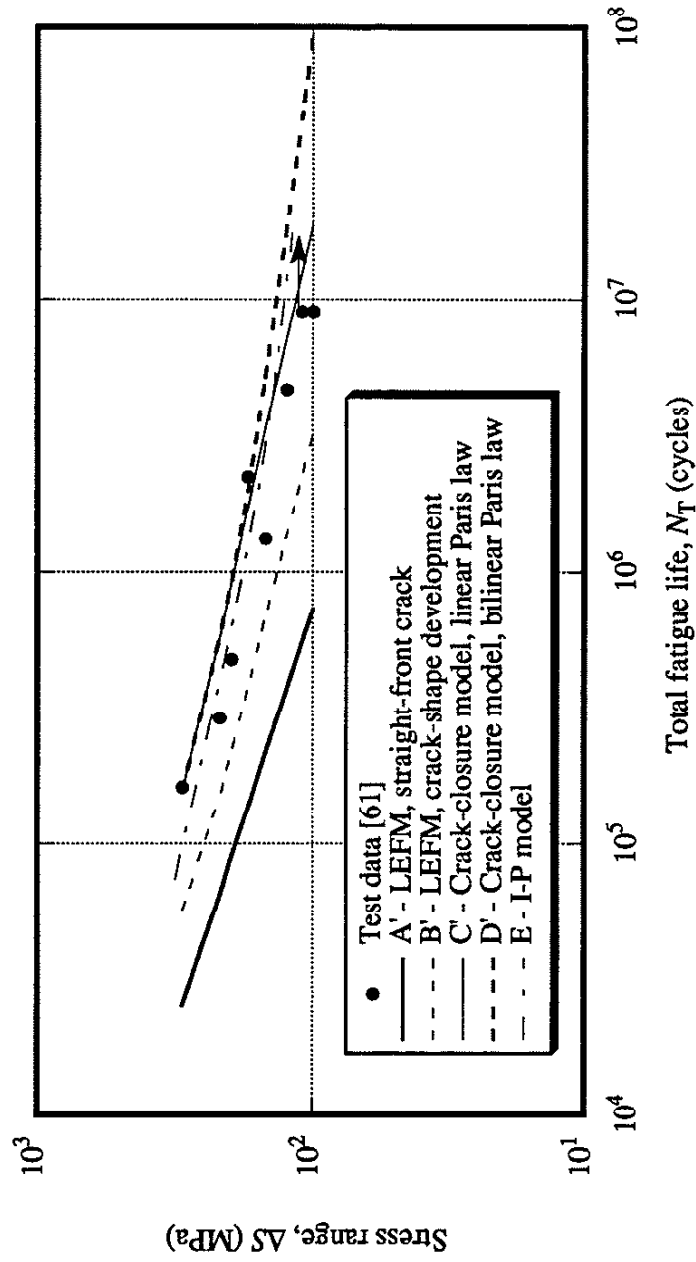


Fig. 35(a) Comparison of the model predictions with the tested total fatigue lives for a plate thickness $t = 16$ mm.

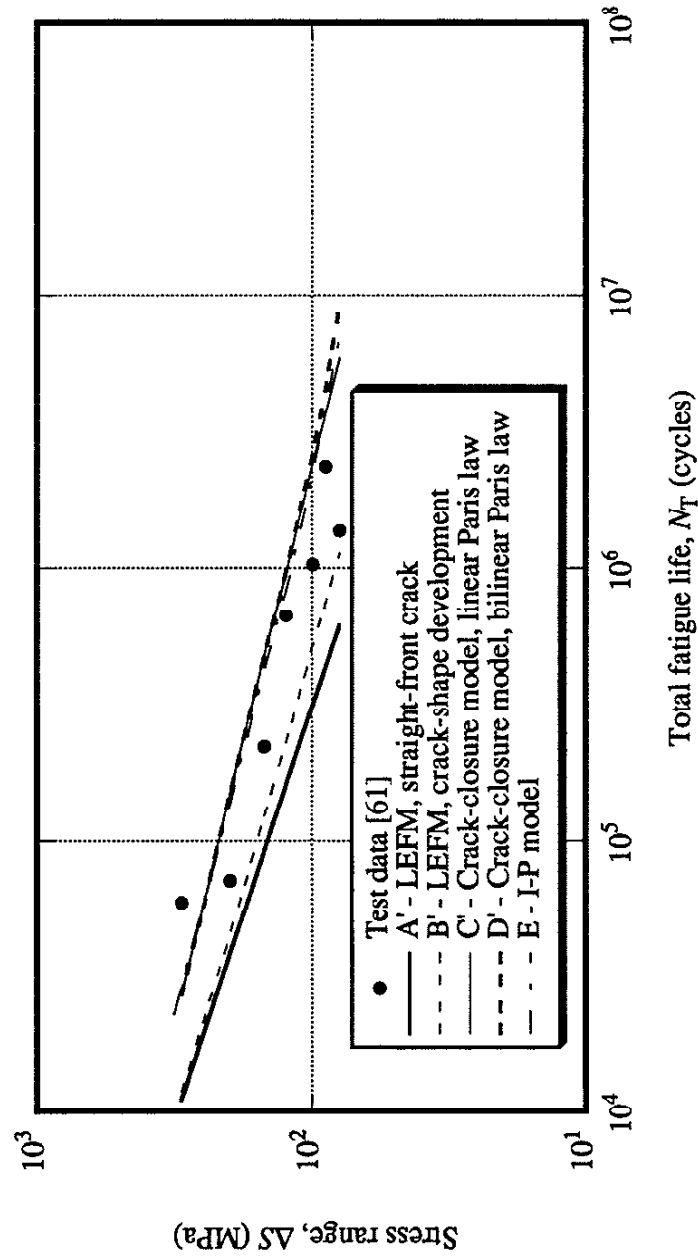


Fig. 35(b) Comparison of the model predictions with the observed total fatigue lives for a plate thickness $t = 78$ mm.

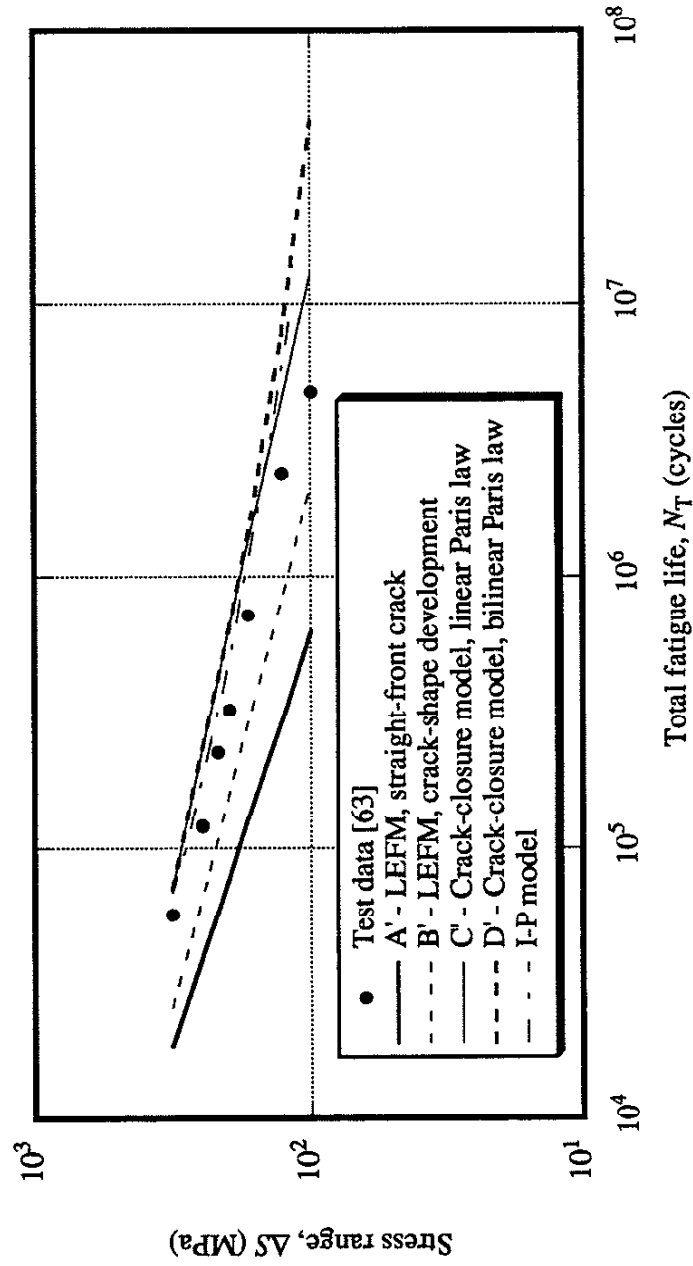
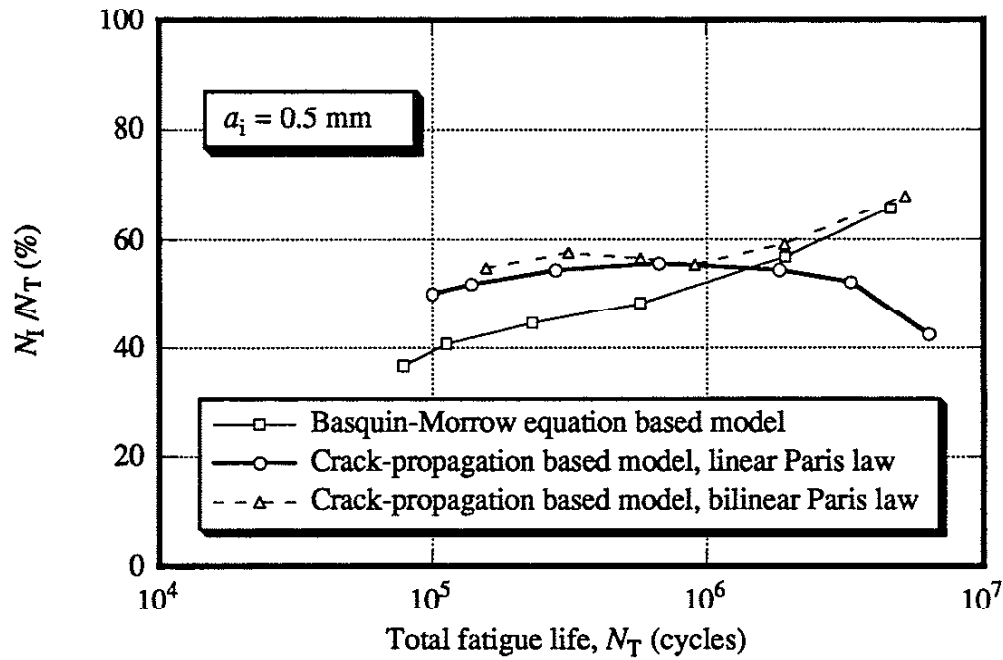
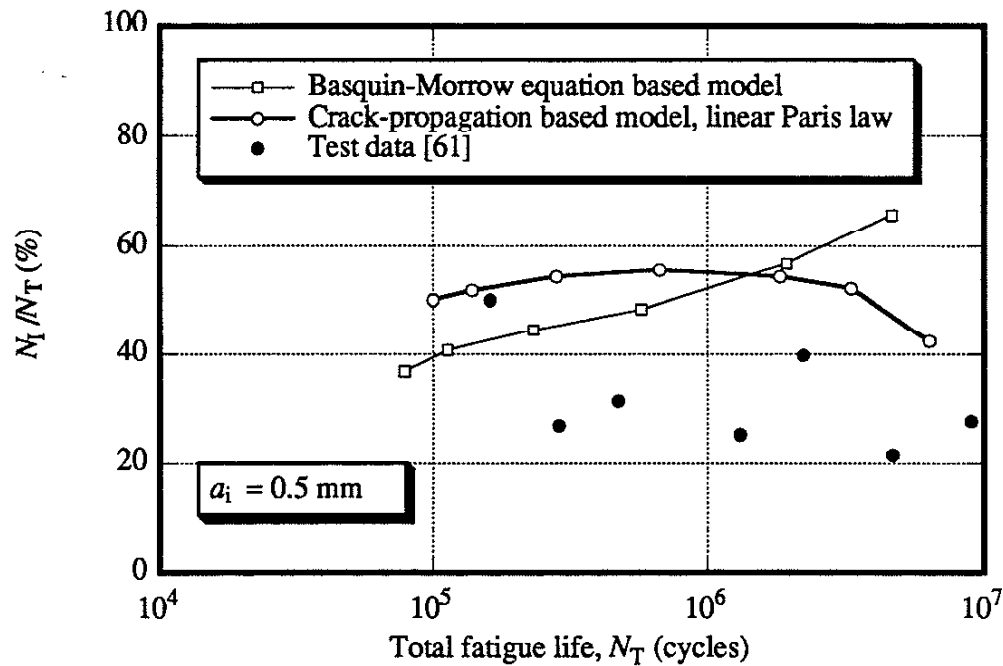


Fig. 35(c) Comparison of the model predictions with the observed total fatigue lives for a plate thickness $t = 22$ mm.

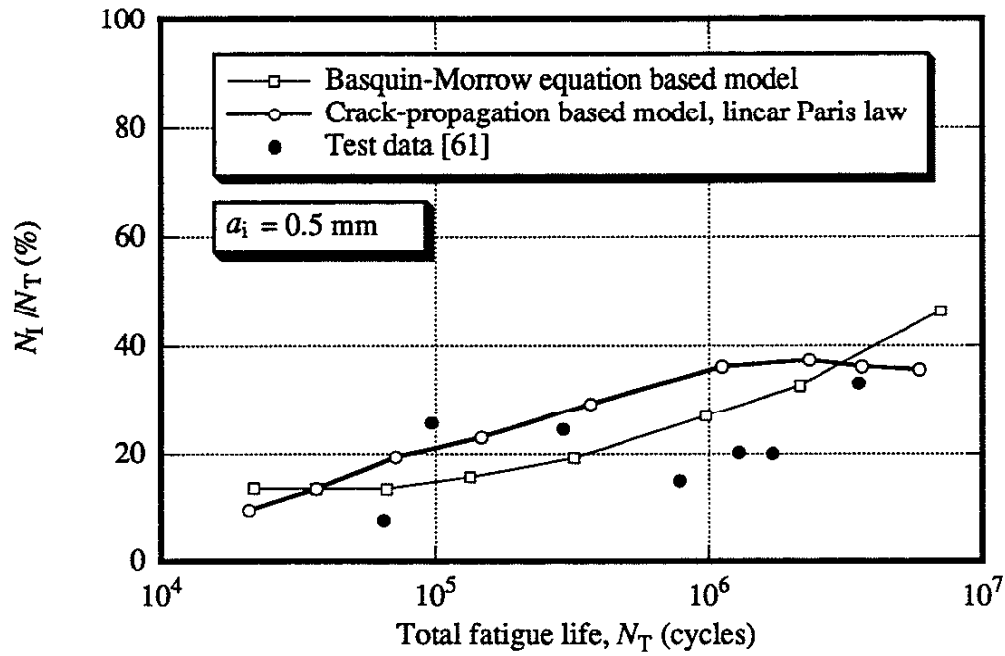


(a)

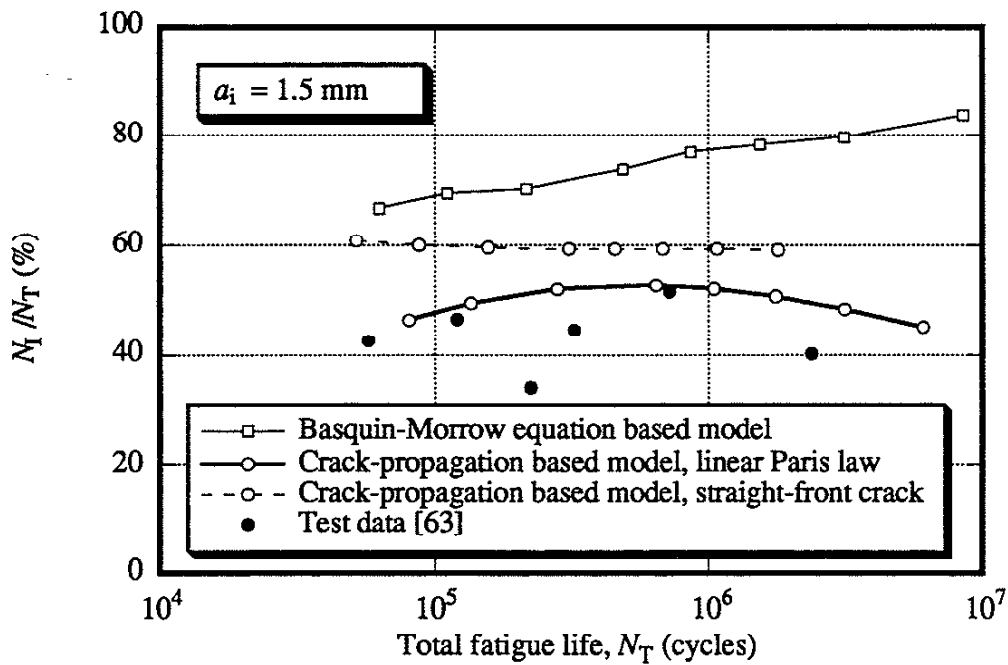


(b)

Fig. 36 The predicted values of N_I/N_T for a T-joint with plate thickness of 16 mm: (a) comparison of model predicted results (b) comparison with test data.



(c)



(d)

Fig. 36 The predicted values of N_I/N_T from the Basquin-Morrow equation based and crack-propagation based model for N_I : (c) $t = 78$ mm (d) $t = 22$ mm.

REFERENCES

1. Elber, W., "The Significance of Fatigue Crack Closure", *Damage Tolerance in Aircraft Structure, ASTM STP 486*, American Society for Testing and Materials, 1971, pp. 230-242.
2. Walker, N. and Beevers, C. J., "A Fatigue Crack Closure Mechanism in Titanium", *Fatigue Fract. Engng. Mater. Struct.*, Vol. 1, 1979, pp. 135-148.
3. Steward, A. T., "The Influence of Environment and Stress Ratio on Fatigue Crack Growth at Near Threshold Stress Intensities in Low-Alloy Steels", *Engineering Fracture Mechanics*, Vol. 13, 1980, pp. 463-478.
4. Ritchie, R. O., Suresh, S. and Moss, C. M., "Near Threshold Fatigue Crack Growth in 2%Cr-1Mo Pressure Vessel Steel in Air and Hydrogen", *Journal of Engineering Materials and Technology*, Vol. 102, pp. 293-299.
5. Suresh, S., "Fatigue Crack Deflection and Fracture Surface Contact: Micromechanical Models", *Metallurgical Transactions A*, Vol. 16A, 1985, pp. 249-260.
6. LLorca, J., "Roughness-Induced Fatigue Crack Closure: A Numerical Study", *Fatigue Fract. Engng. Mater. Struct.*, Vol. 15, 1992, pp. 655-669.
7. Suresh, S., Parks, D. M. and Ritchie, R. O., "Crack Tip Oxide Formation and Its Influence on Fatigue Threshold", *Fatigue Thresholds*, Vol. 1, 1981, pp. 391-408, EMAS Publ. Ltd., Warleg, England.
8. Budiansky, B. and Hutchinson, J. W., "Analysis of Closure in Crack Growth", *Journal of Applied Mechanics*, Vol. 45, 1978, pp. 267-275.
9. Newman, J. C., Jr., "A Finite Element Analysis of Fatigue Crack Closure", *Mechanics of Crack Growth, ASTM STP 590*, American Society for Testing and Materials, 1976, pp. 281-301.
10. Fleck, N. and Newman, J. C., Jr., "Analysis of Crack Closure under Plane Strain Conditions", *Mechanisms of Crack Closure, ASTM STP 982*, American Society for Testing and Materials, 1988, pp. 319-341.
11. Sun, W., "Finite Element Simulations of Fatigue Crack Growth and Closure", *Ph. D. Thesis*, Department of Mechanical Engineering, University of Illinois at Urbana-Champaign.
12. McClung, R. C. and Sehitoglu, H., "On the Finite Element Analysis of Fatigue Crack Closure - 1. Basic Modeling Issues", *Engineering Fracture Mechanics*, Vol. 33, 1989, pp. 237-252.
13. Newman, J. C., Jr., "A Crack-Closure Model for Predicting Fatigue Crack Growth Under Aircraft Spectrum Loading", *Methods and Models for Predicting Fatigue Crack Growth Under Random Loading, ASTM STP 748*, American Society for Testing and Materials, 1983, pp. 53-84.
14. Newman, J. C., Jr., "A Nonlinear Fracture Mechanics Approach to the Growth of Small Cracks", *AGARD Report 328*, 1983, pp. 6.1-6.26.

15. de Koning, A. U. and Liefeling, G., "Analysis of Crack Opening Behavior by Application of a Discretized Strip Yield Model", *Mechanics of Crack Closure*, ASTM STP 982, American Society for Testing and Materials, 1988, pp. 437-458.
16. Wang, G. S. and Blom, A. F., "A Strip Model for Fatigue Crack Growth Predictions Under General Load Conditions", *Engineering Fracture Mechanics*, Vol. 40, 1991, pp. 507-533.
17. Newman, J. C., Jr., "Fracture Mechanics Parameters for Small Fatigue Cracks", *Small-Crack Test Methods*, ASTM STP 1149, American Society for Testing and Materials, 1992, pp. 6-33.
18. Irwin, G. R., "Plastic Zone Near a Crack and Fracture Toughness", *Proceedings of the 7th Sagamore Conference*, 1960, pp. IV63-IV 76.
19. Paris, P. C. and Erdogan, F., "A Critical Analysis of Crack Propagation Laws", *Trans. ASME, Journal of Basic Engineering*, Vol. D85, 1963, pp. 528-534.
20. Bueckner, H. F., "A Novel Principle for the Computation of Stress Intensity Factors", *ZAMM*, Vol. 50, 1970, pp. 529-546.
21. Rice, J. R., "Some Remarks on Elastic Crack-Tip Stress Fields", *International Journal of Solid Structures*, Vol. 8, 1972, pp. 751-758.
22. Dowling, N. E., "Fatigue at Notches and the Local Strain and Fracture Mechanics Approaches", *Fracture Mechanics*, ASTM STP 677, American Society for Testing and Materials, 1979, pp. 247-273.
23. Smith, R. A. and Miller, K. J., "Fatigue Cracks at Notches", *International Journal of Mechanical Science*, Vol. 19, 1977, pp. 11-22.
24. Dowling, N. E., "Crack Growth During Low-Cycle Fatigue of Smooth Axial Specimens", *Cyclic Stress-Strain and Plastic Deformation Aspects of Fatigue Crack Growth*, ASTM STP 637, American Society for Testing and Materials, 1977, pp. 97-121.
25. El Haddad, M. H., Dowling, N. E., Topper, T. H. and Smith, K. N., "J Integral Applications for Short Cracks at Notches", *International Journal of Fracture*, Vol. 16, 1980, pp. 15-30.
26. Sehitoglu, H., "Fatigue Life Prediction of Notched Members Based on Local Strain and Elastic-Plastic Fracture Mechanics Concepts", *Engineering Fracture Mechanics*, Vol. 18, 1983, pp. 609-621.
27. Leis, B. N., "Displacement Controlled Fatigue Crack Growth in Inelastic Notch Fields: Implications for Short Cracks", *Engineering Fracture Mechanics*, Vol. 22, 1985, pp. 279-293.
28. Shin, C. S. and Smith, R. A., "Fatigue Crack Growth at Stress Concentrations - The Role of Notch Plasticity and Crack Closure", *Engineering Fracture Mechanics*, Vol. 29, 1988, pp. 301-315.

29. Sehitoglu, H., "Characterization of Crack Closure", *Fracture Mechanics, ASTM STP 868*, American Society for Testing and Materials, 1985, pp. 361-380.
30. Lawrence, F. V., Burk, J. D. and Yung, J.-Y., "Influence of Residual Stress on the Predicted Fatigue Life of Weldments", *Residual Stress Effects in Fatigue, ASTM STP 776*, American Society for Testing and Materials, 1982, pp. 33-43.
31. Jhansale, H. R. and Topper, T. H., "Engineering Analysis of the Inelastic Stress Response of a Structural Metal Under Variable Cyclic Strains", *Cyclic Stress-Strain Behavior -- Analysis, Experimentation, and Failure Prediction, ASTM STP 519*, American Society for Testing and Materials, 1973, pp. 246-270.
32. Parker, A. P., "Stress Intensity Factors, Crack Profiles, and Fatigue Crack Growth Rates in Residual Stress Fields", *Residual Stress Effects in Fatigue, ASTM STP 776*, American Society for Testing and Materials, 1982, pp. 13-31.
33. Glinka, G., "Effect of Residual Stresses on Fatigue Crack Growth in Steel Weldments Under Constant and Variable Amplitude Loads", *Fracture Mechanics, ASTM STP 677*, American Society for Testing and Materials, 1979, pp. 198-214.
34. Nelson, D. V., "Effects of Residual stress on Fatigue Crack Propagation", *Residual Stress Effects in Fatigue, ASTM STP 776*, American Society for Testing and Materials, 1982, pp. 172-194.
35. Ohta, A., Kosuge, M., Mawari, T. and Nishijima, S., "Fatigue Crack Propagation in Tensile Residual Stress Fields of Welded Joints Under Fully Compressive Cycling", *International Journal of Fatigue*, Vol. 10, 1988, pp. 237-242.
36. Ohta, A., McEvily, A. J. and Suzuki, N., "Fatigue Crack Propagation in a Tensile Residual Stress Field Under a Two-Step Programmed Test", *International Journal of Fatigue*, Vol. 15, 1993, pp. 9-12.
37. Itoh, Y. Z., Suruga, S. and Kashiwaya, H., "Prediction of Fatigue Crack Growth Rate in Welding Residual Stress Field", *Engineering Fracture Mechanics*, Vol. 33, 1989, pp. 397-407.
38. Kang, K. J., Song, J. H. and Earmme, Y. Y., "Fatigue Crack Growth and Closure Through a Tensile Residual Stress Field Under Compressive Applied Loading", *Fatigue Fract. Engng. Mater. Struct.*, Vol. 12, 1989, pp. 363-376.
39. Lawrence, F. V., Jr., Mattos, R. J., Higashida, Y. and Burk, J. D., "Estimating the Fatigue Crack Initiation Life of Welds", *Fatigue Testing of Weldments, ASTM STP 648*, American Society for Testing and Materials, 1978, pp. 134-158.
40. Ho, N. J. and Lawrence, F. V., Jr., "Constant Amplitude and Variable Load History Fatigue Testing Results and Predictions for Cruciform and Lap Welds", *Theoretical and Applied Fracture Mechanics*, Vol. 1, No. 1, 1984, pp. 3-21.
41. Yung, J.-Y. and Lawrence, F. V., Jr., "Analytical and Graphical Aids for the Fatigue Design of Weldments", *Fatigue Fract. Engng. Mater. Struct.*, Vol. 8, No. 3, 1985, pp. 223-241.

42. Hammouda, M. M., Smith, R. A. and Miller, K. J., "Elastic-Plastic Fracture Mechanics for Initiation and Propagation of Notch Fatigue Cracks", *Fatigue Fract. Engng. Mater. Struct.*, Vol. 2, 1979, pp. 139-154.
43. Socie, D. F., Dowling, N. E. and Kurath, P., "Fatigue Life Estimation of Notched Members", *Fracture Mechanics, ASTM STP 833*, Society for Testing and Materials, 1984, pp. 284-299.
44. Ting, J. C. and Lawrence, F. V., "Modeling the Long-Life Fatigue Behavior of a Cast Aluminum Alloy", *Fatigue Fract. Engng. Mater. Struct.*, Vol. 16, 1993, pp. 631-647.
45. Ting, J. C. and Lawrence, F. V., "A Crack Closure Model for Predicting the Threshold Stresses of Notches", *Fatigue Fract. Engng. Mater. Struct.*, Vol. 16, 1993, pp. 93-114.
46. Ogura, K., Miyoshi, Y. and Nishikawa, I., "Fatigue Crack Growth and Closure of Small Cracks at Notch Root", *Current Japanese Materials Research, MRS*, Society of Material Science, Japan, Vol. I, 1987, pp. 67-91.
47. Verreman, Y., Baillon, J.-P. and Masounave, J., "Fatigue Short Crack Propagation and Plasticity-Induced Crack Closure at the Toe of a Fillet Welded Joint", *The Behavior of Short Fatigue Cracks*, EGF Pub. 1, 1986, Mechanical Engineering Publications, London, pp. 387-404.
48. McClung, R. C. and Sehitoglu, H., "Closure and Growth of Fatigue Cracks at Notches", *Journal of Engineering Materials and Technology*, Vol. 114, 1992, pp. 1-7.
49. Tanaka, K., Nakai, Y. and Yamashita, M., "Fatigue Growth Threshold of Small Cracks", *International Journal of Fracture*, Vol. 17, 1981, pp. 519-533.
50. Hou, C. Y. and Lawrence, F. V., "A Model for Weldment Fatigue Based on Crack-Closure Concepts (CCN Model)", *Proceeding of the 12th International Conference on Offshore Mechanics and Arctic Engineering*, 1993, pp. 513-528.
51. Fleck, N. A., "Influence of Stress State on Crack Growth Retardation", *Basic Questions in Fatigue: Volume I, ASTM STP 924*, American Society for Testing and Materials, 1988, pp. 157-183.
52. Tanaka, K. and Akiniwa, Y., "The Propagation of Short Fatigue Cracks at Notches", *Basic Questions in Fatigue: Volume I, ASTM STP 924*, American Society for Testing and Materials, 1988, pp. 281-298.
53. Verreman, Y., Baillon, J.-P., Masounave, J., "Closure and Propagation Behavior of Short Fatigue Cracks" at Different R-Ratios", *Fatigue 87*, 1987, pp. 371-380.
54. Verreman, Y., Baillon, J.-P. and Masounave, J., "Fatigue Life Prediction of Welded Joints - A Re-Assessment", *Fatigue Fract. Engng. Mater. Struct.*, Vol. 10, 1987, pp. 17-36.
55. Keyvanfar, F. and Nelson, D. V., "Predictions of Fatigue Crack Growth Behavior Using a Crack Closure Ligament Model", *Mechanics of Fatigue Crack Closure, ASTM STP 982*, American Society for Testing and Materials, 1988, pp. 414-436.
56. Pang, H. L. J. and Pukas, S. R., "Residual Stress Measurements in a Cruciform Joint Using Hole Drilling and Strain Gauges", *Strain*, Feb. 1989, pp. 7-13.

57. Pang, H. L. J., "Fatigue Crack Growth Study of Residual-Stress Effects", *International Journal of Fatigue*, Vol. 14, 1992, pp. 233-237.
58. Otegui, J. L., Mohaupt, U. H. and Burns, D. J., "Effect of Welded Process on Early Growth of Fatigue Cracks in Steel T Joints", *International Journal of Fatigue*, Vol. 13, 1991, pp. 45-58.
59. Tao, Y., He, J. and Hu, N., "Effect of Notch Stress Field and Crack Closure on Short Fatigue Crack Growth", *Fatigue Fract. Engng. Mater. Struct.*, Vol. 13, 1990, pp. 423-430.
60. Stephens, R. I., Sheets, E. C. and Njus, G. O., "Fatigue Crack Growth and Life Predictions in Man-Ten Steel Subjected to Single and Intermittent Tensile Overloads", *Cyclic Stress-Strain Behavior -- Analysis, Experimentation, and Failure Prediction*, ASTM STP 519, American Society for Testing and Materials, 1973, pp. 176-191.
61. Bell, R. and Vosikovsky, O., "Fatigue Life Prediction of Welded Joints for Offshore Structures Under Variable Amplitude Loading", *Proceeding of the 10th International Conference on Offshore Mechanics and Arctic Engineering*, 1991, pp. 385-393.
62. Niu, X. and Glinka, G., "Theoretical and Experimental Analyses of Surface Fatigue Cracks in Weldments", *Surface-Crack Growth: Models, Experiments, and Structures*, ASTM STP 982, American Society for Testing and Materials, 1990, pp. 390-413.
63. Yagi, J., Machida, S., Tomita, Y., Matoba, M. and Soya, I., "Influence Factors on Thickness Effect of Fatigue Strength in As-Welded Joints for Steel Structures", *Proceeding of the 10th International Conference on Offshore Mechanics and Arctic Engineering*, 1991, pp. 305-313.
64. Jono, M. and Song, J., "Growth and Closure of Short Fatigue Cracks", *Current Japanese Materials Research, MRS, I*, Society of Material Science, Japan, 1987, pp. 67-91.
65. McMahon, J. C. and Lawrence, F. V., "Predicting Fatigue Properties Through Hardness Measurements", *FCP Report No. 105*, 1984, University of Illinois at Urbana-Champaign.
66. Petroski, H. J. and Achenbach, J. D., "Computation of the Weight Function from a Stress Intensity Factor", *Engineering Fracture Mechanics*, Vol. 10, 1978, pp. 257-266.
67. Görner, F., Mattheck, C., Morawietz, P. and Munz, D., "Limitations of the Petroski-Achenbach Crack Opening Displacement Approximation for the Calculation of Weight Functions", *Engineering Fracture Mechanics*, Vol. 22, 1985, pp. 269-277.
68. Bueckner, H. F., "Field Singularities and Related Integral Representations", *Mechanics of Fracture 1 - Methods of Analysis and Solution of Cracks Handbook*, Del. Research Corporation, 1973.
69. Newman, J. C., Jr., Bigelow, C. A. and Shivakumar, K. N., "Three-Dimensional Elastic-Plastic Finite-Element Analyses of Constraint Variations in Cracked Bodies", *NASA Technical Memorandum No. 107704*, 1993.

APPENDIX A: ADAPTATION OF NEWMAN'S STRIP-YIELD MODEL TO ESTIMATE THE CRACK CLOSURE OF NOTCHED COMPONENTS

A.1 MATHEMATICAL FORMULATION OF THE STRIP-YIELD MODEL FOR NOTCHED COMPONENTS

Since cracks emanating from notches is our concern, the effect of the notch-stress field on crack closure has to be considered. This problem suggests the use of the weight function method to calculate the required stress-intensity factors and crack-face displacements based on the notch-stress distributions. All expressions are based on a single-edge crack because short cracks propagating in notches should be treated as edge cracks even if they start from center notched specimens or double-edge notched specimens. Despite the fact that the single-edge crack formulation for crack closure of other types of long cracks is inadequate, it is believed that the calculated U values using the single-edge crack formulation will be close to the values obtained using the correct formulation which corresponds to the crack geometry considered. Therefore, for simplicity, the crack-closure behavior of long cracks is entirely calculated using the single-edge crack formulation in current study. The equations below show the modifications of Newman's original strip-yield model. The details of the model and the significance of these equations are discussed in Ref. 13.

The weight function derived by Petroski et al. [66] for a single-edge crack was used to calculate notch stress-intensity factor $K(a)$:

$$K(a) = \frac{H}{K_r(a)} \int_0^a \sigma(x) \frac{\partial u_r(a, x)}{\partial a} dx \quad (\text{A.1})$$

where

- | | | |
|-------------|---|---|
| $K_r(a)$ | = | the stress-intensity factor of a reference crack subjected to an arbitrarily chosen reference symmetrical load system |
| $u_r(a, x)$ | = | the known elastic crack-face displacement corresponding to the arbitrarily chosen reference symmetrical load system |
| $\sigma(x)$ | = | the unflawed notch-stress distribution on crack path |
| H | = | E for plane stress
$E/(1-\nu^2)$ for plane strain |

A single-edge crack in a smooth plate subjected remote stress S was used as the arbitrarily chosen reference system: see Fig. A.1(a). Because the corresponding $u_r(a, x)$ is not readily available from stress-intensity factor handbooks, an approximate equation for $u_r(a, x)$ given in Ref. 66 was used. The $u_r(a, x)$ was calculated by the approximate equation:

$$u_r(a, x) = \frac{S}{H\sqrt{2}} \left[4F_r\left(\frac{a}{W}\right)a^{1/2}(a-x)^{1/2} + G_r\left(\frac{a}{W}\right)a^{-1/2}(a-x)^{3/2} \right] \quad (\text{A.2})$$

where

$$F_r\left(\frac{a}{W}\right) = 1.12 - 0.231\left(\frac{a}{W}\right) + 10.55\left(\frac{a}{W}\right)^2 - 21.72\left(\frac{a}{W}\right)^3 + 30.39\left(\frac{a}{W}\right)^4 \quad (\text{A.3})$$

$$G_r\left(\frac{a}{W}\right) = \left[I_1(a) - 4F_r\left(\frac{a}{W}\right)a^{1/2}I_2(a) \right] a^{1/2} / I_3(a) \quad (\text{A.4})$$

$$I_1(a) = \sqrt{2}\pi S \int_0^a F_r\left(\frac{a}{W}\right)^2 a \, da \quad (\text{A.5})$$

$$I_2(a) = \int_0^a \sigma(x)(a-x)^{1/2} \, dx \quad (\text{A.6})$$

$$I_3(a) = \int_0^a \sigma(x)(a-x)^{3/2} \, dx \quad (\text{A.7})$$

The required notch-elastic, crack-face displacement functions were obtained by following procedure. Since $u_r(a, x)$ was calculated based on $K_r(a)$ using Eq. A.2, the same procedure can be applied to calculate the notch crack-face displacement (caused by remote stress, see Fig. A.1(b)) $u_1(a, x)$. Therefore, after the notch stress-intensity factor $K(a)$ is calculated, the $u_1(a, x)$ was obtained using Eq. A.2 and Eq. A.3 through A.7 with the $F_r(a/W)$ and $G_r(a/W)$ replaced by $F(a/W)$ and $G(a/W)$. The $F(a/W)$ was calculated by:

$$F\left(\frac{a}{W}\right) = \frac{K(a)}{S\sqrt{\pi a}} \quad (\text{A.8})$$

Note that $K(a)$ was obtained by Eq. A.1 using the notch stress $\sigma(x)$. It is important to replace the crack length a by $a+p_c$ from Eq. A.2 through A.8 because all the equations are applied to the fictitious crack with crack length of $a+p_c$. Since erroneous results were reported [67] for crack-face displacement caused by yield-strip load using Eq. A.2, the $u_2(a+p_c, x)$ (caused by

the strip-yield load ahead of the crack tip, see Fig. A.1(c)) was calculated by a double integral equation:

$$u_2(a + \rho_c, x) = \sigma_0 \int_0^{a + \rho_c} \int_{a_1}^{a + \rho_c} h(c, a') h(x, a') da' dc \quad (\text{A.9})$$

$$a_1 = \max(c, x)$$

where $h(c, a)$ and $h(x, a)$ are the weight functions derived by Bueckner for single-edge cracks [68]:

$$h(a, x) = \sqrt{\frac{2}{\pi a}} \frac{1}{\sqrt{1 - \frac{x}{a}}} \left[1 + m_1 \left(1 - \frac{x}{a} \right) + m_2 \left(1 - \frac{x}{a} \right)^2 \right] \quad (\text{A.10})$$

$$m_1 = 0.6147 + 17.1844 \left(\frac{a}{W} \right)^2 + 8.7822 \left(\frac{a}{W} \right)^6 \quad (\text{A.11})$$

$$m_2 = 0.2502 + 3.2889 \left(\frac{a}{W} \right)^2 + 70.0444 \left(\frac{a}{W} \right)^6 \quad (\text{A.12})$$

The influence function $g(x_i, x_j)$ (the crack-face displacement at x_i , i.e., element i, caused by a uniformly distributed unit load applied at x_j , i. e., element j, see details in Ref. 13) was also obtained by the double integral equation:

$$g(x_i, x_j) = \int_{x_j - \frac{w_j}{2}}^{x_j + \frac{w_j}{2}} \int_{a_1}^{a + \rho_c} h(c, a') h(x, a') da' dc \quad (\text{A.13})$$

$$a_1 = \max(c, x)$$

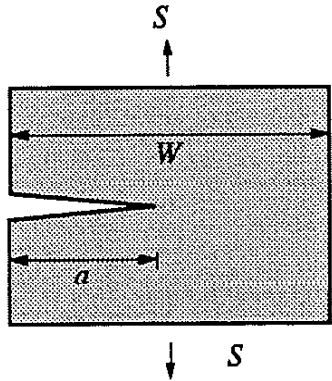
where

w_j = width of element j

A.2 CONSTRAINT FACTOR

Since the constraint factor α used in the strip-yield model is controversial and has a large influence on the calculated results (see detailed explanation in Sec. 2.1.2), Newman et al. [69] rationalized the role of α by performing a series of 3-D FEA for cracks in plates of

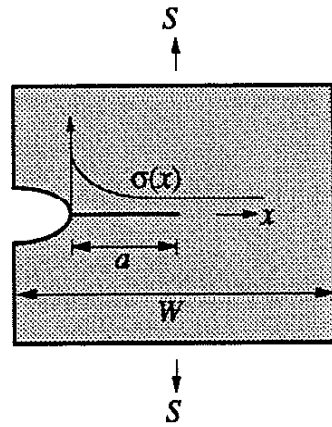
various thickness. They recorded and averaged the loading direction stress values of the yielded elements due to crack-tip stresses and normalized the averaged stress value with respect to σ_0 to obtain a global value α_g . The values of α_g are dependent on plate thickness, stress-intensity factor, flow stress, and plate width. Their results are shown in Fig. A.2. In the present study, the variable α values used in the strip-yield model were obtained from these curves.



$$K_I(a) = F_I \left(\frac{a}{W} \right) S \sqrt{\pi a}$$

$$u_I(a, x) = \frac{S}{H \sqrt{2}} \left[4 F_I \left(\frac{a}{W} \right) a^{1/2} (a-x)^{1/2} + G_I \left(\frac{a}{W} \right) a^{-1/2} (a-x)^{3/2} \right]$$

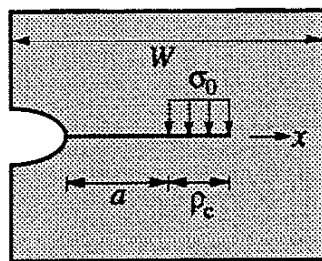
(a)



$$K(a) = \frac{H}{K_I(a)} \int_0^a \sigma(x) \frac{\partial u_I(a, x)}{\partial a} dx = F \left(\frac{a}{W} \right) S \sqrt{\pi a}$$

$$u_1(a, x) = \frac{S}{H \sqrt{2}} \left[4 F \left(\frac{a}{W} \right) a^{1/2} (a-x)^{1/2} + G \left(\frac{a}{W} \right) a^{-1/2} (a-x)^{3/2} \right]$$

(b)



$$u_2(a + \rho_c, x) = \sigma_0 \int_0^{a + \rho_c} \int_{a_1}^{a + \rho_c} h(c, a') h(x, d') da' dc$$

$$a_1 = \max(c, x)$$

(c)

Fig. A.1 The equations for the strip-yield model: (a) The arbitrarily chosen single-edge crack system (b) The notch-stress intensity and crack-face displacement caused by remote load (c) The crack-face displacement caused by the strip-yield load.

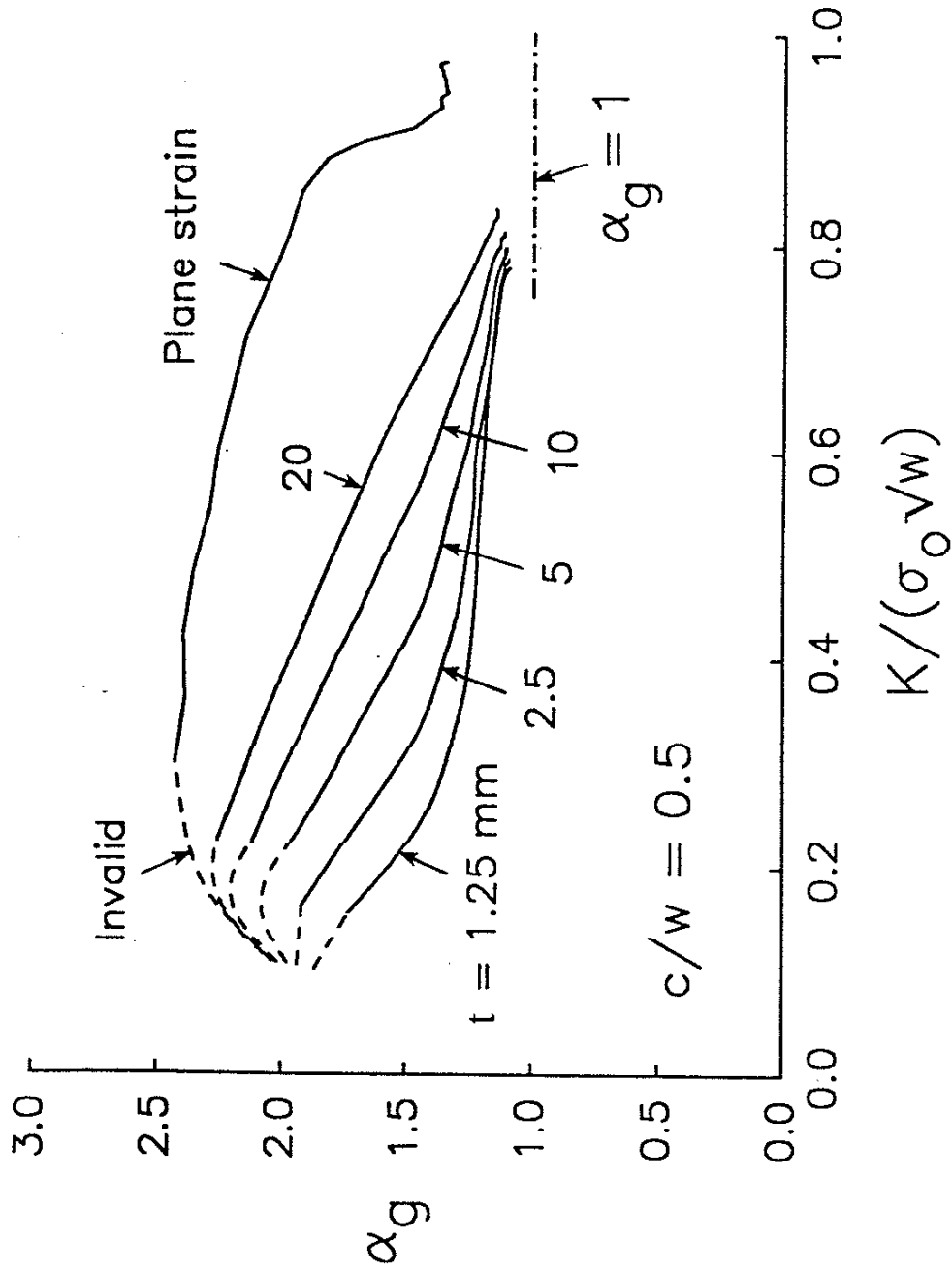


Fig. A.2 The values of α_g obtained from 3-D FEA [69].

APPENDIX B: INTRODUCING THE EFFECTS OF RESIDUAL STRESSES INTO THE STRIP-YIELD MODEL

The basic concept for considering the effects of residual stresses using the strip-yield model is similar to the superposition of the stress-intensity factors: see Eq. 2.7. However, instead of using a stress-intensity factor, crack-face displacements are superposed.

The $K_{\text{res}}(a)$ was obtained by the weight function method, i.e., Eq. 5.2 for a center cracks in smooth plates. For welded joint, Eq. A.1 was used to obtain the $K_{\text{res}}(a)$ for cracks emanating from weld toes. The crack-tip plastic zone size at S_{max} was obtained by substituting $K_{\text{max}}(a) + K_{\text{res}}(a)$ into K_S in Eq. 3.1.

Crack-face displacements caused by residual stresses exist before the external load is applied. This residual crack-face displacement $u_{\text{res}}(a + \rho_{\infty}x)$ was calculated using Eq. A.2 with $K(a)$ and $\sigma(x)$ replaced by $K_{\text{res}}(a)$ and $\sigma_{\text{res}}(x)$. Therefore, at any load level, the $u_{\text{res}}(a + \rho_{\infty}x)$ was added to the calculated crack-face displacement caused by the external load:

$$u'_{\text{max}}(a + \rho_{\infty}x) = u_{\text{max}}(a + \rho_{\infty}x) + u_{\text{res}}(a + \rho_{\infty}x) \quad (\text{B.1})$$

$$u'_{\text{min}}(a + \rho_{\infty}x) = u_{\text{min}}(a + \rho_{\infty}x) + u_{\text{res}}(a + \rho_{\infty}x) \quad (\text{B.2})$$

where

$$\begin{aligned} u'_{\text{max}}(a + \rho_{\infty}x), u'_{\text{min}}(a + \rho_{\infty}x) &= \text{maximum and minimum crack-face} \\ &\quad \text{displacements due to the external stresses and} \\ &\quad \text{residual stresses} \\ u_{\text{max}}(a + \rho_{\infty}x), u_{\text{min}}(a + \rho_{\infty}x) &= \text{maximum and minimum crack-face} \\ &\quad \text{displacements due to the external stresses} \end{aligned}$$

Note that $u_{\text{max}}(a + \rho_{\infty}x)$ and $u_{\text{min}}(a + \rho_{\infty}x)$ are calculated from the elastic crack-face displacements $u_1(a + \rho_{\infty}x)$ and $u_2(a + \rho_{\infty}x)$. It is apparent that the effective stress ratio R' caused by the residual stresses is accounted for by the local crack-face displacements in the current approach. This approach differs from the approach used by Wang and Blom [16] who considered the residual stress effects by converting the local crack-tip stress intensity to a uniform remote load: see Sec. 2.3 for details.